

# Optical properties of cadmium phosphide and cadmium arsenide

**Citation for published version (APA):**

Gelten, M. J. (1985). *Optical properties of cadmium phosphide and cadmium arsenide*. [Phd Thesis 1 (Research TU/e / Graduation TU/e), Applied Physics and Science Education]. Technische Hogeschool Eindhoven. <https://doi.org/10.6100/IR178915>

**DOI:**

[10.6100/IR178915](https://doi.org/10.6100/IR178915)

**Document status and date:**

Published: 01/01/1985

**Document Version:**

Publisher's PDF, also known as Version of Record (includes final page, issue and volume numbers)

**Please check the document version of this publication:**

- A submitted manuscript is the version of the article upon submission and before peer-review. There can be important differences between the submitted version and the official published version of record. People interested in the research are advised to contact the author for the final version of the publication, or visit the DOI to the publisher's website.
- The final author version and the galley proof are versions of the publication after peer review.
- The final published version features the final layout of the paper including the volume, issue and page numbers.

[Link to publication](#)

**General rights**

Copyright and moral rights for the publications made accessible in the public portal are retained by the authors and/or other copyright owners and it is a condition of accessing publications that users recognise and abide by the legal requirements associated with these rights.

- Users may download and print one copy of any publication from the public portal for the purpose of private study or research.
- You may not further distribute the material or use it for any profit-making activity or commercial gain
- You may freely distribute the URL identifying the publication in the public portal.

If the publication is distributed under the terms of Article 25fa of the Dutch Copyright Act, indicated by the "Taverne" license above, please follow below link for the End User Agreement:

[www.tue.nl/taverne](http://www.tue.nl/taverne)

**Take down policy**

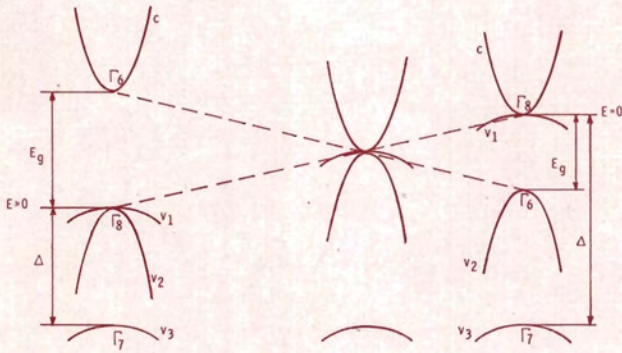
If you believe that this document breaches copyright please contact us at:

[openaccess@tue.nl](mailto:openaccess@tue.nl)

providing details and we will investigate your claim.

# OPTICAL PROPERTIES

## OF CADMIUM PHOSPHIDE AND CADMIUM ARSENIDE



M.J. GELTEN

**OPTICAL PROPERTIES OF CADMIUM PHOSPHIDE AND CADMIUM ARSENIDE**

**OPTICAL PROPERTIES  
OF  
CADMIUM PHOSPHIDE AND CADMIUM ARSENIDE**

**PROEFSCHRIFT**

**TER VERKRIJGING VAN DE GRAAD VAN DOCTOR IN DE  
TECHNISCHE WETENSCHAPPEN AAN DE TECHNISCHE  
HOGESCHOOL EINDHOVEN, OP GEZAG VAN DE RECTOR  
MAGNIFICUS, PROF. DR. S. T. M. ACKERMANS, VOOR EEN  
COMMISSIE AANGEWEEZEN DOOR HET COLLEGE VAN  
DEKANEN IN HET OPENBAAR TE VERDEDIGEN OP  
VRIJDAG 14 JUNI 1985 TE 16.00 UUR**

**DOOR**

**MARINUS JOHANNES GELTEN**

**GEBOREN TE HALSTEREN**

Dit proefschrift is goedgekeurd door de promotoren:

Prof.dr. M.J. Steenland

en

Prof.dr.ir. W.J.M. de Jonge

Aan Ria,  
Aan Marijn en Ronald

## CONTENTS

CHAPTER 1. GENERAL INTRODUCTION	1
CHAPTER 2. EXPERIMENTAL TECHNIQUES	3
2.1. <i>Introduction</i>	3
2.2. <i>A specular reflectance accessory for infrared spectrometers</i>	4
2.3. <i>A gas filled cryogenic sample holder for infrared transmission measurements</i>	6
2.4. <i>Sample preparation</i>	8
CHAPTER 3. INTERBAND ABSORPTION OF $Cd_3P_2$ AND $Cd_3As_2$	10
3.1. <i>Band structure inversion</i>	10
3.2. <i>Band models of <math>Cd_3P_2</math> and <math>Cd_3As_2</math></i>	11
3.3. <i>Optical properties of <math>Cd_3P_2</math></i>	14
3.4. <i>Optical verification of the valence band structure of <math>Cd_3As_2</math></i>	25
CHAPTER 4. FAR INFRARED REFLECTIVITY OF $Cd_3P_2$ AND $Cd_3As_2$	29
4.1. <i>Plasma edge behaviour of <math>Cd_3P_2</math> and <math>Cd_3As_2</math></i>	29
4.2. <i>A new method to determine the coupled mode parameters of a plasmon-multiphonon system</i>	31
4.3. <i>Far infrared optical properties of <math>Cd_3P_2</math> and <math>Cd_3As_2</math></i>	42
4.4. <i>Intrinsic phonon parameters of <math>Cd_3P_2</math></i>	47
4.5. <i>Magnetoplasma reflectivity studies of <math>Cd_3As_2</math></i>	55
CHAPTER 5. RECENT DEVELOPMENTS: THE BODNAR MODEL	68
GENERAL REFERENCES	73
APPENDIX	76
SUMMARY	79
SAMENVATTING	81
DANKWOORD	83
CURRICULUM VITAE	84

## CHAPTER I GENERAL INTRODUCTION

One of the interesting areas of semiconductor physics is formed by the study of narrow gap semiconductors {1,2}. Both, fundamental interest and technical applications, are a strong stimulus for many groups to study these materials extensively. The best known example of a typical narrow gap material is the system  $\text{Hg}_x\text{Cd}_{1-x}\text{Te}$  ( $0 \leq x \leq 1$ ). This system shows the interesting fundamental phenomenon of band structure inversion and is widely used in applications, especially as infrared detectors {3}.

Among the narrow gap semiconductors the II-V compounds form a special class. These materials exhibit in many aspects a typical narrow gap behaviour (e.g. band structure inversion) and on the contrary they show interesting and specific deviations from the standard pattern. Various properties of II-V compounds are reviewed in the literature {4,5,6} while some recent developments are presented in the proceedings of an international symposium {7}.

Typical representatives of the II-V family are formed by the compounds  $\text{Cd}_3\text{P}_2$  and  $\text{Cd}_3\text{As}_2$ , which have been the subject of an extensive research program of our laboratory during the last two decades. After a preliminary study of the thermomagnetic properties of polycrystalline  $\text{Cd}_3\text{As}_2$  {8} Blom succeeded to grow single crystals of both  $\text{Cd}_3\text{P}_2$  and  $\text{Cd}_3\text{As}_2$ . These crystals were highly degenerate n-type materials with high electron mobilities and showed interesting analogies with  $\text{Hg}_x\text{Cd}_{1-x}\text{Te}$ , mentioned above, e.g. a non-parabolic conduction band and very high values of the electron mobility. There were also indications that the system of mixed crystals of  $\text{Cd}_3(\text{As}_x\text{P}_{1-x})_2$  showed band structure inversion (see section 3.1.). Unfortunately, no conclusive evidence for this phenomenon was available because the details of the band structure were not known. Moreover, a large variety of experimental results was not understood at that time. Therefore it was decided to start a comprehensive research program aimed at the experimental study of the details of the band structure of the end compounds  $\text{Cd}_3\text{P}_2$  and  $\text{Cd}_3\text{As}_2$ . To achieve this goal two important tools were used: optical and electrical transport measurements. The electrical transport measurements are reviewed in {9}, {10} and {11} while this thesis describes mainly the results of the optical measurements on  $\text{Cd}_3\text{P}_2$  and  $\text{Cd}_3\text{As}_2$ .



The organisation of this thesis is as follows: In chapter 2 some relevant instrumental information is given. Chapter 3 deals with the results of interband absorption measurements on  $\text{Cd}_3\text{P}_2$  and  $\text{Cd}_3\text{As}_2$ . The experimental proof of band structure inversion is given in this chapter. In chapter 4 the far infrared optical properties of  $\text{Cd}_3\text{P}_2$  and  $\text{Cd}_3\text{As}_2$  are described, yielding a better understanding of the plasma edge behaviour in these materials. Finally, in chapter 5 we present some considerations about recent developments concerning the band structure of our materials.

It will be seen that most sections of the various chapters consist of papers that have been published previously in different journals. All papers are presented in a chronological order linked by some elucidating text. This leads to some inconsistencies that could not be avoided. In this respect we would like to make the following remarks:

- Literature references in the papers are given at the end of each paper. The references in the linking texts are given in braces (like {i}) and listed in the section General References at the end of this thesis.
- Energies are expressed in eV as well as in  $\text{cm}^{-1}$ .
- In section 4.3. the symbol  $\gamma$  is used for the phonon damping parameter instead of  $\Gamma$  and in section 4.5. the symbol  $\Delta\epsilon$  is used for the oscillator strength instead of  $f$ .

## CHAPTER 2 EXPERIMENTAL TECHNIQUES

### 2.1. Introduction

For the optical experiments we used several experimental arrangements with the following characteristic features:

1. A high resolution single beam transmission set up for the near infrared wavelength region ( $1 < \lambda < 3 \mu\text{m}$ ).
2. A medium resolution single beam transmission set up for the near and middle infrared wavelength region ( $2 < \lambda < 15 \mu\text{m}$ ).
3. A standard double beam spectrometer for the infrared wavelength region ( $2.5 < \lambda < 50 \mu\text{m}$ ).
4. A slow scan fourier transform spectrometer for the far infrared wavelength region ( $20 < \lambda < 200 \mu\text{m}$ ).
5. A rapid scan fourier transform spectrometer with superconducting magnet for the far infrared wavelength region ( $15 < \lambda < 100 \mu\text{m}$ ).

In the next chapters the various sections give some details on the experimental techniques used in that particular part. There are, however, some experimental details we would like to treat separately in this chapter. The first topic concerns the modification of the standard double beam spectrometer for reflectivity measurements at room temperature. This system is described in section 2.2. The second topic, described in section 2.3., deals with the construction of a gas filled sample holder for infrared transmission measurements at cryogenic temperatures. Finally, in section 2.4. we give some details about the sample preparation.

## RESEARCH NOTE

### 2.2 A SPECULAR REFLECTANCE ACCESSORY FOR INFRARED SPECTROMETERS

M. J. GELTEN, A. VAN OOSTEROM and C. VAN ES

Department of Physics, Eindhoven University of Technology, Eindhoven, Netherlands

(Received 4 March 1976)

A new trend in the development of u.v.-vis and i.r. spectrometers is the design of a large sample compartment with foci of sample and reference beams in its centre instead of at the entrance slit. Consequently standard accessories like beam condensers, ATR units are not adaptable to these new optical systems and when specular reflectance measurements at small angles of incidence (less than  $20^\circ$ ) are needed and only small samples (diameter less than 10 mm) are available no suitable accessories exist. Therefore, we have designed a device for measuring the near normal incidence reflectivity of small samples on a Beckman IR 4250 spectrometer.

The principle of the device is shown in Fig. 1. The average angle of incidence on the sample  $\beta$  is given by a prism angle  $\alpha = \pi/2 + \beta$ . We chose  $\alpha = 100^\circ$  for  $\beta = 10^\circ$ . All components are mounted on a base plate which is rigidly fixed to the base of the spectrometer. The prism is made of a single block of aluminum, the two reflecting surfaces being made on a special milling machine with hydrodynamic bearings and supports

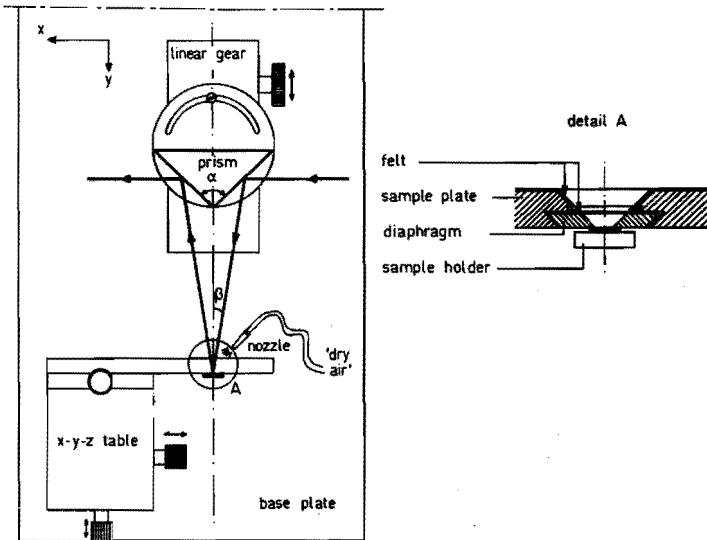


Fig. 1. Sketch of the principle of the specular reflectance accessory.

giving extremely low vibration levels and perfectly flat surfaces. The prism can be rotated about the Z-axis and moved linearly in the y-direction. Sample holders with different diaphragms for various sample diameters fit accurately in the sample plate by means of a dovetail construction. The sample plate in turn is mounted rigidly on a standard x-y-z micrometer translation stage. A complementary version of the device fitted with a calibration mirror directly behind the sample diaphragms is placed in the reference beam.

In using the device one must take care to align all components in such a way that the 100% reflectance line of the instrument remains flat within the specification. The most crucial point appears to be to avoid a step in the 100% R line at the grating change ( $650\text{ cm}^{-1}$ ). The best way to achieve this is to look at the focus points of both reference and sample beam at the entrance slit of the monochromator and to adjust the prisms and sample holders so that the spots coincide. It was found that once adjusted all reflectance curves reproduced very well even when the diaphragms in the sample and reference holders are changed and only slight readjustments with the 100% T knob of the spectrometer were needed to get an exact 100% R line. Care should also be taken that the slit width never exceeds the sample diameter, because this results in an incorrect 100% R line.

As a calibration mirror we tried optically flat machined silver and aluminum and evaporated gold, silver and aluminum on glass substrates. The best results were obtained with thick evaporated gold films giving a constant reflectivity of  $98 \pm 1\%$  in the wavelength range  $2.5\text{--}50\ \mu\text{m}$ .<sup>(1-3)</sup>

Special attention must be given to the blackening of the sample holders and sample plate. Since black surfaces absorb all incident energy, their temperature is raised and they emit radiation which causes errors. With a diaphragm diameter of 4 mm we detected more than 15% deviation from the 0% R line in the range  $20\text{--}50\ \mu\text{m}$ . This problem was overcome by blowing dry air through a nozzle against the blackened surface around the diaphragms, using part of the output of the pneumatic air dryer of the purging system of the spectrometer. The best material was found to be black felt which reflected less than 0.2% in the whole wavelength range except for a small increase up to 1.5% in the range  $40\text{--}50\ \mu\text{m}$ .

After correct adjustments it is possible to measure the near normal incidence reflectivity of samples as small as 4 mm in diameter. The deviations from linearity and 100% R line are no larger than those for the un-modified instrument. No polarisation effects were observed.

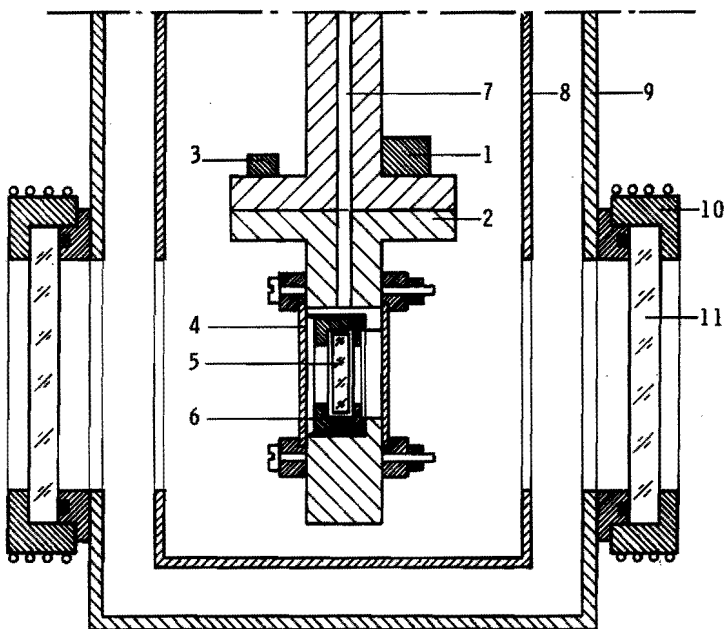
#### REFERENCES

1. BENNETT, H. I., J. M. BENNETT & E. J. ASHLEY, *J. Opt. Soc. Am.* **52**, 1245 (1962).
2. DICKSON, P. F. & M. C. JONES, *Cryogenics* **8**, 24 (1968).
3. TOULOUKIAN, Y. S. & D. P. DEWITT, *Thermal Radiative Properties of Solids*, Vol. 7. IFI-Plenum Press, New York.

### *2.3. A gas filled cryogenic sample holder for infrared transmission measurements*

In solid state spectroscopy it is often desirable to perform measurements at low temperatures. In the present study of optical properties of  $\text{Cd}_3\text{P}_2$  and  $\text{Cd}_3\text{As}_2$  it appeared even necessary to do transmission measurements at cryogenic temperatures down to liquid helium because the materials are highly degenerate. Only at low temperatures the shape of the optical absorption edge is dominated by the band structure instead of by the broadened free carrier distribution function.

At low temperatures it is very important to pay special attention to strain free mounting of the samples. A suitable way to achieve this is to mount a sample free standing in a sample holder which is cooled by some cryogenic liquid. For a good thermal contact between sample and sample holder it is necessary to use contact gas (e.g. helium). This implies, however, that for optical transmission measurements the sample holder should be closed by two vacuum tight windows transmitting radiation in the desired wavelength region. For our purpose the most interesting wavelength region ranges from several microns to several tens of microns. It is known from literature [12] that silver chloride is a suitable material for such cryogenic vacuum tight infrared transmitting windows ( $1 < \lambda < 25 \mu\text{m}$ ). Using this result we equipped a standard continuous flow cryostat (Oxford Instruments type CF 100) with a special sample holder. A schematic drawing of this sample holder is given in fig. 2.1. The outer wall of the cryostat contains KBr windows (diameter 38 mm, thickness 7 mm) heated slightly above room temperature because of their hygroscopic nature. The AgCl windows are standard commercially available windows for room temperature gas cells in infrared spectrometers (diameter 16 mm, thickness 0.3 mm). They can be mounted directly between two flat flanges because AgCl itself is sufficiently ductile. The flanges should be bolted together with at least 12 screws to achieve a homogeneous distribution of the applied force. It should be noted that AgCl is strongly corroded by all metals which are less noble than silver. Therefore the vacuum flanges should be heavily electroplated with gold and great care should be taken that not one single part of the window makes contact with other metals than gold. To our experience pure copper is a suitable flange



- |                       |                     |
|-----------------------|---------------------|
| 1. Heater             | 7. Gas filling tube |
| 2. Cold finger        | 8. Radiation shield |
| 3. Temperature sensor | 9. Outer wall       |
| 4. AgCl window        | 10. Heated flange   |
| 5. Sample             | 11. KBr window      |
| 6. Sample diaphragm   |                     |

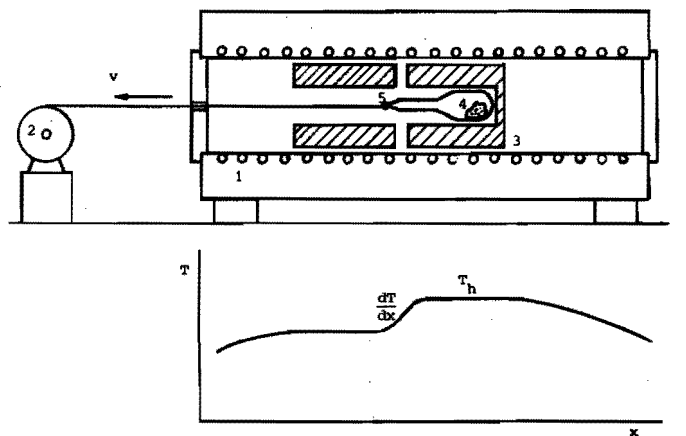
Fig. 2.1. Schematic drawing of the gas filled sample holder.

material to be gold plated to form a chemically stable system in contact with AgCl. We found for instance that AgCl reacted strongly with gold plated brass. We believe that this may be explained by the Kirkendall effect {13}. In our case the zinc from the brass diffuses more rapidly through the gold than the copper and reacts more strongly. It is our experience that infrared transmitting AgCl windows mounted between gold plated copper flanges remain vacuum tight after several temperature cycles between 4.2 K and 300 K. Even after a sample change a demounted window can be used again.

## 2.4. Sample preparation

Polycrystalline  $\text{Cd}_3\text{As}_2$  is prepared by weighting stoichiometric quantities of high purity cadmium and arsenic in a silica ampoule which has been carbon coated by pyrolysis of benzene vapour. The ampoule is evacuated, sealed off and placed into a vertical furnace. The ampoule is slowly heated (in 24 hours from room temperature to  $775^\circ\text{C}$ ) in order to prevent a violent chemical reaction. The melt is kept at  $775^\circ\text{C}$  during 8 hours and cooled down to room temperature in 2 hours. After this procedure an ingot of polycrystalline  $\text{Cd}_3\text{As}_2$  is formed which can be powdered to serve as starting material for crystal growth.

As starting material for the growth of single crystals of  $\text{Cd}_3\text{P}_2$  we used commercially available high purity polycrystalline lumps (CERAC PURE, Milwaukee, Wisconsin, 53233, USA). All starting materials were regularly checked for composition and purity by both wet chemical analysis and Debye-Scherrer X-ray powder diffraction measurements.



- |                     |                      |
|---------------------|----------------------|
| 1. Furnace          | 4. Starting material |
| 2. Motor drive      | 5. Single crystal    |
| 3. Aluminium blocks |                      |

Fig. 2.2. Experimental set up for crystal growth

Single crystals of  $\text{Cd}_3\text{As}_2$  are grown by a modified vapour transport method [14]. Approximately 6 grams of starting material are put into a specially shaped silica ampoule with a very sharp point and a total length of 15 cm (see fig. 2.2).

The starting material is kept at a constant temperature  $T_h$  of 560 °C and the point of the ampoule is pulled slowly through a small temperature gradient. Typical values are a velocity  $v = 1$  mm/day and a temperature gradient  $dT/dx = 1$  °C/cm. After 3 weeks a single crystal-line ingot is formed with a diameter in the order of 6 mm and a length of approximately 30 mm.

$\text{Cd}_3\text{P}_2$  single crystals are grown in a similar way. The crystallinity of all samples is checked by von Laue X-ray diffraction measurements. The further preparation of samples for optical measurements is described in the relevant papers.



3.1. Band structure inversion

In the early days of interest in the study of II-V compounds some fifteen years ago, it became clear that the electronic properties of  $\text{Cd}_3(\text{As}_x\text{P}_{1-x})_2$  showed strong resemblance to those of the famous system  $\text{Hg}_x\text{Cd}_{1-x}\text{Te}$  ( $0 \leq x \leq 1$ ). Preliminary (magneto) optical measurements suggested that the system  $\text{Cd}_3(\text{As}_x\text{P}_{1-x})_2$  would show the interesting phenomenon of band structure inversion [15,16] in analogy with  $\text{Hg}_x\text{Cd}_{1-x}\text{Te}$ . A schematic illustration of this phenomenon is given in fig. 3.1.

$\text{CdTe}$  has a band structure similar to the one of  $\text{InSb}$  [17]. A Kane like conduction band  $c$  of  $\Gamma_6$  symmetry is separated from two valence bands  $v_1$  and  $v_2$  of  $\Gamma_8$  symmetry. The valence band  $v_2$  is of the Kane type and  $v_1$  is parabolic, degenerate with  $v_2$  at the  $\Gamma$ -point. The bands show a normal open bandgap  $E_g = E(\Gamma_6) - E(\Gamma_8)$ . A third valence band  $v_3$  of  $\Gamma_7$  symmetry is located below  $v_1$  and  $v_2$  with a separation energy equal to the spinorbit splitting energy  $\Delta$ . Because of relativistic interactions in  $\text{HgTe}$  the symmetries of bands  $c$  and  $v_2$  are interchanged: the conduc-

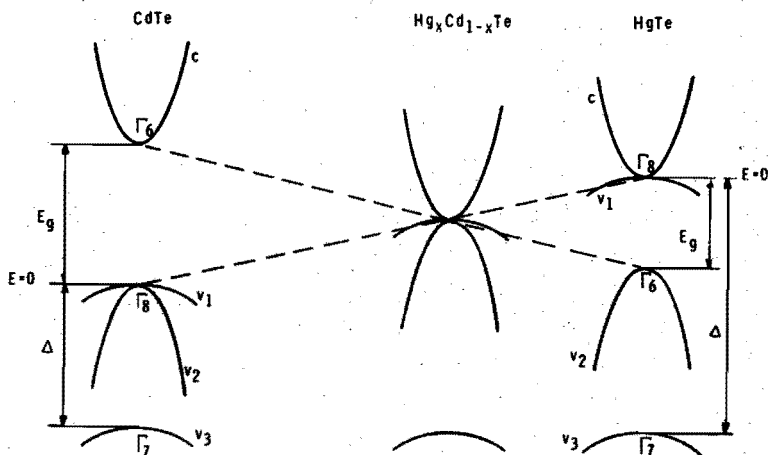


Fig. 3.1.  $E$ - $k$  plots illustrating the principle of the band structure inversion in the system  $\text{Hg}_x\text{Cd}_{1-x}\text{Te}$ .

tion band has  $\Gamma_8$  symmetry whereas the valence band  $v_2$  now has  $\Gamma_6$  symmetry. Both these bands remain of the Kane type. The parabolic band  $v_1$  is not affected by these interactions and remains parabolic with  $\Gamma_8$  symmetry. The degeneracy now occurs with the  $\Gamma_8$  conduction band. The split off band  $v_3$  is not affected by the interaction either. The band-gap  $E_g = E(\Gamma_6) - E(\Gamma_8)$  is now a negative parameter because of the band inversion. If mixed crystals of CdTe and HgTe are considered we get a continuous change from the normal to the inverted situation with increasing mercury content (see fig. 3.1.). It should be noted that the thermal bandgap in the  $\text{Hg}_x\text{Cd}_{1-x}\text{Te}$  system is zero above a certain value of  $x$  corresponding to  $E_g = 0$ .

The preliminary measurements mentioned earlier indicated that  $\text{Cd}_3\text{P}_2$  had a normal band structure and  $\text{Cd}_3\text{As}_2$  an inverted one. Because more details were needed for conclusive evidence the main purposes of our research were to prove the band structure inversion of the system  $\text{Cd}_3(\text{As}_x\text{P}_{1-x})_2$  and to determine more qualitative and quantitative details of the electronic properties.

### 3.2. Band models of $\text{Cd}_3\text{P}_2$ and $\text{Cd}_3\text{As}_2$

A suitable description of the band models of both the normal and inverted structure is given by Kane [17], Zawadzki [18] and Szymanska [19] using k.p approximation. The  $E(k)$  relations for the four bands in the region near  $k = 0$  can be determined from the following set of secular equations.

For the bands  $c$ ,  $v_2$  and  $v_3$ :

$$E'(E' + \Delta)(E' - E_g) - k^2 P^2 (E' + \frac{2}{3} \Delta) = 0 \quad (3.1)$$

For the band  $v_1$ :

$$E' = 0 \quad (3.2)$$

where  $E' = E - \hbar^2 k^2 / 2m_0$ . Here  $E_g = E(\Gamma_6) - E(\Gamma_8)$ ,  $\Delta$  is the spin orbit splitting energy,  $P$  is the Kane matrix element and  $m_0$  is the free

electron mass. In this simple k.p model the band  $v_1$  is formally given by  $E' = 0$  but it is well established {17} that due to higher order corrections this simple solution should be replaced by a parabolic heavy hole band with effective mass  $m_{v_1}$  given by

$$E_{v_1} = -\frac{\hbar^2 k^2}{2m_{v_1}} \quad (3.3)$$

It should be emphasized that this band model is valid only for cubic crystals with isotropic band properties. Because of the tetragonal crystal structure of  $Cd_3P_2$  and  $Cd_3As_2$ , this band model should be modified in principle. However, the deviations from a cubic structure are so small that in a first approximation the band structure may be considered to be isotropic {20,21}. It appears that tetragonal corrections near the bandgap in the centre of the Brillouin zone only give rise to slight modification {22-25} especially in the case of  $Cd_3P_2$ . Besides it was known from transport measurements that anisotropy effects only play a minor role in  $Cd_3P_2$  {11} and therefore it seems a reasonable assumption that the band structure of  $Cd_3P_2$  can be described by the relations given in eqs. (3.1) and (3.3). A detailed analysis of the band structure of  $Cd_3P_2$  is presented in section 3.3.

The situation in  $Cd_3As_2$  is slightly different. Like  $Cd_3P_2$ ,  $Cd_3As_2$  showed no pronounced anisotropy effects but there were strong indications from transport measurements (see e.g. Appendix) that the valence band  $v_1$  of this material could not be described correctly by eq. (3.3). Moreover, Aubin {26} and Caron et al. {27} found from a number of transport data taken from the literature a strong indication that the valence band  $v_1$  could not be parabolic with its maximum at  $k = 0$ . They proposed an isotropic valence band with its maximum shifted from the  $\Gamma$ -point. In analogy with Harman {28} we introduced for the  $E(k)$  relation of the heavy hole band in  $Cd_3As_2$  on a phenomenological basis the following expression:

$$E_{v_1} = \left(\frac{k}{k_1}\right)^4 (E_R - E_T) - 2\left(\frac{k}{k_1}\right)^2 (E_R - E_T) + E_R \quad (3.4)$$

Here  $k_1$  is the wave vector of the maximum energy  $E_T$  and  $E_R$  is the residual gap at  $k = 0$  ( $\Gamma$ -point). The other bands are still supposed to

be described adequately by eq. (3.1).

All considerations mentioned above give rise to band structure models of  $\text{Cd}_3\text{P}_2$  and  $\text{Cd}_3\text{As}_2$  as indicated in fig. 3.2. Notice from this figure that the thermal energy gap  $E_T$  is no longer necessarily equal to zero. Also indicated in this figure is the approximate position of the fermi level which indicates that the interband absorption curves will show a large Burstein-Moss shift [29]. More details on the band structure of  $\text{Cd}_3\text{As}_2$  are presented in section 3.4.

After completion of this work new information about the anisotropy effects became available. Some comments on these recent developments are given in chapter 5.

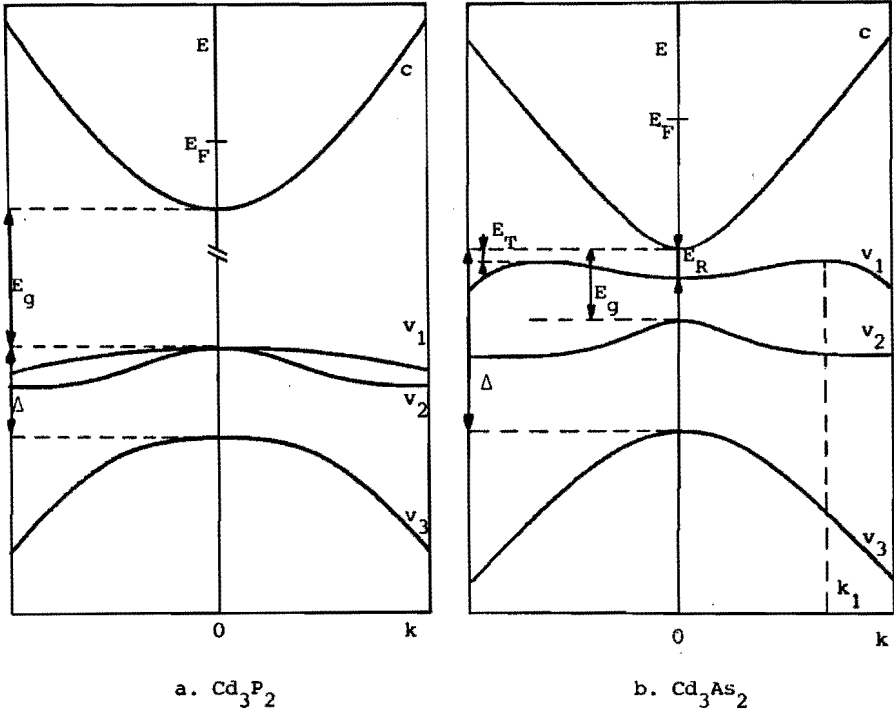


Fig. 3.2. Band structure models of  $\text{Cd}_3\text{P}_2$  and  $\text{Cd}_3\text{As}_2$

### 3.3

## Optical properties of $\text{Cd}_3\text{P}_2$

M J Gelten, A van Lieshout, C van Es and F A P Blom

Department of Physics, Eindhoven University of Technology, Eindhoven, Netherlands

Received 18 July 1977, in final form 25 August 1977

**Abstract.** Absorption measurements at room temperature and 90 K on single crystals of  $\text{Cd}_3\text{P}_2$  are given. Free carrier absorption can be interpreted in the simple classical model while the interband absorption is interpreted in the Kane band model using exact solutions of the secular equation and without neglecting the free electron term. The best fit of the theory to experimental points is found for  $E_g(300\text{ K}) = 0.53\text{ eV}$ ,  $E_g(90\text{ K}) = 0.56\text{ eV}$ ,  $P = 6.7 \times 10^{-10}\text{ eVm}$ ,  $\Delta = 0.1\text{ eV}$  and  $m_{v_1} = 0.5 m_0$ . Some results of thermomagnetic transport properties are discussed in the same model.

### 1. Introduction

In the past few years some progress has been made in the determination of the shape of the conduction band of  $\text{Cd}_3\text{P}_2$  from measurements of thermomagnetic transport properties (Blom and Burg 1977, Radautsan *et al* 1974). These measurements indicate a non-parabolic conduction band which can be described in a simplified Kane model with approximate values of the band parameters of 0.5 eV for the band gap and  $7 \times 10^{-10}\text{ eVm}$  for the Kane matrix element  $P$ . Concerning optical properties Haacke and Castellion (1964) did some preliminary measurements of interband absorption followed by more extensive measurements by Radoff and Bishop (1972 and 1973). Also from photoconductivity and photoluminescence measurements (Bishop *et al* 1969) and interband magneto absorption data (Wagner *et al* 1970) a value of the band gap could be derived. All these optical measurements show that the band gap is approximately 0.5 eV, but in general a satisfactory interpretation in terms of a particular band model could not be given. In this paper we present absorption measurements on single crystals of  $\text{Cd}_3\text{P}_2$  at room temperature and low temperatures which are interpreted in the exact non-parabolic Kane model. Moreover, it appears that earlier reports as well as some new results on thermomagnetic transport properties can be explained in the same model.

### 2. Sample preparation

Single crystals of degenerate n-type  $\text{Cd}_3\text{P}_2$  were grown by a sublimation technique described by Blom and Burg (1977). For optical experiments the large single crystals were cut with a multi-wire saw into many platelets with a thickness of about 800  $\mu\text{m}$  and a diameter of approximately 5 mm. These platelets were ground on both sides and the electron concentration  $N$  and the mobility  $\mu$  were measured at room temperature

by means of the four point Van der Pauw method (Van der Pauw 1958). Contacts were soldered on small electrolytically deposited copper spots as described by Zdanowicz and Wojakowski (1965). Afterwards the samples were ground to the desired thickness and polished flat and plane-parallel with  $1\ \mu\text{m}$  and  $\frac{1}{4}\ \mu\text{m}$  diamond paste. The flatness of the sample surfaces was determined by an interference method with an optically flat glass plate. Very thin samples (thickness less than  $50\ \mu\text{m}$ ) were glued on a sapphire substrate before polishing. As a glue we used cellulose caprate (cellulose tridecanoate, manufactured by Kodak Ltd) or Loctite adhesive 312 because these materials which could be produced in a very thin layer, of only a few microns thick, had a good infrared transmission and could be cycled to cryogenic temperatures. In order to get samples with lower electron concentration some crystals were compensated by doping with copper which acts as an acceptor in  $\text{Cd}_3\text{P}_2$  (Radoff and Bishop 1973). For this purpose one of the end faces of a cylindrical bar was electrolytically covered with an amount of copper equal to  $N_a V$  where  $N_a$  is the desired concentration if this copper were homogeneously distributed into the sample with volume  $V$ . The copper was diffused into the sample by heating it in an evacuated ampoule to  $550^\circ\text{C}$  during 96 h. To determine the penetration depth the bar was cut into slices and for every slice the electron concentration and mobility were measured. The results are given in figure 1 as a function of distance from the copper covered end face of the crystal. From this figure it can be seen that the Cu atoms diffuse into the sample to a depth of 5–10 mm. Therefore we may assume the platelets of  $800\ \mu\text{m}$  thickness to be homogeneously doped. For the actual measurements we mostly took one platelet of as-grown material, covered it completely with copper and applied the heat treatment.

### 3. Experimental methods

The optical interband absorption measurements were performed on a standard single beam system consisting of a quartz halogenlamp as a light source, a 400 Hz chopper

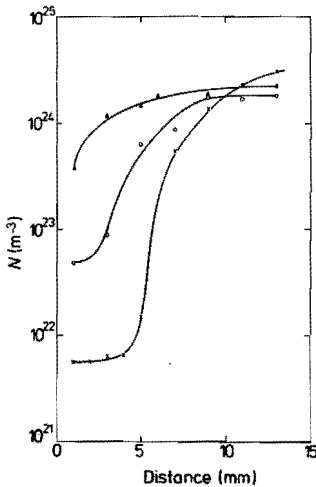


Figure 1. Electron concentration  $N$  as a function of distance from end face for various copper concentrations  $N_a$ :  $1 \times 10^{24}\ \text{m}^{-3}$  ( $\Delta$ );  $2 \times 10^{24}\ \text{m}^{-3}$  ( $\circ$ );  $5 \times 10^{24}\ \text{m}^{-3}$  ( $\times$ ).

and an InSb (77 K) photovoltaic detector with phase sensitive amplifier. As the absorption coefficient of  $Cd_3P_2$  rises very steeply at the band edge (Haacke and Castellion 1964) we used a grating monochromator (Hilger and Watts monospek 1000) equipped with a  $2 \mu\text{m}$  blazed grating resulting in a spectral resolution of  $0.003 \mu\text{m}$  for 1 mm slit width. The samples (or substrates) were mounted on the cold finger of a liquid helium cryostat. The temperature of the samples was measured with thin thermocouples. The free carrier absorption beyond the near infrared was measured on a Beckman IR 4250 double beam spectrometer. For measurements of the reflectivity of thick samples this instrument was fitted with a specular reflectance accessory described elsewhere (Gelten *et al* 1976). The absorption coefficient  $K$  of freely mounted samples was determined from the transmission  $T$  using (as  $Kd$  always  $> 1$ ):

$$I/I_0 = T = (1 - R)^2 \exp(-Kd) \quad (1)$$

where  $R$  is the reflectivity of the sample and  $d$  its thickness. For samples on a substrate,  $K$  was determined by assuming that the refractive indices of sapphire and glue are equal, so that we may use:

$$T = (1 - R_0)(1 - R')(1 - R) \exp(-Kd). \quad (2)$$

Here  $R_0$  is the reflectivity of sapphire calculated from its refractive index  $n_0$  and  $R'$  is the reflectivity of the glue-sample interface given by  $R' = (n - n_0)^2 / (n + n_0)^2$  where  $n$  is the refractive index of  $Cd_3P_2$ .

#### 4. Theory

$Cd_3P_2$  has a tetragonal crystal structure which differs only slightly from a cubic one (Lin-Chung 1971). The conduction band is Kane-like and therefore we assume that the band structure of  $Cd_3P_2$  is similar to that of InSb. Neglecting the influence of higher bands we have the following set of secular equations (Kane 1957)

$$E' = 0, \quad (3a)$$

$$E'(E' - Eg)(E' + \Delta) - k^2 P^2 (E' + \frac{2}{3}\Delta) = 0, \quad (3b)$$

where  $E' = E - \hbar^2 k^2 / 2m_0$ . (3c)

Here  $\Delta$  is the spin-orbit splitting energy,  $Eg$  the band gap,  $P$  the Kane matrix element and  $m_0$  the free electron mass. For  $Cd_3P_2$  we may not make the assumption  $\Delta \gg Eg$  like in the case of InSb. For a binary compound Braunstein and Kane (1962) give the relation:

$$\Delta = A[x\Delta_1 + (1 - x)\Delta_2], \quad (4)$$

where  $\Delta_1$  and  $\Delta_2$  are the atomic spin-orbit splittings of the atom 1 and 2 and  $x$  is a parameter related to the ionicity of the compound.  $A$  is a constant which may be taken as 1.45, being the exact value of  $A$  for germanium. Braunstein and Kane (1962) find a value of  $x = 0.35$  for III-V compounds. Cardona (1969) uses equation (4) with  $x = 0.2$  for II-VI compounds and  $x = 0$  for I-VII compounds. For  $Cd_3P_2$  Radautsan *et al* (1974) use  $x = 0.35$  and obtain  $\Delta = 0.15 \text{ eV}$  while Zivitz and Stevenson (1974) obtain  $\Delta = 0.067 \text{ eV}$ . Using (4) Sobolev and Syrbu (1974) obtain  $\Delta = 0.15 \text{ eV}$  starting from atomic Cd and P and  $0.2 \text{ eV}$  ( $0.52 \text{ eV}$ ) starting from singly (doubly) ionised Cd and P respectively. The above arguments indicate that a reasonable value of  $\Delta$  is  $0.1 \text{ eV}$  which

means that for  $\text{Cd}_3\text{P}_2$   $\Delta \approx E_g$  or even  $\Delta \ll E_g$ . This makes it necessary to solve equation (3b) exactly. In that case it appears that for small values of  $\Delta$  the bands are much less curved than in the Kane approximation so that the free electron term  $\hbar^2 k^2/2m_0$  can no longer be neglected.

According to Kane (1957) equation (3a) gives rise to the parabolic heavy hole band  $v_1$  with effective mass  $m_{v_1}$ . Equation (3b) can be solved numerically. A handy way to do this with a pocket calculator is given in the Handbook of Chemistry and Physics (1962).

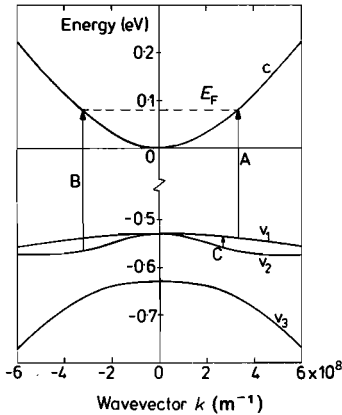


Figure 2. Energy bands of  $\text{Cd}_3\text{P}_2$  for  $E_g = 0.53$  eV,  $\Delta = 0.1$  eV,  $P = 6.7 \times 10^{-10}$  eV m and  $m_{v_1} = 0.5 m_0$ .

In figure 2 the band structure of  $\text{Cd}_3\text{P}_2$  is given for a set of relevant parameters. It can be seen from this figure that there are three possible direct interband transitions called *A*, *B* and *C*. The absorption coefficient  $K_{ij}$  for each transition from band *i* to band *j* is given by:

$$K_{ij} = (\pi e^2 / \epsilon_0 n c m_0^2 \omega) M_{ij}^2 \rho_{ij} f_{ij} \quad (5)$$

Here  $\omega$  is the photon frequency and  $\epsilon_0 = 8.85 \times 10^{-12}$  ASV $^{-1}$ m $^{-1}$ .  $M_{ij}$  and  $\rho_{ij}$  are the momentum matrix element and the joint density of states between band *i* and *j* respectively. Because  $\text{Cd}_3\text{P}_2$  is an n-type degenerate material with a large Burstein–Moss shift the factor  $f_{ij}$  has been introduced taking into account the distribution of unoccupied states in band *j* and the occupied states in band *i*. As all energies involved in the absorption processes are much larger than  $k_0 T$  we may assume that the lowest band *i* is completely occupied and we need only take into account the unoccupancy of the highest band *j*.

In this case  $f_{ij}$  is simply related to the Fermi–Dirac distribution of band *j*:

$$f_{ij} = 1 - f_j,$$

with

$$f_j = \{1 + \exp [(E_j - E_F)/k_0 T]\}^{-1} \quad (6)$$



For our isotropic bands  $\rho_{ij}$  is given by :

$$\rho_{ij} = k^2 \left/ \left( 2\pi^2 \left| \frac{dE_j}{dk} - \frac{dE_i}{dk} \right|_{(E_j - E_i = \hbar\omega)} \right) \right. \quad (7)$$

$dE/dk$  can be determined by differentiating the secular equation (3b) and using (3c) :

$$\frac{dE}{dk} = \frac{\hbar^2 k}{m_0} + \frac{2kP^2(E' + \frac{2}{3}\Delta)}{(E' - E_g)(E' + \Delta) + E'(E' + \Delta) + E'(E' - E_g) - k^2P^2} \quad (8)$$

According to Kane (1957) the interband matrix element  $M_{ij}$  is given by

$$M_{ij}^2 = (2m_0^2P^2/3\hbar^2) [(a_jc_i + c_ja_i)^2 + (a_jb_i - b_ja_i)^2] \quad (9)$$

where the coefficients  $a$ ,  $b$  and  $c$  are given by :

$$\begin{aligned} a_i &= kP(E'_i + 2\Delta/3)/N_i \\ b_i &= (\sqrt{2\Delta/3})(E'_i - E_g)/N_i \\ c_i &= (E'_i - E_g)(E'_i + 2\Delta/3)/N_i \quad \text{for } i = c, v_2, v_3, \end{aligned} \quad (10)$$

$N_i$  is a normalising factor so that  $a_i^2 + b_i^2 + c_i^2 = 1$ . For the heavy hole band  $v_1$  we use  $a_{v_1} = c_{v_1} = 0$ ,  $b_{v_1} = 1$ . Now for a given value of  $k$  the band energies  $E$  or  $E'$  can be calculated and substituted into equation (6), (7) and (9). The next step is to determine for this particular  $k$  value the three (different) photon energies involved in the transitions A, B and C using the relation

$$\hbar\omega_{ij} = E_j(k) - E_i(k). \quad (11)$$

By stepping the value of  $k$ , three curves of  $K_{ij}(\hbar\omega_{ij})$  can be calculated in this way. The total interband absorption coefficient  $K$  can be determined graphically using :

$$K = K_A + K_B + K_C. \quad (12)$$

As the temperature and the refractive index are known, we have as parameters in the calculation : the matrix element  $P$ , the band gap  $E_g$ , the spin-orbit splitting  $\Delta$ , the heavy hole effective mass  $m_{v_1}$  and the Fermi energy  $E_F$ . Only for large electron concentrations in the high-degeneracy limit we may calculate the wavevector  $k_F$  at the Fermi level from :

$$k_F = (3\pi^2N)^{1/3}. \quad (13)$$

In this case the Fermi energy can be simply calculated from the secular equation. However, for arbitrary degeneracy the Fermi energy must be calculated from the electron concentration using :

$$N = (1/3\pi^2) (k_0T/P)^3 {}^0\mathcal{X}_0^{3/2} \quad (14)$$

where  ${}^0\mathcal{X}_0^{3/2}$  is an integral of the type  ${}^n\mathcal{X}_k^m$ . These integrals are generalised  ${}^n\mathcal{L}_k^m$  integrals (Zawadski 1974) by fully taking into account the exact solutions of the secular equation as well as the free electron term  $\hbar^2k^2/2m_0$ . The above  $\mathcal{X}$  integral is in fact the same as the one introduced by Ermolovich and Kravchuk (1976).

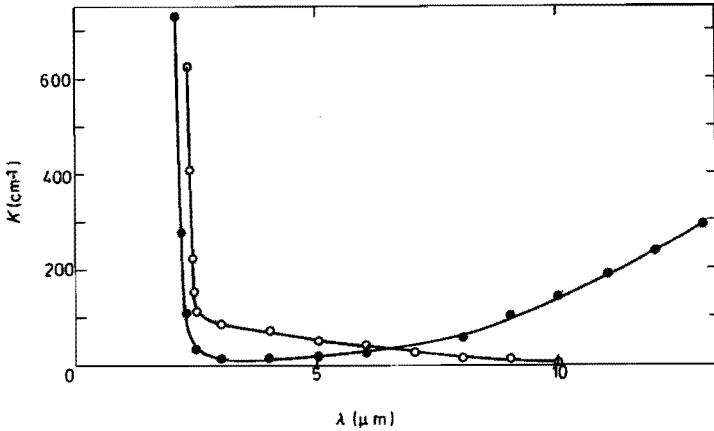


Figure 3. Total absorption coefficient  $K$  at room temperature of as-grown (●) and copper-doped (○)  $\text{Cd}_3\text{P}_2$  as a function of wavelength  $\lambda$ .

## 5. Results and discussion

A typical example of a complete absorption curve of as-grown and Cu-doped  $\text{Cd}_3\text{P}_2$  is given in figure 3. In this figure we notice a very steep band edge for both samples. The as-grown sample with high electron concentration gives rise to marked free carrier absorption at larger wavelengths which is completely absent in the Cu-doped samples, because of their low electron concentration. However, the Cu-doped samples show always a very broad shoulder in the absorption coefficient at wavelengths just longer than the edge. A similar effect was observed by Radoff and Bishop (1973) and its origin is not quite clear yet. Some of the samples showed interference maxima and minima in the transmission due to multiple reflection. Using the relation  $2nd = m\lambda$  the average value of the refractive index could be determined and appeared to be  $n = 3.6 \pm 0.2$  in the wavelength range from 2–10  $\mu\text{m}$ . This result is in good agreement with the measured reflectivity having a constant value of  $33 \pm 2\%$  in this wavelength range. Furthermore  $n$  appeared independent of the concentration of the copper dope.

The long wavelength absorption coefficient can always be described by the empirical formula:

$$K = a\lambda^2 + b. \quad (15)$$

The factor  $a$  can be interpreted in the well-known Drude theory neglecting collision effects ( $\omega\tau \gg 1$ ) and is given by (Zawadzki 1974)  $a = (e^3 N / 4\pi^2 c^3 n \epsilon_0) (1/m^{*2} \mu)$ . The constant  $b$  which has usually a small value is probably caused by small errors in the determination of the light intensities  $I$  and  $I_0$  or a small light scattering factor of the sample. An example of the free carrier absorption plotted against  $\lambda^2$  is given in figure 4. If we make the simplifying assumption  $\langle 1/m^{*2} \mu \rangle = 1/\langle m^* \rangle^2 / \langle \mu \rangle$  we determine for this sample a value of  $m^* = 0.06 m_0$  at 300 K and  $m^* = 0.05 m_0$  at 90 K which is in good agreement with values found in the literature for the same electron concentration. A more detailed analysis of the effective mass against electron concentration could not be done due to lack of samples with a sufficiently wide range of carrier concentration. The results of interband absorption measurements on as-grown

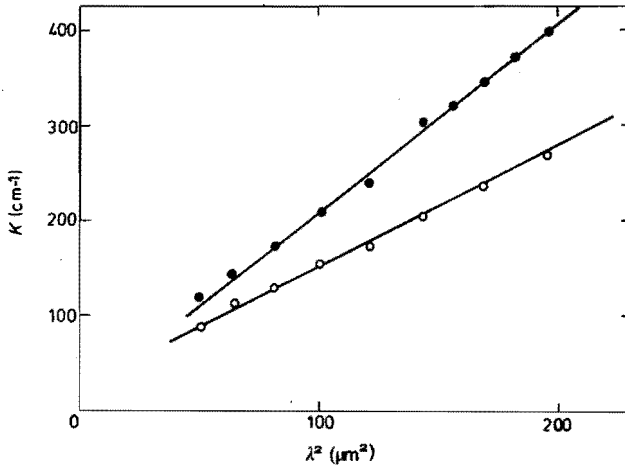


Figure 4. Free carrier absorption of  $Cd_3P_2$  against  $\lambda^2$  for two different temperatures (●) 300 K, (○) 90 K. ( $N = 1.2 \times 10^{24} \text{ m}^{-3}$ ).

and Cu-doped samples are shown in figures 5 and 6 respectively. The absorption curves have been determined up to high values of  $K$  and free carrier contribution can be neglected in this wavelength range. Also shown in figures 5 and 6 are theoretical curves, obtained in the following way. We started to fit the absorption curve of an as-grown sample at room temperature because these samples are strain free and their electron concentration is known. From  $N$  the Fermi energy can be calculated using equation (14). A typical result is shown in figure 7 where the Fermi energy  $\epsilon_F$  above the bottom of the conduction band is plotted against the electron concentration for a relevant set of band parameters ( $E_g$ ,  $P$ ,  $\Delta$ ) and for various temperatures. With the same set of parameters

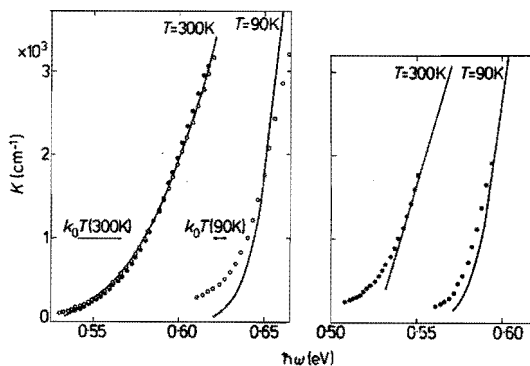
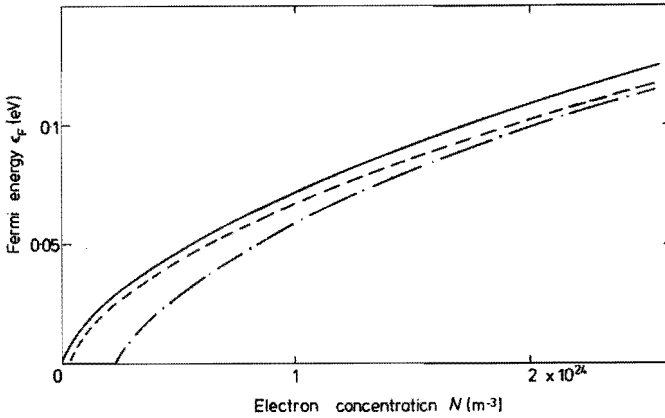


Figure 5. Interband absorption coefficient of as-grown  $Cd_3P_2$  for two different samples with the same electron concentration ( $N = 1.3 \times 10^{24} \text{ m}^{-3}$ ). Full curves are theoretical results. (○) P3-9, (●) Px-1.

Figure 6. Interband absorption coefficient of copper doped  $Cd_3P_2$ . Full curves are theoretical results. (●) P9-29.



**Figure 7.** Calculated Fermi energy  $\epsilon_F$  above the bottom of the conduction band against electron concentration for different temperatures: full curve, 4.2 K; dashed curve, 90 K; chain curve, 300 K. ( $E_g$ ,<sub>300</sub> = 0.53 eV,  $E_g$ ,<sub>90</sub> =  $E_g$ ,<sub>4.2</sub> = 0.56 eV,  $\Delta$  = 0.1 eV,  $P$  =  $6.7 \times 10^{-10}$  eV m).

and an additional value of  $m_{v1}$  an absorption curve can be calculated. The best fit at room temperature is obtained for  $E_g = 0.53$  eV,  $\Delta = 0.1$  eV,  $P = 6.7 \times 10^{-10}$  eV m and  $m_{v1} = 0.5 m_0$ . The next step is to fit the results at low temperature (90 K). We assumed  $P$ ,  $\Delta$ ,  $m_{v1}$  and  $n$  independent of temperature. As the curves of figure 7 change negligibly with small changes in  $E_g$ , and the electron concentration is constant as a function of temperature, the fermi energy at 90 K can be read directly from figure 7. By changing only  $E_g$  a best fit at 90 K can be obtained for  $E_g = 0.56$  eV. The electron concentration measurements on Cu-doped samples might be somewhat in error because we do not know the influence of the Cu-dope on the conduction mechanism. Therefore we have taken the parameter set ( $E_g$ ,  $P$ ,  $\Delta$ ,  $m_{v1}$ ) of the as-grown sample at 300 K and used  $\epsilon_F$  as a fitting parameter for the room temperature absorption curve of Cu-doped  $\text{Cd}_3\text{P}_2$ . The best fit is shown in figure 6. Once  $\epsilon_F$  at 300 K is known, the electron concentration can be read from figure 7, which in turn gives directly  $\epsilon_F$  at 90 K. Now all parameters for the Cu-doped  $\text{Cd}_3\text{P}_2$  are fixed and the absorption curve calculated without any fitting is given in figure 6. In an earlier paper (Blom and Burg 1977) some thermomagnetic transport properties of  $\text{Cd}_3\text{P}_2$  were reported. The results, i.e., the dependence of the zero-field Seebeck coefficient on electron concentration and the reversal of sign of the transverse Nernst effect at a certain electron concentration, could be quantitatively well described by a two-band Kane-model with  $E_g = 0.50$  eV,  $m_g^* = 0.040 m_0$ , and a scattering parameter  $r = -1$ . In the mean time we succeeded in growing samples with higher electron concentration than those considered in that study. Of these new samples we studied particularly the transverse Nernst effect in order to confirm experimentally the 'saturation' of the normalised zero-field transverse Nernst coefficient for high concentrations, as predicted by theory. See figure 8 in the paper by Blom and Burg (1977). We also calculated the transport coefficients given by equations (8)–(11) of that paper for the three-band model by replacing the  $\mathcal{L}$  by the  $\mathcal{N}$  integrals with the appropriate indices. Adopting the values of the band gap and of its temperature dependence obtained from the optical measurements, we found an even better fit to both the older and newer experimental results for temperature independent value of  $P$  and  $\Delta$  of  $6.7 \times 10^{-10}$  eV m and 0.10 eV,

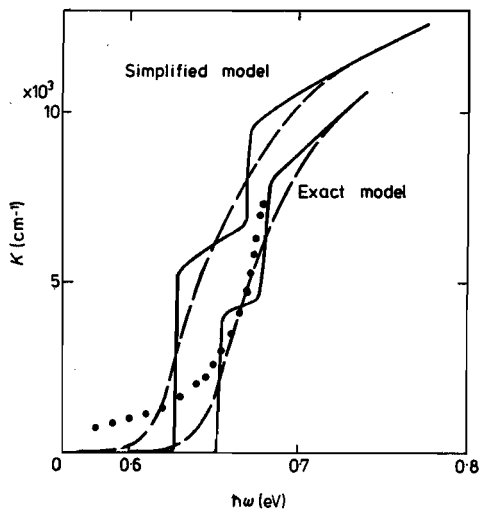


Figure 8. Calculated absorption curves including transitions A and B for both the exact ( $\Delta = 0.1$  eV) and simplified ( $\Delta = \infty$ ) band models. Full curves are for  $T = 4.2$  K, dashed curves for  $T = 90$  K. ( $E_{g,90} = E_{g,4.2} = 0.56$  eV,  $P = 6.7 \times 10^{-10}$  eVm,  $m_{v_1} = 0.5 m_0$ ,  $N = 1.3 \times 10^{24} \text{ m}^{-3}$ ). Dots are measured points of a very thin sample, measured at liquid helium temperature.

respectively. The scattering parameter was again taken as  $r = -1$ . The resulting bottom-of-the-band masses at 90 K and 300 K are  $0.047 m_0$  and  $0.045 m_0$  respectively.

In order to get insight into the accuracy of the values of the determined parameters we generated a large number of theoretical curves for wide ranges of all parameters. Roughly spoken it turned out that changes in  $E_g$  and  $\epsilon_F$  shift the curves along the energy axis while changes in  $P$  and  $m_{v_1}$  influence mainly the steepness of the curves. It is obvious that deviations due to changes of one parameter can be partly compensated by changing another parameter. Moreover, we have experimental errors in the determined values of the refractive index ( $n = 3.6 \pm 0.2$ ) and in the electron concentration of approximately 10%, determined by the finite area of the electrical contacts (van der Pauw 1958). Note for instance that an error of 10% in  $N$  gives rise to an error of 0.005 eV in  $\epsilon_F$ . Considering all these data we arrive at the set of band parameters given in table 1 for 300 K and 90 K.

Table 1. Values of the best fit band parameters of  $\text{Cd}_3\text{P}_2$  at 300 K and 90 K.

	300 K	90 K
$E_g$ (eV)	$0.53 \pm 0.025$	$0.56 \pm 0.025$
$\Delta$ (eV)	0.1	0.1
$P$ (eVm)	$6.7 \pm 0.5 \times 10^{-10}$	$6.7 \pm 0.5 \times 10^{-10}$
$m_{v_1}$ ( $m_0$ )	$0.5 \pm 0.1$	$0.5 \pm 0.1$
$m_e^*$ ( $m_0$ )	$0.045 \pm 0.005$	$0.047 \pm 0.005$

From figures 5 and 6 we notice some deviation of the experimental points from the theoretical curves at the tail. For the measurements at 90 K this might be due to strain in the samples which is an inevitable consequence of making a good thermal contact, while for the Cu-doped samples the broad absorption shoulder mentioned earlier might be of influence here.

Up to now we only needed transition A (figure 2) in the calculations because transition B has its onset at higher energies and the values of  $K$  due to transition C can be neglected in the whole range of energies. If we consider the absorption curve up to very high values of  $K$  we might see the influence of transition B analogous to the measurements on InSb by Gobeli and Fan (1960). In figure 8 some theoretical absorption curves are given for different temperatures including transitions A and B. In this figure are also given the curves calculated from the simplified quadratic Kane equation for bands c and  $v_2(\Delta = \infty)$ :

$$E_{c,v_2} = \frac{1}{2}E_g \pm \frac{1}{2}(E_g^2 + \frac{8}{3}P^2k^2)^{1/2}. \quad (16)$$

For low temperatures we see a marked step in  $K(\hbar\omega)$  at the energy where transition B sets in. The width of the step is noticeable in the model with the simplified solution but drops by more than factor of two in the model using the exact solution. This can be explained easily by remembering that the valence bands in the exact model are much flatter than in the simple Kane model. We have prepared very thin samples of approximately 10  $\mu\text{m}$  thickness and measured the absorption curve up to very high values of  $K$ . The results are shown in figure 8. It should be emphasised that the quality of these samples was poor which made it impossible to measure  $N$ . The samples were not plane-parallel and only an average value of  $d$  could be determined, leading to inaccurate values of  $K$  and no exact fitting was possible. However, the shape of the curves is correct and indicates no detectable steps. This leads to an additional argument for the use of the model with the exact solutions of the secular equation.

## 6. Conclusions

In conclusion we can say that both optical and thermomagnetic transport measurements on  $\text{Cd}_3\text{P}_2$  can be explained very well in the exact Kane band model including the free electron term. At 300 K and 90 K we find values of  $E_g$  of 0.53 eV and 0.56 eV respectively. For the other band parameters we find  $\Delta = 0.1$  eV,  $P = 6.7 \times 10^{-10}$  eVm and  $m_{v_1} = 0.5 m_0$ , independent of temperature. Additional measurements of the free electron absorption and interpretation in terms of the effective mass might give additional information to support these values.

## Acknowledgment

We greatly appreciate the assistance of Mr P A M Nouwens for growing the crystals and Dr W Batenburg for calculating many  $\mathcal{K}$  integrals. We are also indebted to Professor M J Steenland for careful reading of the manuscript.

**References**

- Bishop S G, Moore W J and Swiggard E M 1969 *Proc. 3rd Int. Conf. Photoconductivity* ed E M Bell (Oxford: Pergamon Press)
- Blom F A P and Burg J W 1977 *J. Phys. Chem. Solids* **38** 19–25
- Braunstein R and Kane E O 1962 *J. Phys. Chem. Solids* **23** 1423–31
- Cardona M 1969 *Solid St. Phys. Suppl.* vol **11** eds F Seitz and D Turnbull (New York: Academic Press)
- Ermolovich Yu B and Kravchuk A F 1976 *Sov. Phys.-Semicond* **10** 1173–4
- Gelten M J, Oosterom A van and Es C M van 1976 *Infrared Physics* **16** 661–2
- Gobeli G W and Fan H Y 1960 *Phys. Rev.* **119** 613–20
- Haacke G and Castellion G A 1964 *J. Appl. Phys.* **35** 2484–7
- Handbook of Chemistry and Physics 1962 44th ed, ed C D Hodgman (Cleveland: The Chemical Rubber Corp) p 320
- Kane E O 1957 *J. Phys. Chem. Solids* **1** 249–61
- Lin-Chung P J 1971 *Phys. Stat. Solidi (b)* **47** 33–9
- van der Pauw L J 1958 *Philips Res. Rep.* **13** 1–9
- Radautsan S I, Arushanov E K and Nateprov A N 1974 *Phys. Stat. Solidi (a)* **23** K59–61
- Radoff P L and Bishop S G 1972 *Phys. Rev. B* **5** 442–8
- 1973 *Mat. Res. Bull.* **8** 219–28
- Sobolev V V and Syrbu N N 1974 *Phys. Stat. Solidi (b)* **64** 423–29
- Wagner R J, Palik E D and Swiggard E M 1971 *The Physics of semimetals and narrow gap semiconductors* eds D L Carter and R T Bates (Oxford: Pergamon)
- Zawadzki W 1974 *Adv. Phys.* **23** 435–522
- Zdanowicz W and Wojakowski A 1965 *Phys. Stat. Solidi* **8** 569–75
- Zivitz M and Stevenson J R 1974 *Phys. Rev. B* **10** 2457–68



### 3.4 OPTICAL VERIFICATION OF THE VALENCE BAND STRUCTURE OF CADMIUM ARSENIDE

M.J. Gelten, C.M. van Es, F.A.P. Blom and J.W.F. Jongeneelen

Department of Physics, Eindhoven University of Technology, Eindhoven, The Netherlands

(Received 30 November 1979 by A. R. Miedema)

Optical absorption measurements were performed on thin single crystalline samples of  $\text{Cd}_3\text{As}_2$  at temperatures of 300 K and 10 K. At low temperature the interband absorption coefficient shows clearly two steps due to direct transitions from the heavy hole and light hole valence bands to the conduction band. The absorption coefficient can be interpreted quantitatively in an isotropic inverted Kane band model with a modified heavy hole band with its maximum shifted from the  $\Gamma$ -point.

Cadmium arsenide ( $\text{Cd}_3\text{As}_2$ ) is a degenerate n-type semiconducting  $\text{II}_3\text{-V}_2$  compound which properties are similar to those of the well known narrow-gap semiconductors  $\text{HgTe}$  and  $\text{HgSe}$ . In contrast with these cubic compounds,  $\text{Cd}_3\text{As}_2$  has an anisotropic band structure due to the tetragonal crystal field interaction, as has been shown by Bodnar<sup>2</sup>. Particular in low concentration samples this band structure leads to very interesting anisotropy effects, such as the energy dependent anisotropy of the cyclotron mass and the effective g-factor of the conduction electrons<sup>1</sup>. However, for electron concentrations around the characteristic value of  $2 \times 10^{18} \text{ cm}^{-3}$  the anisotropy is only weak and most of the electronic transport effects can be satisfactorily described by an isotropic Kane-type conduction band<sup>1</sup>.

Although it is generally accepted now that  $\text{Cd}_3\text{As}_2$  has an inverted band structure<sup>1,2,6,12</sup>, the problems regarding the heavy-hole band are not clearly solved yet. Wagner et al.<sup>3</sup> first assumed a heavy-hole band at the  $\Gamma$  point, degenerate with the conduction band. Aubin et al.<sup>4</sup> proposed a parabolic heavy-hole band with its maximum away from  $k = 0$  and showing a small overlap with the conduction band. The shape of this band is smoothed out towards  $\Gamma$  and reveals a residual gap with the conduction band at  $\Gamma$ . Recently Blom and Gelten<sup>5</sup> found from transport measurements that the heavy-hole band can be assumed to be parabolic with a slightly open gap with respect to the bottom of the conduction band. Up to now no direct experimental data exist on the position of the light hole valence band whose maximum can be expected at an energy  $E_0$  below the bottom of the conduction band. In this paper we present interband absorption measurements showing clearly the valence band structure of  $\text{Cd}_3\text{As}_2$ .

The measurements were performed on a standard single beam optical transmission set up in the wavelength range from 3 - 15  $\mu\text{m}$ . The reflectivity was measured with a modified Beckman IR 4250 spectrophotometer<sup>7</sup>. Thin samples were prepared by polishing, lapping and etching techniques. After the final stage the electron concentration and Hall mobility were measured by means of the four point vander Pauw

method. Then the samples were removed from the substrate and annealed for 40 hours in an evacuated ampoule at a temperature of 150°C. By handling them very carefully the samples were mounted strainfree in a closely fitting sample holder and covered with a suitable diaphragm. The sample holder was mounted inside a hollow cooling finger of a continuous flow cryostat. The cooling finger was closed with cryogenic vacuum tight AgCl windows permitting the sample to be cooled by means of helium contact gas, without introducing any strain.

Both transmission and reflection measurements on thin samples showed large interferences due to multiple reflection. From these interferences the thickness of the samples could be determined very accurately by fitting the interferences pattern to the calculated dielectric constant using the set of band parameters as given below in an iterative way. An example of such a fit is given in figure 1.

The absorption coefficient of sample As-18-11 at 300 K and 10 K is given in figure 2. We clearly see at low temperature two distinct steps in the absorption edge which disappear at room temperature due to broadening of the Fermi-Dirac distribution function. The same effect has been observed by Szuskiewicz on  $\text{HgSe}$ <sup>6</sup>. Also the free carrier contribution to the absorption coefficient becomes very small at low temperature because of a decrease in the electron concentration and a strong increase in the mobility. It should be emphasized that a very important condition for the observation of the steps appeared to be the strain free mounting of the samples. If annealing was omitted, or if the sample was glued only at one point to the cooling finger, the steps in the absorption curves at 10 K completely disappeared and the curve was nearly identical with that measured at 300 K. Also by bending the sample intentionally the steps at 10 K disappeared completely. The steps in the absorption curve could always be reproduced by applying a heat treatment to the sample (40 hours at 150°C in vacuum). None of the above mentioned comments did effect the absorption curve at 300 K in a significant way. This leads us to the conclusion that not



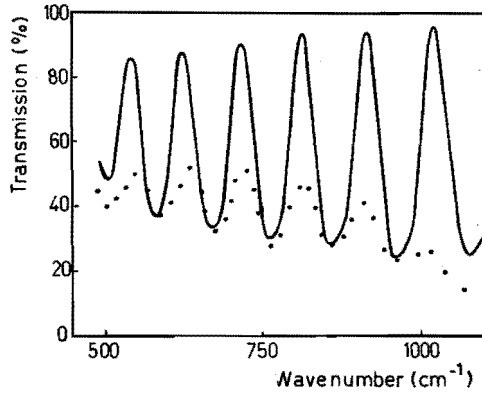


Fig. 1. Transmission of sample AS-18-11 at 10 K. The solid line was calculated from the dielectric constant  $\epsilon$  using the parameters given in the text and a thickness of 10.7  $\mu\text{m}$ .

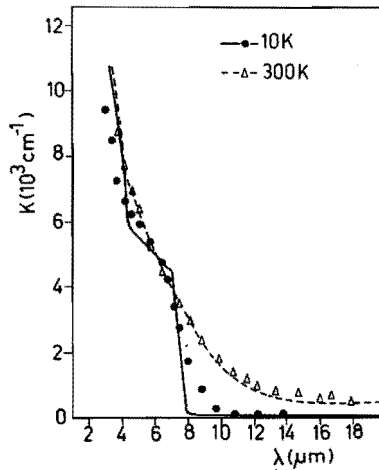


Fig. 2. Absorption coefficient of  $\text{Cd}_3\text{As}_2$  sample AS-18-11 as a function of wavelength. The dotted and solid lines are theoretical fits at 300 K and 10 K respectively.

only mechanical strain but also the introduction of dislocations affects the absorption curve strongly. Possibly the effects are so dramatic in  $\text{Cd}_3\text{As}_2$  because the crystal structure contains many inherent vacancies in a very large unit cell<sup>3</sup>, so that only very little stress is needed to disturb the crystal lattice permanently. This of course also explains why these low energy dislocations can be removed easily by a simple heat treatment at moderate temperatures. The full lines in figure 2 are best fits

of the theoretical absorption coefficient calculated in the following way. Because of the relatively high value of the electron concentration we applied an isotropic inverted Kane model like in HgTe. The secular equation describing the conduction band c, the light hole valence band  $v_2$  and the spin orbit split valence band  $v_3$  is given by:

$$E'(E' + \Delta)(E' + |E_0|) - k^2 P^2 (E' + \frac{2}{3}\Delta) = 0, \quad (1)$$

with  $E' = E - \hbar^2 k^2 / 2m_0$ .

Here  $m_0$  is the free electron mass,  $E_0$  is the energy gap (negative for inverted band structures),  $\Delta$  is the spin orbit splitting energy and  $P$  is the  $k$ - $p$  interaction matrix element. For the heavy hole valence band we used an empirical  $E(k)$  relation resulting in a maximum shifted from  $k = 0$ :

$$E_{v1} = \left(\frac{k}{k_1}\right)^4 (E_R - E_T) - 2 \left(\frac{k}{k_1}\right)^2 (E_R - E_T) + E_R \quad (2)$$

Here  $k_1$  is the wave vector of maximum energy  $E_T$  and  $E_R$  is the residual gap at  $k = 0$ . Notice that  $E_T$  is the real (thermal) band gap in our model. Eq. (2) reflects the proposals of Aubin<sup>4</sup> and can also be considered as a directional average of the valence band energies given by Bodnar<sup>2</sup>. A schematic drawing of the band structure is given in figure 3. In this figure A and B denote the two relevant direct interband transitions being of interest in our measurements.

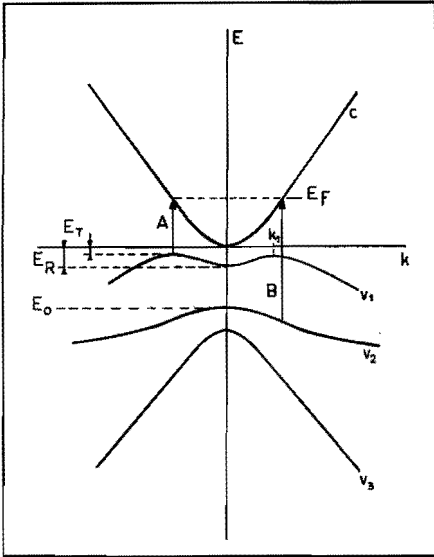


Fig. 3. Schematic band structure of Cd<sub>3</sub>As<sub>2</sub>.

The total dielectric function of Cd<sub>3</sub>As<sub>2</sub> can be written as  $\epsilon_c^2 = \epsilon = \epsilon_1 - i\epsilon_2 = \epsilon'(\omega) + \epsilon_{fc} + \epsilon_A + \epsilon_B$ . Here  $\epsilon_{fc}$  is the free carrier contribution and is given by:

$$\epsilon_{fc} = -\frac{Ne^2}{m^* \epsilon_0} \frac{\tau^2}{\omega^2 \tau^2 - i\omega\tau}$$

where  $N$  is the electron concentration,  $m^*$  the effective mass at the Fermi level and  $\tau = m^* \mu / e$  is the relaxation time of the electrons. The quantities  $\epsilon_A$  and  $\epsilon_B$  are the contributions due to the interband transition A and B respectively and are given by  $\epsilon_{A,B} = \epsilon_{1A,B} - i\epsilon_{2A,B}$ .  $\epsilon'(\omega)$  is the quasi high frequency dielectric constant and is assumed to be real and constant in our case. This quantity is related to the well known and generally used high frequency dielectric constant

$\epsilon(\omega)$  by the relation  $\epsilon(\omega) = \epsilon'(\omega) + \lim_{\omega \rightarrow 0} (\epsilon_{1A} + \epsilon_{1B})$ .

The real part  $\epsilon_{1A}$  was calculated by Kramers-Kronig relations from the imaginary part  $\epsilon_{2A}$  given by<sup>10</sup>:

$$\epsilon_{2A} = \frac{e^2}{2m_0^2 c^2} M_A^2 \rho_A f_{v1} (1 - f_c)$$

where  $M_A$  is the interband momentum matrix element,  $\rho_A$  is the density of states given by:

$$\rho_A = k^2 / 2\pi^2 \left| \frac{dE_C}{dk} - \frac{dE_{v1}}{dk} \right|$$

and  $f_i$  denotes the Fermi-Dirac distribution functions of the participating bands. A similar expression holds for  $\epsilon_{2B}$ . The matrix elements  $M_A$  and  $M_B$  were calculated using the equation given by Kane<sup>10</sup> and the wavefunction coefficients for the inverted structure given by Szymanska et al.<sup>11</sup>. Finally the absorption coefficient  $K$  was calculated from  $\epsilon_1$  and  $\epsilon_2$  via the real and imaginary parts of  $n_c$ . The parameters for the calculation were obtained in the following way:

- (1) The band parameters  $E_0$ ,  $\Delta$ ,  $P$  and  $E_T$  which were taken from ref. 5 have the values  $E_0 = -0.12 - 3.3 \cdot 10^{-8} T$  eV,  $\Delta = 0.3$  eV,  $P = 7.0 \cdot 10^{-6}$  eVcm and  $E_T = -26$  meV.
- (2) From these parameters and the value of the electron concentration, at 300 K the electron concentration at low temperatures and the Fermi energy  $E_F$  can be calculated with the method given in ref. 5.
- (3) The parameter  $\epsilon'(\omega)$  was given such a value that  $\epsilon(\omega) = 16$  which is in good agreement with all our reflectivity measurements.
- (4) The effective mass  $m^*$  at the Fermi level is calculated from the secular equation (1) and is given by:

$$\frac{m^* / m_0}{1 - m^* / m_0} = \frac{\hbar^2 k_F^2}{2m_0} \left[ \frac{1}{E_F^2} + \frac{1}{E_F^2 + \Delta} + \frac{1}{E_F^2 + |E_0|} - \frac{1}{E_F^2 + 2\Delta/3} \right]$$

The only fitting parameters left are  $E_R$  and  $k_1$ . The solid lines in figure 2 are the best fits of the theoretical absorption curve to the experimental points. The values of  $E_R$  and  $k_1$  obtained in this way are  $E_R = -30$  meV and  $k_1 = 4 \cdot 10^8$  m<sup>-1</sup>.

Notice that the cut-off wavelength corresponding to transition B strongly depends on the value of  $E_0$ . Because  $E_0$  was not used as a fitting parameter, the good fit in figure 2 not only proves the inverted character of the band structure of Cd<sub>3</sub>As<sub>2</sub> but also confirms the value of the bandgap determined from transport measurements<sup>5</sup>. Furthermore it turns out that only suitable fits to the experimental data of strain free samples can be obtained with a heavy hole valence band shifted from the  $\Gamma$ -point. In our opinion this is the first experimental verification of the model proposed by Aubin et al.<sup>4</sup>. Finally the necessity of strain free mounting might explain the differences in the absorption curves reported in the literature<sup>13</sup>.

Acknowledgement. We would like to thank P. Nouwens for growing the crystals and Prof. Dr. M.J. Steenland for many helpful discussions.

## REFERENCES

1. F.A.P. Blom, Proc. Int. Summer School on Narrow Gap Sem., Physics and Applications, Nimes 1979 (to be published).
2. J. Bodnar, Proc. Int. Conf. on Physics of Narrow Gap Sem., Warsaw 1977, p.311.
3. R.J. Wagner, E.D. Palik and E.M. Swiggard, "The Physics of Semimetals and Narrow Gap Semiconductors", Ed. D.L. Carter and R.T. Bates, J. Phys. Chem. Solids Suppl. 1, 471 (1971).
4. M.J. Aubin, L.G. Caron and J.-P. Jay-Gerin, Phys. Rev. B15, 3872 (1977).
5. F.A.P. Blom and M.J. Gelten, Phys. Rev. B19, 2411 (1979).
6. J. Cisowski, E.K. Arushanov, J. Bodnar and K. Kloc, Proc. 14th Int. Conf. Phys. Sem., Edinburgh 1978, p.253.
7. M.J. Gelten, A. van Oosterom and C.M. van Es, Infrared Physics 16, 661 (1976).
8. W. Szuszkiewicz, Phys. Stat. Sol. (b) 91, 361 (1979).
9. P.J. Lin Chung, Phys. Rev. 188, 1272 (1969).
10. E.O. Kane, J. Phys. Chem. Solids 1, 249 (1957).
11. W. Szymanska, P. Boguslawski and W. Zawadzki, Phys. Stat. Sol. (b) 65, 641 (1974).
12. B. Dowgiallo-Plenkiewicz and P. Plenkiewicz, Phys. Stat. Sol. (b) 94, K57 (1979).
13. L. Zdanowicz and T. Czaplá, see ref. 2, p.271.

4.1. Plasma edge behaviour of  $Cd_3P_2$  and  $Cd_3As_2$

The samples of both  $Cd_3P_2$  and  $Cd_3As_2$  are highly degenerate n-type materials with electron concentrations in the order of  $10^{24} m^{-3}$ . This leads to the well known phenomenon of plasma reflectivity {29} occurring in the infrared region of the spectrum at wavelengths between 10  $\mu m$  and 100  $\mu m$ . The most important parameter which describes this phenomenon is the plasma frequency  $\omega_p$ . In highly degenerate materials  $\omega_p$  is given by:

$$\omega_p^2 = \frac{Ne^2}{\epsilon_0 \epsilon(\infty) m_F^*} \quad (4.1)$$

Here N is the electron concentration,  $\epsilon(\infty)$  the high frequency dielectric constant and  $m_F^*$  the effective mass at the fermi level which depends on N in materials with a non parabolic band structure. Using eq. (3.1) and the transport theory reviewed by Zawadzki {18}  $m_F^*$  is determined by

$$\frac{m_F^*}{m_0 - m_F^*} = \frac{\hbar^2 k_F^2}{2m_0} \left[ \frac{1}{E_F'} + \frac{1}{E_F' + \Delta} + \frac{1}{E_F' - E_g} - \frac{1}{E_F' + 2\Delta/3} \right] \quad (4.2)$$

Here  $k_F$  is the electron wave vector at the fermi level and  $E_F' = E_F - \hbar^2 k_F^2 / 2m_0$  where  $E_F$  is the fermi energy, counted from the  $\Gamma_8$ -point (see fig. 3.1).  $E_F'$  can be determined using eq. (3.1) in combination with the relation

$$k_F = (3\pi^2 N)^{1/3} \quad (4.3)$$

If the materials are not highly degenerate the quantity  $m_F^*$  should be replaced by an average value {17}. It is clear that knowledge of the plasma frequency can give strong support to the determination of the band structure parameters.

The optical phonons of  $Cd_3P_2$  and  $Cd_3As_2$  are active in the plasma frequency region. Therefore plasmon-phonon coupling will occur {30}.

Because  $\text{Cd}_3\text{P}_2$  has 40 atoms in its unit cell and  $\text{Cd}_3\text{As}_2$  even 160 one might expect an unusually complicated plasmon-phonon system due to the many different optical phonon modes. This results in infrared reflectivity spectra with many pronounced structures. This will complicate a detailed and careful analysis. Nevertheless, for the interpretation of electrical transport measurements it is important to know the values of the phonon parameters {31,32}, especially when the electron mobility is dominated by optical phonon scattering. We were therefore challenged to develop a suitable interpretation method of complex reflectivity spectra. We started with the development of a new and general method for the analysis of reflectivity spectra of plasmon-multiphonon systems. This method is described in section 4.2. The method was applied to room temperature reflectivity measurements of  $\text{Cd}_3\text{P}_2$  and  $\text{Cd}_3\text{As}_2$ . The results are presented in section 4.3. Though the interpretation of the experimental data is rather satisfactory it has to be concluded that the phonon spectra of our materials are such complicated that our new method is not powerful enough for a detailed analysis in this case. Therefore it was decided to extend the measurements to low temperatures in order to be able to analyse them with a less general and more conventional method. We described the reflectivity spectrum on the basis of a dielectric function simply determined by the sum of a number of harmonic oscillators in analogy with the first results of Thielemann et al. {33} on  $\text{Cd}_3\text{As}_2$ . Our results on  $\text{Cd}_3\text{P}_2$  are described in section 4.4.

The analysis of the spectra obtained for  $\text{Cd}_3\text{As}_2$  leads to an additional complication because the plasma edge of this material shows a unique oscillatory structure at wavelengths just below the plasma edge. This phenomenon has also been reported in the literature {34,35} but could not be explained satisfactorily. We expected that application of a magnetic field would influence the structure in such a way to enable us to find a key to the solution of this peculiar effect. Therefore we decided to set up a series of magneto-reflectivity measurements in cooperation with the Max Planck Institute in Grenoble. The results of this study, with a suitable explanation of the oscillatory effect, are presented in section 4.5. This section also contains some additional values of phonon parameters of  $\text{Cd}_3\text{As}_2$  at low temperature.

phys. stat. sol. (b) **106**, 635 (1981)

Subject classification: 6 and 13.5.2; 20.1; 22

*Department of Physics, Eindhoven University of Technology<sup>1)</sup>*

### 4.3 A New Method to Determine the Coupled Mode Parameters of a Plasmon–Multiphonon System

By

M. J. GELTEN and L. A. BOSCH

A new (numerical) method is described to determine all coupled mode parameters of a complex plasmon–phonon system in a semiconductor. First a general theoretical description is given of the complex dielectric function describing such a system. Some practically important relations are deduced. Starting from an experimentally determined reflectivity spectrum, the dielectric function is determined at a number of discrete frequencies by means of Kramers-Kronig analysis. A complete background is given for a numerical method to determine all relevant mode parameters, especially the coordinates of poles and zeros in the complex frequency plane, from this spectrum. Finally the new method is applied to a test spectrum. The results are discussed and compared with those of other methods.

Es wird über eine neue (numerische) Methode zur Bestimmung von allen gekoppelten Modeparametern eines komplizierten Plasmon–Phonon-Systems in einem Halbleiter berichtet. Eine allgemeine theoretische Beschreibung der Dielektrizitätsfunktion eines solchen Systems wird gegeben. Einige praktisch wichtige Beziehungen werden abgeleitet. Mit einem experimentell bestimmten Reflexionsspektrum als Ausgangspunkt wird aus einer Kramers-Kronig-Analyse die dielektrische Funktion für eine große Menge von diskreten Frequenzen berechnet. Alle erforderlichen Informationen für eine numerische Methode zur Bestimmung aller relevanter Modeparameter werden angegeben, besonders der komplexen Polstellen und Nullstellen. Schließlich wird die neue Methode geprüft mit einem Testspektrum. Die Resultate werden diskutiert und mit Resultaten anderer Methoden verglichen.

#### 1. Introduction

Infrared spectroscopy is a powerful tool in the study of plasmon–phonon coupling in semiconductors. Especially if we know the reflectivity in a large enough frequency range, we can apply a special set of Kramers-Kronig relations by which it is possible to calculate the real part  $\epsilon_1$  and the imaginary part  $\epsilon_2$  of the dielectric function as a function of frequency  $\omega$ . A well established method to determine the parameters of LO and TO modes from these data is described by Balkanski [1]. With this method a plot is made of  $\omega\epsilon_2$  versus  $\omega$  and one reads directly the frequencies of the TO modes from the peak frequencies in this plot. Twice the damping constant of the TO modes is given by the halfwidth of these peaks, while the peak values of  $\omega\epsilon_2$  give information about the static dielectric constant and the oscillator strength of the modes. In a similar way the LO mode parameters may be determined from a plot of  $\omega\epsilon_2/(\epsilon_1^2 + \epsilon_2^2)$  versus  $\omega$ . This method will be referred to as method I in this paper. Though this method is often used, even for complicated systems with many modes [2, 18, 19], one should realise that the method described in [1] only applies exactly to the case of an intrinsic semiconductor with only one LO and TO phonon mode having equal damping constants and real frequency independent oscillator strengths. In systems containing more infrared active phonon modes this method is only an approximation and leads

<sup>1)</sup> P. O. Box 513, 5600 Eindhoven, The Netherlands.

to experimental errors [19], especially concerning the damping parameters. If free carriers are introduced into the system we get the phenomenon of plasmon-phonon coupling [3, 19]. In this case curves of  $\omega\epsilon_2$  and  $\omega\epsilon_2/(\epsilon_1^2 + \epsilon_2^2)$  are determined mainly by the plasmon properties and the phonon structures are hardly resolved. In these cases method I is no longer applicable. As an alternative one tries in practical cases to fit the optical data to some suitable model for the dielectric function by means of numerical least-squares procedures, but this method is limited to cases with only one or two coupled modes, because of the large number of unknown parameters [4, 5, 20]. Recently Kim and Spitzer [6] succeeded to fit reflectivity data of  $\text{Ga}_{1-x}\text{Al}_x\text{As}$  to a three-mode model (one plasmon and two TO phonons). They used, however, values for some parameters already known from other experiments.

In this paper we describe a simple method to determine all relevant parameters of the coupled modes of a semiconductor with a plasmon and many phonons. First we give a treatment of the necessary model dielectric functions. Then a numerical procedure is described to calculate the relevant parameters, starting with the reflectivity spectrum as input data. Finally the new method is applied to a test spectrum and the results are discussed.

2. Theory

The most general way to describe the dielectric function of a coupled mode system, consisting of a plasmon and several phonons, is given by Kukharskii [4, 7]. From general arguments he derives the so-called factorised dielectric function, which is given by

$$\hat{\epsilon}(\hat{\omega}) = \epsilon_\infty \frac{\prod_{j=1}^{n+1} (\hat{\omega}^2 - 2i\Omega_{2j}\hat{\omega} - |\Omega_j|^2)}{\hat{\omega} (\hat{\omega} - i\gamma_p) \prod_{j=1}^n (\hat{\omega}^2 - 2i\Gamma_{1j}\hat{\omega} - \omega_{1j}^2)} \tag{1}$$

Here  $\hat{\omega}$  is the complex frequency defined by  $\hat{\omega} = \omega + i\eta$ ,  $\epsilon_\infty$  the well-known high-frequency dielectric constant,  $n$  the number of TO phonon modes, and  $\gamma_p$  the damping constant of the plasmon given by  $\gamma_p = 1/\tau = e/m^*\mu$ . The zeros of  $\hat{\epsilon}(\hat{\omega})$  are given by  $\hat{\omega} = \Omega_j = \pm \Omega_{1j} + i\Omega_{2j}$ . The complex frequencies of the coupled LO modes are defined by these zeros of  $\hat{\epsilon}(\hat{\omega})$  with positive real part. The poles of  $\hat{\epsilon}(\hat{\omega})$  are given by  $\hat{\omega} = 0$ ,  $\hat{\omega} = i\gamma_p$ , and  $\hat{\omega} = \theta_j = \pm\theta_{1j} + i\theta_{2j} = \pm(\omega_{1j}^2 - \Gamma_{1j}^2)^{1/2} + i\Gamma_{1j}$ . The complex frequencies of the TO modes are defined by these poles of  $\hat{\epsilon}(\hat{\omega})$  with positive real part.

Kukharskii [4] pointed out that the eigenfrequencies of the longitudinal (transverse) coupled modes are given by  $|\Omega_j|$  ( $|\theta_j| = \omega_{1j}$ ), while their damping constants are given by  $\Omega_{2j}$  and  $\Gamma_{1j}$ , respectively. It follows from the causality principle that  $\hat{\epsilon} = \epsilon_1 - i\epsilon_2$  has only poles and zeros in the upper half-plane (including the real axis) [8]. For clarity the lay-out of poles and zeros for a three-mode system is given in Fig. 1.

There is, however, another way to describe the dielectric function of a plasmon-phonon system. As pointed out by Varga [9] we may consider the dielectric function

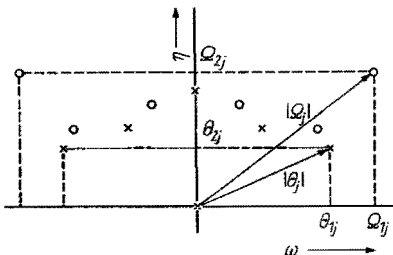


Fig. 1. Lay-out of poles (x) and zeros (o) in the complex frequency plane for a three-mode system

as the sum of two separate contributions: one of the intrinsic material consisting only of the lattice contribution and one of the free carriers. In the framework of poles and zeros the most general equation for the lattice part of the dielectric function is given by Berreman and Unterwald [10],

$$\hat{\epsilon}_L(\hat{\omega}) = \epsilon_\infty \frac{\prod_{j=1}^n (\hat{\omega}^2 - 2i\Gamma_{lj}\hat{\omega} - \omega_{lj}^2)}{\prod_{j=1}^n (\hat{\omega}^2 - 2i\Gamma_{tj}\hat{\omega} - \omega_{tj}^2)}. \quad (2)$$

Due to the fact that TO phonon modes do not couple to plasmon modes because they generate no macroscopic electric fields, equations (1) and (2) contain the same parameters  $\omega_{lj}$  and  $\Gamma_{lj}$ .

Notice that  $\hat{\epsilon}_L$  is described, in contrast to  $\hat{\epsilon}$ , by intrinsic material parameters being the LO phonon frequencies and damping constants ( $\omega_{lj}$ ,  $\Gamma_{lj}$ ) and the TO phonon parameters ( $\omega_{tj}$ ,  $\Gamma_{tj}$ ). The free-carrier contribution to the dielectric function  $\hat{\epsilon}_{fc}(\hat{\omega})$  can be very well described by the Drude equation [11],

$$\hat{\epsilon}_{fc}(\hat{\omega}) = -\epsilon_\infty \frac{\omega_p^2}{\hat{\omega}(\hat{\omega} - i\gamma_p)}. \quad (3)$$

In this equation  $\gamma_p$  is the plasmon damping constant and  $\omega_p$  is the plasma frequency defined by  $\omega_p^2 = Ne^2/\epsilon_0\epsilon_\infty m^*$  ( $N$  is the free-carrier concentration,  $m^*$  the effective mass). The total dielectric function is now given by [9]

$$\tilde{\epsilon}(\hat{\omega}) = \hat{\epsilon}_L(\hat{\omega}) + \hat{\epsilon}_{fc}(\hat{\omega}). \quad (4)$$

Both dielectric functions  $\hat{\epsilon}(\hat{\omega})$  and  $\tilde{\epsilon}(\hat{\omega})$  describe the same physical system and may be compared to each other.

Equation (1) may be split into the following sum:

$$\hat{\epsilon}(\hat{\omega}) = \epsilon_\infty + \frac{A_1}{\hat{\omega}} + \frac{A_2}{\hat{\omega} - i\gamma_p} + \sum_{k=1}^n \left( \frac{B_k^+}{\hat{\omega} - \theta_{tk} - i\Gamma_{tk}} + \frac{B_k^-}{\hat{\omega} + \theta_{tk} - i\Gamma_{tk}} \right) \quad (5)$$

with  $\theta_{tk} = (\omega_{tk}^2 - \Gamma_{tk}^2)^{1/2}$ . The (complex) constants in equation (5) may be determined from the residue theorem,

$$A_1 = \{\text{Res } \hat{\epsilon}\}_{\hat{\omega}=0} = \frac{\epsilon_\infty \prod_{j=1}^{n+1} |\Omega_j|^2}{i\gamma_p \prod_{j=1}^n \omega_{tj}^2}, \quad (6a)$$

$$A_2 = \{\text{Res } \hat{\epsilon}\}_{\hat{\omega}=i\gamma_p} = \epsilon_\infty \frac{\prod_{j=1}^{n+1} (-\gamma_p^2 + 2\gamma_p\Omega_{2j} - |\Omega_j|^2)}{i\gamma_p \prod_{j=1}^n (-\gamma_p^2 + 2\gamma_p\Gamma_{tj} - \omega_{tj}^2)}, \quad (6b)$$

$$\begin{aligned} B_k^\pm &= \{\text{Res } \hat{\epsilon}\}_{\hat{\omega}=\pm\theta_{tk}+i\Gamma_{tk}} = \\ &= \epsilon_\infty \frac{\prod_{j=1}^{n+1} (\theta_{tk}^2 \pm 2i\theta_{tk}\Gamma_{tk} - \Gamma_{tk}^2 \mp 2i\theta_{tk}\Omega_{2j} + 2\Gamma_{tk}\Omega_{2j} - |\Omega_j|^2)}{\pm 2\theta_{tk} (\pm\theta_{tk} + i\Gamma_{tk}) (\pm\theta_{tk} + i\Gamma_{tk} - i\gamma_p)} \times \\ &\times \frac{1}{\prod_{\substack{j=1 \\ j \neq k}}^n \{(\pm\theta_{tk} + i\Gamma_{tk} - \theta_{tj} - i\Gamma_{tj}) (\pm\theta_{tk} + i\Gamma_{tk} + \theta_{tj} - i\Gamma_{tj})\}}. \end{aligned} \quad (6c)$$



From equation (6c) it can be easily verified that  $B_k^\pm = (-B_k^-)^*$ . We can also split  $\tilde{\varepsilon}(\hat{\omega})$  into a sum

$$\tilde{\varepsilon}(\hat{\omega}) = \varepsilon_\infty + \frac{\varepsilon_\infty \omega_p^2}{i\gamma_p \hat{\omega}} - \frac{\varepsilon_\infty \omega_p^2}{i\gamma_p (\hat{\omega} - i\gamma_p)} + \sum_{k=1}^n \left( \frac{D_k^+}{\hat{\omega} - \theta_{tk} - i\Gamma_{tk}} + \frac{D_k^-}{\hat{\omega} + \theta_{tk} - i\Gamma_{tk}} \right) \quad (7)$$

with

$$\begin{aligned} D_k^\pm &= \{ \text{Res } \hat{\varepsilon}_L \}_{\hat{\omega} = \pm \theta_{tk} + i\Gamma_{tk}} = \\ &= \varepsilon_\infty \frac{\prod_{j=1}^n (\theta_{tk}^2 \pm 2i\theta_{tk}\Gamma_{tk} - \Gamma_{tk}^2 \mp 2i\theta_{tk}\Gamma_{tj} + 2\Gamma_{tk}\Gamma_{tj} - \omega_{tj}^2)}{\pm 2\theta_{tk} \prod_{\substack{j=1 \\ j \neq k}}^n (\pm \theta_{tk} + i\Gamma_{tk} - \theta_{tj} - i\Gamma_{tj}) (\pm \theta_{tk} + i\Gamma_{tk} + \theta_{tj} - i\Gamma_{tj})} \end{aligned} \quad (8)$$

If we compare the different terms in (5) and (7) and use equations (6) and (8) we can deduce the following relations:

(i) From the  $1/\hat{\omega}$  term

$$\omega_p^2 = \frac{\prod_{j=1}^{n+1} |\Omega_j|^2}{\prod_{j=1}^n \omega_{tj}^2} \quad (9)$$

This is the generalised Lyddane-Sachs-Teller relation for a coupled mode system [4].

(ii) From the  $1/(\hat{\omega} - i\gamma_p)$  term

$$\omega_p^2 = - \frac{\prod_{j=1}^{n+1} (-\gamma_p^2 + 2\gamma_p \Omega_{2j} - |\Omega_j|^2)}{\prod_{j=1}^n (-\gamma_p^2 + 2\gamma_p \Gamma_{tj} - \omega_{tj}^2)} \quad (10)$$

This relation gives a second possibility to determine the plasma frequency from the experimental parameters.

(iii) From the other terms we get

$$B_k^\pm = D_k^\pm \quad (k = 1, 2, \dots, n). \quad (11)$$

The important consequence of this relation is the following: from equation (8) we see that the coefficients  $D_k^\pm$  are determined completely by intrinsic phonon parameters, while from equation (6c) we see that the coefficients  $B_k^\pm$  are determined both by intrinsic and coupled mode parameters. This means that with a change in free carrier concentration the coupled mode parameters change in such a way that the coefficients  $B_k^\pm$  remain constant: they form an invariant set, completely determined by intrinsic material parameters. The static dielectric constant  $\varepsilon_s$  of the intrinsic material follows from equation (2) and from (7) and (11) by putting  $\omega_p = \hat{\omega} = 0$ ,

$$\varepsilon_s = \varepsilon_\infty \frac{\prod_{j=1}^n \omega_{tj}^2}{\prod_{j=1}^n \omega_{tj}^2} = \varepsilon_\infty - \sum_{k=1}^n \frac{\theta_{tk}(B_k^+ - B_k^-) - i\Gamma_{tk}(B_k^+ + B_k^-)}{\omega_{tk}^2} \quad (12)$$

The first relation in (12) is the well-known Lyddane-Sachs-Teller relation for a multiphonon system. The second relation leads to calculation of  $\epsilon_s$  from the coupled mode parameters. Note that  $\epsilon_s$  is real and constant as can be verified by putting  $B_k^\pm = \pm a + ib$ .

At this point we can make some general remarks. In the literature one often uses for the lattice dielectric function the sum equation

$$\tilde{\epsilon}_L(\hat{\omega}) = \epsilon_\infty - \sum_{j=1}^n \frac{f_j \omega_{tj}^2}{\hat{\omega}^2 - 2i\Gamma_{tj}\hat{\omega} - \omega_{tj}^2}. \quad (13)$$

Here  $f_j$  is the oscillator strength which is taken as a real constant. As we have seen the lattice contribution to the dielectric function also can be written in an "additive form" (see, for example, (7) with  $\omega_p = 0$ ). Reducing this form to one like equation (13) leads to the following result:

$$\tilde{\epsilon}_L(\hat{\omega}) = \epsilon_\infty + \sum_{k=1}^n \frac{(\hat{\omega} - i\Gamma_{tk})(D_k^+ + D_k^-) + \theta_{tk}(D_k^+ - D_k^-)}{\hat{\omega}^2 - 2i\Gamma_{tk}\hat{\omega} - \omega_{tk}^2}. \quad (14)$$

We see that now a complex and frequency dependent oscillator strength is obtained; a situation which is equivalent to frequency dependent transverse eigenfrequencies and damping constants [10]. The relation  $B_k^\pm = D_k^\pm$  physically means that the introduction of free carriers in a system does not even change the frequency dependence of the transverse eigenfrequencies and damping constants (or oscillator strengths). Only when our  $D_k^\pm$  is real we find the real and constant oscillator strength of equation (13). Giehler and Jahne [12] indeed showed in a general treatment of the dielectric function for a two-mode system (one plasmon + one phonon) that in the special case when there is no interaction between plasmon and transverse phonon, the oscillator strength is real and the use of (13) is correct.

### 3. Numerical Procedure

Suppose that we know from an experiment the reflectivity  $R$  of a sample in such a large range of real frequencies  $\omega$  that the spectrum may be correctly extrapolated to  $\omega = 0$  and  $\omega = \infty$ . From this  $R(\omega)$  we determine numerically  $\hat{\epsilon} = \epsilon_1 - i\epsilon_2$  by means of a special Kramers-Kronig relation [13]. After this numerical calculation the results for  $\epsilon_1$  and  $\epsilon_2$  are discretised. So we start our method by assuming that  $\hat{\epsilon}$  is known for a large number of discrete frequencies  $\omega_k$  ( $k = 0, 1, 2, \dots, M - 1$ ) on the real  $\omega$ -axis, separated by a sampling distance  $h = \omega_{k+1} - \omega_k$ . These discrete values of  $\hat{\epsilon}$  will be denoted by  $\hat{\epsilon}(\omega_k)$ .

The basic idea of our method is now to replace the unknown continuous dielectric function  $\hat{\epsilon}(\omega)$  by a set of  $M$  functions  $\hat{\epsilon}_k(\omega)$  from which each element  $\hat{\epsilon}_k(\omega)$  is a good approximation of the dielectric function in a small region around  $\omega_k$ . These approximations can be determined using the experimental values of  $\hat{\epsilon}$  in our sampling points on the real  $\omega$ -axis. Replacing  $\omega$  in  $\hat{\epsilon}_k(\omega)$  by a complex frequency  $\hat{\omega}$  defined by  $\hat{\omega} = \omega + i\eta$  leads to a set of functions  $\hat{\epsilon}_k(\hat{\omega})$  extended in the complex frequency plane. The complex zeros with positive imaginary part of each function  $\hat{\epsilon}_k(\hat{\omega})$  can be determined. It can be shown that this set of zeros has accumulation (or cluster) points in the complex frequency plane, which can be identified with the zeros of the true dielectric function  $\hat{\epsilon}(\hat{\omega})$ . In the same way the poles of the dielectric function can be determined by applying the method to the quantity  $1/\hat{\epsilon}(\hat{\omega})$ .

We will give now some more details on our method. We can expand the continuous dielectric function for every  $\omega_k$  in a Taylor series on the real axis,

$$\hat{\varepsilon}(\omega) = \hat{\varepsilon}(\omega_k) + \left. \frac{d\hat{\varepsilon}}{d\omega} \right|_{\omega=\omega_k} (\omega - \omega_k) + \left. \frac{1}{2} \frac{d^2\hat{\varepsilon}}{d\omega^2} \right|_{\omega=\omega_k} (\omega - \omega_k)^2 + G_0(\omega, \omega_k) \quad (15)$$

$(k = 0, 1, 2, \dots, M - 1)$ .

It can be shown [14] that the residual term  $G_0(\omega, \omega_k)$  is given by

$$G_0(\omega, \omega_k) = \left. \frac{1}{6} \frac{d^3\hat{\varepsilon}}{d\omega^3} \right|_{\omega=\zeta} (\omega - \omega_k)^3, \quad (16)$$

where  $\zeta$  is some frequency between  $\omega$  and  $\omega_k$ .

The first and second derivatives in equation (15) may be estimated from the sampling points as follows [14]:

$$\left. \frac{d\hat{\varepsilon}}{d\omega} \right|_{\omega=\omega_k} = \frac{\hat{\varepsilon}(\omega_{k+m}) - \hat{\varepsilon}(\omega_{k-m})}{2mh} + G_1(mh) \quad (17)$$

with

$$G_1(mh) = - \left. \frac{m^2 h^2}{6} \frac{d^3\hat{\varepsilon}}{d\omega^3} \right|_{\omega=\zeta^1} \quad (18)$$

and

$$\left. \frac{d^2\hat{\varepsilon}}{d\omega^2} \right|_{\omega=\omega_k} = \frac{\hat{\varepsilon}(\omega_{k+m}) - 2\hat{\varepsilon}(\omega_k) + \hat{\varepsilon}(\omega_{k-m})}{m^2 h^2} + G_2(mh) \quad (19)$$

with

$$G_2(mh) = - \left. \frac{m^2 h^2}{12} \frac{d^4\hat{\varepsilon}}{d\omega^4} \right|_{\omega=\zeta^1}, \quad (20)$$

where  $\zeta^1$  is some frequency between  $\omega_{k-m}$  and  $\omega_{k+m}$  and  $m$  is an integer. After substitution of equations (17) and (19) into (15) and extending  $\omega$  into the complex frequency plane, we can write the dielectric function as a sum of two terms,

$$\hat{\varepsilon}(\hat{\omega}) = \hat{\varepsilon}_k(\hat{\omega}) + \Delta\hat{\varepsilon}_k(\hat{\omega}) \quad (k = 0, 1, 2, \dots, M - 1) \quad (21)$$

with

$$\hat{\varepsilon}_k(\hat{\omega}) = \hat{\varepsilon}(\omega_k) + \frac{\hat{\varepsilon}(\omega_{k+m}) - \hat{\varepsilon}(\omega_{k-m})}{2mh} (\hat{\omega} - \omega_k) + \frac{1}{2} \frac{\hat{\varepsilon}(\omega_{k+m}) - 2\hat{\varepsilon}(\omega_k) + \hat{\varepsilon}(\omega_{k-m})}{m^2 h^2} (\hat{\omega} - \omega_k)^2 \quad (22)$$

and

$$\Delta\hat{\varepsilon}_k(\hat{\omega}) = G_0(\hat{\omega}, \omega_k) + G_1(mh) (\hat{\omega} - \omega_k) + \frac{1}{2} G_2(mh) (\hat{\omega} - \omega_k)^2. \quad (23)$$

Using (22) each  $\hat{\varepsilon}_k(\hat{\omega})$  can be calculated and each element of the set of functions  $\hat{\varepsilon}_k(\hat{\omega})$  ( $k = 0, 1, 2, \dots, M - 1$ ) is a good approximation for the true dielectric function around  $\hat{\omega} = \omega_k$ , because  $\Delta\hat{\varepsilon}_k(\hat{\omega}) \rightarrow 0$  as  $\hat{\omega} \rightarrow \omega_k$ . From (18) and (20) it is seen that both  $G_1(mh)$  and  $G_2(mh)$  are proportional to  $m^2$ . So, the errors  $G_1(mh)$  and  $G_2(mh)$  are minimized by choosing  $m$  as small as possible ( $m = 1$ ).

Consider now  $\hat{\varepsilon}_k(\hat{\omega})$  as an approximation of the true dielectric function.  $\hat{\varepsilon}_k(\hat{\omega})$  is a quadratic polynomial and has two zeros in the complex frequency plane, which can be determined numerically by standard procedures [14, 15]. In all practical situations, where we used our method, it appeared that one of the zeros fell below the real axis and one was always lying above it. As has been pointed out in the theory, only the zeros with positive imaginary part are relevant for us. So, with  $M$  discrete frequencies

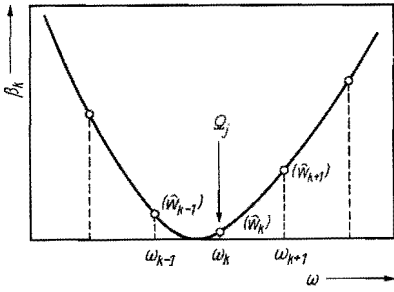


Fig. 2. Determination of the zero  $\Omega_j$  from the parameter  $\beta_k$ . The parameters between brackets indicate the zeros of equation (22) corresponding to each  $\omega_k$

$\omega_k$  on the real axis a set of  $M$  zeros  $\hat{w}_k$  in the upper half of the complex frequency plane can be obtained. Now  $\hat{\epsilon}_k(\hat{\omega})$  is a better approximation for  $\hat{\epsilon}(\hat{\omega})$  in a region around  $\hat{w}_k$  as  $\hat{w}_k$  lies closer to  $\hat{\omega}$ ; so  $\hat{w}_k$  is a better approximation for the true zero  $\Omega_j$  in question as  $\hat{w}_k$  lies closer to  $\omega_k$ . We can conclude that the set of  $M$  zeros has accumulation points in the complex frequency plane and that the true zeros  $\Omega_j$  of the dielectric function will be best approximated by the respective accumulation points of  $\hat{w}_k$ .

The accumulation points are given by those complex zeros for which the expression  $|\hat{w}_k - \omega_k|$  is a minimum or, leading to the same result, when  $\beta_k = |\text{Re}(\hat{w}_k) - \omega_k|$  is a minimum [14]. The best approximation of the actual zero  $\Omega_j$  is the particular value of  $\hat{w}_k$  belonging to the lowest value of  $\beta_k$  as is indicated in Fig. 2.

The poles in the dielectric function can be determined in an analogous way by applying the method to the quantity  $1/\hat{\epsilon}(\omega)$ , because poles in  $\hat{\epsilon}(\hat{\omega})$  are zeros in  $1/\hat{\epsilon}(\hat{\omega})$ .

Before we apply our new method, we have to solve the problem that arises because of the fact that we do not know the dielectric function exactly in the sampling points. The Kramers-Kronig algorithm determines the dielectric function with an error  $\delta\hat{\epsilon}$ ; and if we denote the experimentally determined values of  $\hat{\epsilon}$  at the frequencies  $\omega_k$  by  $\hat{\epsilon}_k$ , then  $\hat{\epsilon}(\omega_k) = \hat{\epsilon}_k + \delta\hat{\epsilon}$ . In practice we can only use the values  $\hat{\epsilon}_k$  instead of the exact values  $\hat{\epsilon}(\omega_k)$  and this results in additional errors in the first and the second derivatives as can be seen by substitution in (17) and (19) [14],

$$\left. \frac{d\hat{\epsilon}}{d\omega} \right|_{\omega=\omega_k} = \frac{\hat{\epsilon}_{k+m} - \hat{\epsilon}_{k-m}}{2mh} + G_1(mh) + \delta_1(mh) \quad \text{with} \quad |\delta_1(mh)| \leq \frac{|\delta\hat{\epsilon}|}{mh}, \quad (24)$$

$$\left. \frac{d^2\hat{\epsilon}}{d\omega^2} \right|_{\omega=\omega_k} = \frac{\hat{\epsilon}_{k+m} - 2\hat{\epsilon}_k + \hat{\epsilon}_{k-m}}{m^2h^2} + G_2(mh) + \delta_2(mh) \quad \text{with} \quad |\delta_2(mh)| \leq \frac{4|\delta\hat{\epsilon}|}{m^2h^2}. \quad (25)$$

Equations (24) and (25) show, together with equations (18) and (20), that there is a limit in the accuracy with which we can approximate the first and second derivatives.  $G_1(mh)$  and  $G_2(mh)$  are proportional to  $m^2$ , whereas  $\delta_1(mh)$  and  $\delta_2(mh)$  are proportional to  $1/m$  and  $1/m^2$ , respectively, so we have two contradictory demands in minimizing the errors in the derivatives. The total error in the derivatives is a minimum for some optimum value of  $m$ . This is the reason why we did not use only nearest-neighbour points ( $m = 1$ ) in our derivatives.

#### 4. Application to a Test Spectrum

We apply our method to a three-mode system (two TO phonons + one plasmon) with the test parameters given in Table 1. The test reflectivity spectrum is calculated

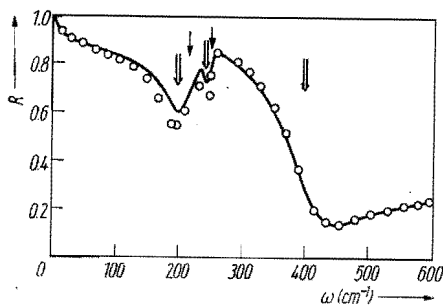


Fig. 3

Fig. 3. The test spectrum (—). The marks denote the LO eigenfrequencies  $|\Omega_j|$  ( $\Downarrow$ ) and TO eigenfrequencies  $|\theta_j|$  ( $\downarrow$ ),  $\circ$  after method II

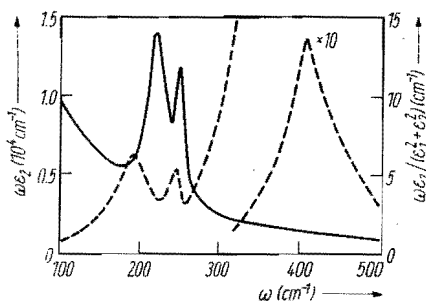


Fig. 4

Fig. 4.  $\omega\epsilon_2$  (solid line) and  $\omega\epsilon_2/(\epsilon_1^2 + \epsilon_2^2)$  (dashed line) as a function of  $\omega$ , determined from the test spectrum

as a function of the frequency using equation (1) and the relation

$$R = \left| \frac{\sqrt{\hat{\epsilon}(\omega)} - 1}{\sqrt{\hat{\epsilon}(\omega)} + 1} \right|^2 \quad (26)$$

and is shown in Fig. 3. For the sampling interval we have taken  $h = 1 \text{ cm}^{-1}$ . From this test spectrum the  $\hat{\epsilon}_k$  are calculated using the Kramers-Kronig relations.

Table 1

Parameter sets determined in different ways. For  $\epsilon_\infty$  a value of 14 was taken. The lower part of the table contains the quantities derived from the parameters in the upper part of the table

parameter	test value	method I	method II with Kramers-Kronig analysis	method II without Kramers-Kronig analysis
$ \Omega_1 $ ( $\text{cm}^{-1}$ )	200.2	192	193.9	193.7
$ \Omega_2 $ ( $\text{cm}^{-1}$ )	247.2	246	245.1	244.2
$ \Omega_3 $ ( $\text{cm}^{-1}$ )	412.9	416	416.0	412.9
$\Omega_{21}$ ( $\text{cm}^{-1}$ )	24.0	$\approx 20$	24.5	24.3
$\Omega_{22}$ ( $\text{cm}^{-1}$ )	6.1	—	8.9	9.0
$\Omega_{23}$ ( $\text{cm}^{-1}$ )	41.1	44	40.7	40.0
$\omega_{t1}$ ( $\text{cm}^{-1}$ )	222.0	222	223.0	222.9
$\omega_{t2}$ ( $\text{cm}^{-1}$ )	250.0	250	250.8	250.9
$\Gamma_{t1}$ ( $\text{cm}^{-1}$ )	14.0	$\approx 15$	14.6	14.6
$\Gamma_{t2}$ ( $\text{cm}^{-1}$ )	4.7	—	6.1	5.8
$\gamma_p$ ( $\text{cm}^{-1}$ )	104.8	—	105.0	105.0
$B_1^\pm$ ( $\text{cm}^{-1}$ ) (6c)	$\mp 666$	—	$\mp 736 - 81i$	$\mp 738 - 344i$
$B_2^\pm$ ( $\text{cm}^{-1}$ ) (6c)	$\mp 125$	—	$\mp 284 - 4i$	$\mp 333 - 21i$
$\epsilon_s$ (12)	21	—	22.9	22.6
$\omega_p$ ( $\text{cm}^{-1}$ ) (9)	368.2	—	353.5	351.9
$\omega_p$ ( $\text{cm}^{-1}$ ) (10)	368.2	—	355.1	353.5

Application of method I then leads to Fig. 4. Clearly visible are the peaks of  $\omega\varepsilon_2$ , representing the two transverse eigenfrequencies and the peaks of  $\omega\varepsilon_2/(\varepsilon_1^2 + \varepsilon_2^2)$ , representing the longitudinal eigenfrequencies. The results of method I are given in Table 1.

Now we apply our new method (method II) to the test spectrum. For some values of  $m$  (generally between 1 and 10) the zeros  $\hat{\omega}_k$  of all  $\hat{\varepsilon}_k(\hat{\omega})$  are determined numerically by means of the Muller procedure [14, 15]. The quantity  $\beta_k$  is calculated and plotted against frequency. Fig. 5a, b, and c show such plots of  $\beta_k$  for three different values of  $m$ .

In Fig. 5a,  $\beta_k$  heavily oscillates at the first and third zero. Only in the neighbourhood of the second zero we get the expected smooth curve with a sharp minimum. As was shown these oscillations are due to the fact that we do not know the dielectric function exactly. Although a Kramers-Kronig analysis gives us the dielectric function in most

frequency regions with a relative error smaller than 2% ( $|\delta\hat{\varepsilon}/\hat{\varepsilon}| \leq 2\%$ ), the choice of a too small value of  $m$  can lead to errors  $\delta_1$  and  $\delta_2$  of 100% (equations (24) and (25)), causing numerical instability. The errors  $\delta_1$  and  $\delta_2$  are independent of the magnitude of the first and second derivative, respectively, so a small error in  $\hat{\varepsilon}$  can cause a large error in the derivatives.

According to this theory the oscillations in  $\beta_k$  at the first and third zero should disappear, when we take a larger value of  $m$ . The result of this is given in Fig. 5b and c. It can be concluded that the optimum value for  $m$  is found where the oscillations in  $\beta_k$  have just disappeared.

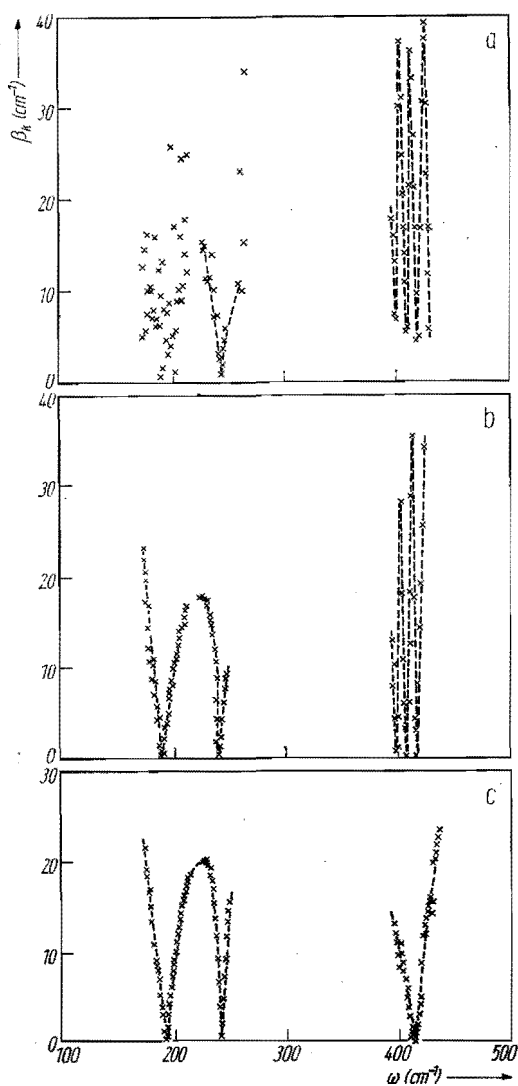


Fig. 5. The parameter  $\beta_k$  as a function of frequency for different values of  $m$ . a)  $m = 1$ , b) 6, c) 9

It is not necessary that the optimum value of  $m$  is the same for all zeros (poles); this depends upon the magnitude of the error in  $\hat{\epsilon}_k$  from Kramers-Kronig analysis. It appeared to be that for  $\Omega_1$ ,  $\Omega_2$ , and  $\Omega_3$  the optimum values are  $m = 6$ ,  $m = 1$ , and  $m = 9$ , respectively. As can be seen from Fig. 5,  $m$ -values larger than the optimum also give smooth curves. The reason for this is that in these cases the errors  $\delta_1$  and  $\delta_2$  are small; the errors  $G_1$  and  $G_2$ , however, have become larger in these cases, so we have passed the optimum  $m$ -value. Finding the correct value of  $m$  is a matter of trial and error. The same arguments hold in the determination of the poles.

In Table 1 the complex frequencies, found with our new method (method II) are given. The results of our new method can be compared with the results of method I and the test values. Applying method II without using the Kramers-Kronig analysis, but using directly the exact values of  $\hat{\epsilon}(\omega_k)$ , calculated from (5) by substituting the test parameters, we never found oscillations in plots like Fig. 5a, b, and c in accordance with theory. The results of such a calculation are given in Table 1 for comparison. It should be noted here that the plasmon damping constant  $\gamma_p$  could only be determined in our case without using the Kramers-Kronig analysis (last column of Table 1).

This is due to the fact that our numerical procedure for the Kramers-Kronig analysis was too inaccurate near  $\omega = 0$ . Improvement of this procedure, which fell beyond the scope of this work, will lead to a correct determination of  $\gamma_p$  in this case. It is for this reason that we have taken in column 4 of Table 1 a value of  $\gamma_p = 105 \text{ cm}^{-1}$ . In practical cases, however,  $\gamma_p$  may also be determined from other experiments like four-point van der Pauw Hall measurements [17, 20].

Using the data of Table 1 the parameters  $B_k^\pm$ ,  $\epsilon_s$ , and  $\omega_p$  may be calculated from equations (6c), (12), and (9) or (10), respectively. The results are also given in Table 1. The test values of our model have been chosen in such a way that the values of the parameters  $B_k^\pm$  are real. From the fourth and fifth columns of Table 1 it is seen that in practice the parameters  $B_k^\pm$  are not found to be real. Although the parameters  $B_k^\pm$  do not fit too well, the use of these coefficients in the calculation of the static dielectric constant and the plasma frequency (in two ways) gives satisfactory results. It is seen that both equations (9) and (10) give the same result for the plasma frequency. Also the reflectivity spectrum, calculated with the experimental parameters of method II without Kramers-Kronig analysis, fits quite well the test spectrum (Fig. 3). Probably the coefficients  $B_k^\pm$  are strongly dependent on the precise structure of a reflectivity spectrum, whereas the other parameters are not influenced so much by the local structure of a reflectivity spectrum.

## 5. Discussion and Conclusions

The analysis of our (arbitrarily chosen) test spectrum clearly verifies the theoretical backgrounds of our numerical procedure, especially concerning the numerical instabilities and the choice of the parameter  $m$ . The results given in Table 1 also show that our method II is more general and as such more powerful in the determination of the mode parameters than method I, especially if we consider the damping parameters. Method I can only lead to correct results in the case of phonon systems with weakly damped and widely separated modes [19]. From the results that can be obtained with method I it is actually impossible to determine the parameters  $B_k^\pm$  and  $\epsilon_s$  (see Table 1). With method II we can determine  $B_k^\pm$ ,  $\epsilon_s$ , and  $\omega_p$  even in two different ways. All these arguments emphasise the power of method II compared to method I. Besides, one should realise that method II will even be better if the number of modes in the system is increased. If we compare the differences of the data in Table 1 with the test parameters, we may conclude that our method II is even more accurate than

method I. It should be noted here that a numerical fitting procedure to the reflectivity spectrum is even impossible with our large number of unknown parameters.

We have also applied our method to some experimental data, obtained on  $\text{Cd}_3\text{P}_2$  and the preliminary results have been reported elsewhere [16].

In conclusion we would like to say that we have developed a relatively simple method to determine all coupled mode parameters of a complex plasmon-phonon system.

### Acknowledgements

We greatly appreciate the assistance of Ir. C. M. van Es with the numerical calculation and the careful reading of the manuscript and helpful discussion with Prof. Dr. M. J. Steenland.

### References

- [1] M. BALKANSKI, in: Optical Properties of Solids, Ed. F. ABELES, North-Holland Publ. Co., Amsterdam 1972.
- [2] S. W. MCKNIGHT, P. M. AMIRTHARAJ, and S. PERKOWITZ, Solid State Commun. **25**, 357 (1978).
- [3] I. YOKOTA, Progr. theor. Phys. (Kyoto), Suppl. **57**, 97 (1975).
- [4] A. A. KUKHARSKII, Soviet Phys. — Solid State **14**, 1501 (1972).
- [5] O. K. KIM and W. G. SPITZER, J. appl. Phys. **50**, 4362 (1979).
- [6] O. K. KIM and W. G. SPITZER, Phys. Rev. B **20**, 3258 (1979).
- [7] A. A. KUKHARSKII, Solid State Commun. **13**, 1761 (1973).
- [8] L. D. LANDAU and E. M. LIFSHITS, Electrodynamics of Continuous Media, Pergamon Press, Oxford 1960.
- [9] B. B. VARGA, Phys. Rev. **137**, A1896 (1965).
- [10] D. W. BERREMAN and F. C. UNTERWALD, Phys. Rev. **174**, 791 (1968).
- [11] T. S. MOSS, G. J. BURRELL, and B. ELLIS, Semiconductor Opto-Electronics, Butterworths, London 1974.
- [12] M. GIEHLER and E. JAHNE, phys. stat. sol. (b) **73**, 503 (1976).
- [13] M. CARDONA, in: Optical Properties of Solids, Ed. S. NUDELMAN and S. S. MITRA, Plenum Press, New York 1969.
- [14] F. B. HILDEBRAND, Introduction to Numerical Analysis, McGraw-Hill Publ. Co., London 1956.
- [15] D. E. MULLER, A Method for Solving Algebraic Equations Using an Automatic Computer, Vol. 10, The National Research Council, Washington 1956 (p. 208 to 215).
- [16] M. J. GELTEN, Proc. I. Internat. Symp. Phys. and Chem. of II-V Compounds, Ed. M. J. GELTEN and L. ZDANOWICZ, Mogyilany, Eindhoven 1981.
- [17] L. VAN DER PAUW, Philips Res. Rep. **13**, 1 (1958).
- [18] I. F. CHANG, S. S. MITRA, J. N. PLENDL, and L. C. MANSUR, phys. stat. sol. **28**, 663 (1968).
- [19] J. F. BAUMARD and F. GERVAIS, Phys. Rev. B **15**, 2316 (1977).
- [20] S. PERKOWITZ and R. H. THORLAND, Solid State Commun. **16**, 1093 (1975).

(Received April 30, 1981)

Note: The next section is a reprint of a paper published in Proc. 4th. Int. Conf. Phys. Narrow Gap Semicond. Linz, 1981 Lecture Notes in Physics 152 p. 167 (Springer Verlag, Berlin, 1982).



## 4.3 FAR INFRARED OPTICAL PROPERTIES OF $\text{Cd}_3\text{P}_2$ AND $\text{Cd}_3\text{As}_2$

M.J. Gelten, C.M. van Es  
Department of Physics  
Eindhoven University of Technology  
5600 MB EINDHOVEN  
The Netherlands

Abstract:  $\text{Cd}_3\text{P}_2$  and  $\text{Cd}_3\text{As}_2$  are degenerate n-type semiconductors showing plasmon-phonon coupling. From infrared and far-infrared reflectivity measurements at 300 K, the dielectric function  $\epsilon(\omega)$  can be determined by means of Kramers-Kronig analysis. With a special numerical method the complex poles and zeros of  $\epsilon(\omega)$  can be calculated giving directly the TO-phonon and LO coupled mode parameters. From a general factorised equation describing  $\epsilon(\omega)$  the static dielectric constant of the material can be determined. Some experimental results will be given and discussed.

### I. Introduction

$\text{Cd}_3\text{P}_2$  and  $\text{Cd}_3\text{As}_2$  form an interesting class of n-type degenerate narrow gap semiconductors. Both materials have a tetragonal crystal structure with a large number of atoms in the unit cell (40 for  $\text{Cd}_3\text{P}_2$  and 160 for  $\text{Cd}_3\text{As}_2$ ). This might lead to complicated infrared phonon spectra which are however difficult to study experimentally because of the phenomenon of plasmon-phonon coupling, which is very pronounced in these degenerate materials. This is the reason why from direct optical measurements no information is available on the values of the intrinsic phonon parameters (eigenfrequencies and damping constants) and the static dielectric constant  $\epsilon_s$ . Only some preliminary values for  $\text{Cd}_3\text{P}_2$  are given in [1] while some indirect and controversial values for  $\epsilon_s$  are given in [2-5]. In this paper we present (far)infrared reflectivity measurements in such a large spectral region that Kramers-Kronig analysis leads to accurate values of the dielectric function  $\hat{\epsilon} = \epsilon_1 - i\epsilon_2$ . By numerical analysis of these data it is possible to determine the intrinsic TO phonon parameters and the LO coupled mode parameters. Besides the value of  $\epsilon_s$  can be determined.

### II. Experimental

Single crystalline samples of  $\text{Cd}_3\text{P}_2$  and  $\text{Cd}_3\text{As}_2$  were polished with 1.0 and 0.25  $\mu\text{m}$  diamond powder and etched with a 15% bromine-ethanol solution in order to get reproducible reflectivity spectra. Reflecting area's were approx. 5 mm diameter. From each sample the electron concentration  $N$  and the Hall mobility  $\mu$  were measured by the 4-point Van der Pauw method. The reflectivity  $R$  was measured in the wave number range from 200-4000  $\text{cm}^{-1}$  by means of a Beckman IR 4250 double beam spectrometer with a special reflectivity attachment described in [6]. In the wave number range from 50-500  $\text{cm}^{-1}$  the reflectivity was measured with a Grubb Parson Fourier Transform Spectrometer as indicated in figure 1. All measurements were performed at room temperature with evaporated gold as a calibrating mirror. For wave numbers  $\nu > 4000 \text{ cm}^{-1}$   $R$  was extrapolated as a constant value and for  $\nu < 50 \text{ cm}^{-1}$  the reflectivity was extrapolated smoothly to  $R=1$  at  $\nu=0 \text{ cm}^{-1}$ . It turned out that these extrapolations had no significant influence on the final results of  $\hat{\epsilon}$  because of the large experimental wave number range. From the complete spectrum,  $\hat{\epsilon}$  is determined by Kramers-Kronig analysis for a large number of discrete frequencies  $\omega_k$  with a sampling distance  $h = \omega_{k+1} - \omega_k$ . In all cases  $h = 1 \text{ cm}^{-1}$ .

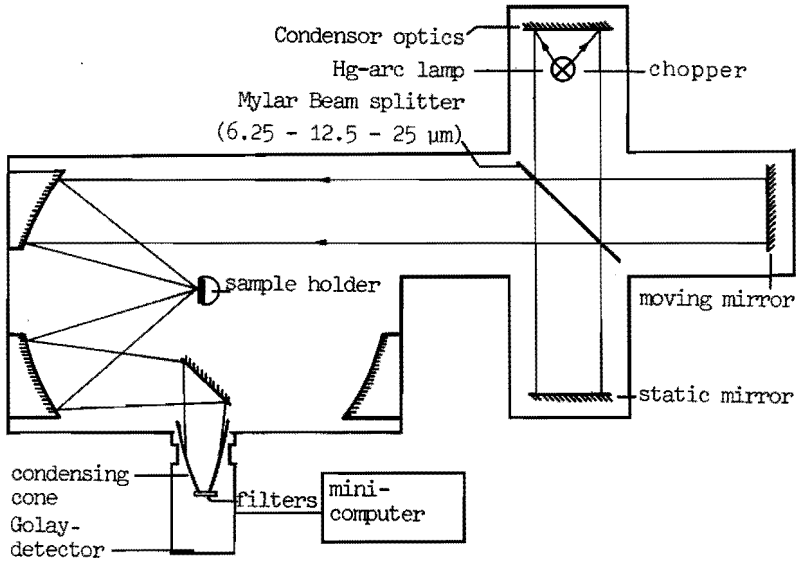


Fig. 1. Far-infrared experimental set-up.

### III. Theory

The most general way to describe the dielectric function of a coupled mode system, consisting of a plasmon and several phonons, is given by Kukharskii [7,8] as the so-called factorised dielectric function:

$$\hat{\epsilon}(\hat{\omega}) = \epsilon_{\infty} \frac{\prod_{j=1}^{n+1} (\hat{\omega}^2 - 2i\Gamma_{lj}\hat{\omega} - \Omega_{lj}^2)}{\hat{\omega}(\hat{\omega} - i\gamma_p) \prod_{j=1}^n (\hat{\omega}^2 - 2i\gamma_{tj}\hat{\omega} - \omega_{tj}^2)} \quad (1)$$

Here  $\hat{\omega}$  is the complex frequency defined by  $\hat{\omega} = \omega + i\eta$ ,  $\epsilon_{\infty}$  is the well known high frequency dielectric constant,  $n$  is the number of TO phonon modes and  $\gamma_p$  is the damping constant of the plasmon given by  $\gamma_p = 1/\tau_p = e/m^*\mu$ . The zeros of  $\hat{\epsilon}(\hat{\omega})$  are given by  $\hat{\omega} = \Omega_j = \pm\Omega_{1j} + i\Omega_{2j} = \pm(\Omega_{lj}^2 - \Gamma_{lj}^2)^{1/2} + i\Gamma_{lj}$ . The complex frequencies of the coupled LO modes are defined by these zeros of  $\hat{\epsilon}(\hat{\omega})$  with positive real part. The poles of  $\hat{\epsilon}(\hat{\omega})$  are given by  $\hat{\omega} = 0$ ,  $\hat{\omega} = i\gamma_p$  and  $\hat{\omega} = \Theta_j = \pm\Theta_{1j} + i\Theta_{2j} = \pm(\omega_{tj}^2 - \gamma_{tj}^2)^{1/2} + i\gamma_{tj}$ . The complex frequencies of the TO modes are defined by these poles of  $\hat{\epsilon}(\hat{\omega})$  with positive real part. Kukharskii pointed out that the eigenfrequencies of the transverse and longitudinal coupled modes are given by  $|\Theta_j| = \omega_{tj}$  and  $|\Omega_j| = \Omega_{lj}$  respectively, while their damping constants are given by  $\gamma_{tj}$  and  $\Gamma_{lj}$  respectively.

There is however another way to describe the dielectric function of a plasmon-phonon system. As pointed out by Varga [9] we may consider the dielectric function as the sum of two separate contributions:  $\hat{\epsilon}_I(\hat{\omega})$  of the intrinsic material consisting only of the lattice contribution and  $\hat{\epsilon}_{FC}(\hat{\omega})$  of the free carriers. In the framework of poles and zeros the summed dielectric function  $\hat{\epsilon}(\hat{\omega})$  is now given by [10]:

$$\tilde{\epsilon}(\omega) = \tilde{\epsilon}_L(\omega) + \tilde{\epsilon}_{rc}(\omega) = \epsilon_\infty + \frac{A_1}{\omega} + \frac{A_2}{\omega - i\gamma_p} + \sum_{k=1}^n \left( \frac{B_k^+}{\omega - \theta_{1k} - i\gamma_{tk}} + \frac{B_k^-}{\omega + \theta_{1k} - i\gamma_{tk}} \right) \quad (2)$$

with  $\theta_{1k} = (\omega_{tk}^2 - \gamma_{tk}^2)^{\frac{1}{2}}$ . Expressions for the (complex) constants  $A_1$ ,  $A_2$  and  $B_k^\pm$  in eq. (2) are given in [10]. It is also shown in [10] that  $B_k^\pm$  are intrinsic material parameters for which the relation  $B_k^+ = (-B_k^-)^*$  holds. Some important relations for the plasma frequency  $\omega_p$  and the static dielectric constant are obtained in [10] and given by:

$$\omega_p^2 = \frac{\sum_{j=1}^{n+1} \Omega_{lj}^2}{\sum_{j=1}^n \omega_{tj}^2} \quad \text{or} \quad \omega_p^2 = - \frac{\sum_{j=1}^{n+1} (-\gamma_p^2 + 2\gamma_p \Gamma_{lj} - \Omega_{lj}^2)}{\sum_{j=1}^n (-\gamma_p^2 + 2\gamma_p \gamma_{tj} - \omega_{tj}^2)} \quad (3a, 3b)$$

and

$$\epsilon_s = \epsilon_\infty - \sum_{k=1}^n \frac{\theta_{1k} (B_k^+ - B_k^-) - i\gamma_{tk} (B_k^+ + B_k^-)}{\omega_{tk}^2} \quad (4)$$

The relation in eq. (3a) is the generalised Lyddane-Sachs-Teller relation for a plasmon-multiphonon system. The relation in eq. (4) leads to the determination of  $\epsilon_s$  from the coupled mode parameters. Note that  $\epsilon_s$  is real and constant as can be verified by putting  $B_k^\pm = \pm a + ib$ . We developed in [10] a numerical method to determine from the discrete set of experimental data points of  $\tilde{\epsilon}$ , all the (coupled) mode parameters from the poles and zero's in the complex frequency plane and the method will be applied to measurements on  $\text{Cd}_3\text{P}_2$  and  $\text{Cd}_3\text{As}_2$ .

#### IV. Results and Discussion

A particular result of the reflectivity spectrum of  $\text{Cd}_3\text{P}_2$  is given in figure (2). Analysis of these data with the method of [10] leads to

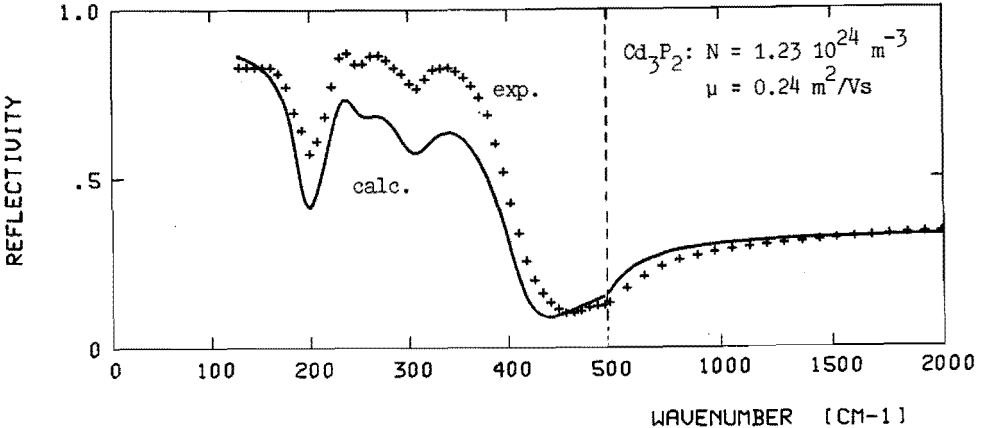


Fig. 2. Room temperature reflectivity spectrum of a particular sample of  $\text{Cd}_3\text{P}_2$ .

the following set of parameters:  $(\omega_{tj}, \gamma_{tj}) = (227, 10.6); (255, 22.2); (318, 25)\text{cm}^{-1}$  and  $(\Omega_{lj}, \Gamma_{lj}) = (195, 12.8); (248, 16.2); (303, 23.9); (417, 27.7)\text{cm}^{-1}$ . The value of  $\gamma_p$  could not be determined from the data

of the corresponding pole in the complex frequency plane because of lack of accurate experimental data near  $\nu=0$  [10]. Therefore  $\gamma_p$  was determined from the experimental value of the mobility and the known value of the effective mass of  $\text{Cd}_3\text{P}_2$  [11], leading to  $\gamma_p=69 \text{ cm}^{-1}$ . Now with all these parameters and the value of  $\epsilon_\infty=14$  (as determined from the high frequency reflectivity) the reflectivity was calculated using the dielectric function of eq. (1). The result is given as the solid line in fig. (2). It is clear that the structure in the experimental data is very well described by this reconstructed reflectivity curve but the absolute value of  $R$  does not fit completely. This might be explained by the existence of some weak TO modes near  $\nu=100 \text{ cm}^{-1}$  which do not show up at room temperature because of the high degeneracy of the samples. Therefore low temperature measurements are being prepared. From the parameters of poles and zeros the plasma frequency was calculated using equations (3a) and (3b). This leads for this particular sample to  $\omega_p=331 \text{ cm}^{-1}$  and  $\omega_p=337 \text{ cm}^{-1}$  respectively, which is in reasonable agreement with the value of  $\omega_p=377 \text{ cm}^{-1}$  calculated from transport data ( $\omega_p^2=Ne^2/\epsilon_0\epsilon_\infty m^*$ ). We measured different samples of  $\text{Cd}_3\text{P}_2$  with electron concentrations in the range of  $1-2 \cdot 10^{24} \text{ m}^{-3}$  and the analysis now always leads to 3 intrinsic TO phonon modes with reproducible parameter sets, instead of the 2 phonon modes reported in [1]. The average values of the TO phonon parameters are given in table (1) together with the average value of  $\epsilon_s$  determined from eq. (4) and the values of  $B_k^\pm$  determined from their equations given in [10]. It appears that the value of  $\epsilon_s$  reproduces within 10% from sample to sample though the values of  $B_k^\pm$  show rather large deviations. It is clear from eq. (4) that in fact from the coupled mode parameters only the difference  $\Delta\epsilon=\epsilon_s-\epsilon_\infty$  can be determined. Our value of  $\Delta\epsilon$  is in good agreement with the value of  $\Delta\epsilon=9$  reported in [2].

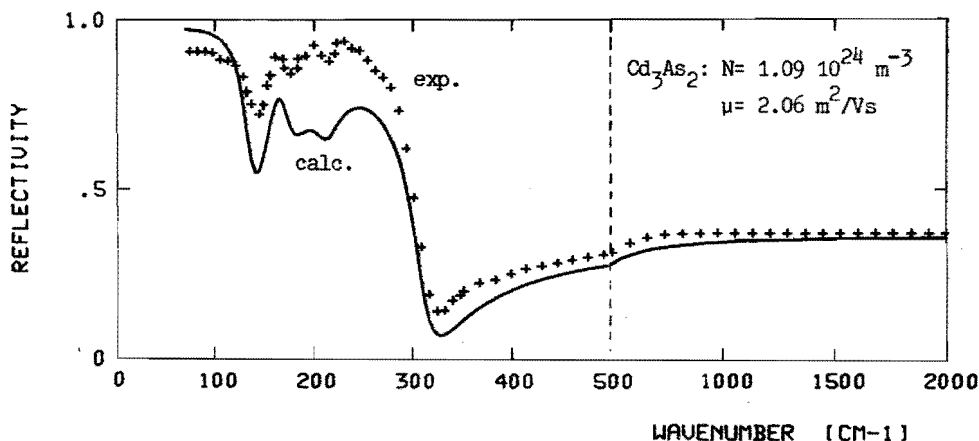


Fig. 3. Room temperature reflectivity spectrum of a particular sample of  $\text{Cd}_3\text{As}_2$ .

The same procedure as given above was applied to some  $\text{Cd}_3\text{As}_2$  samples. A typical spectrum is given in fig. (3) and the average results of the intrinsic parameters that reproduce in every spectrum are given in table (1). We were not able up to now to determine a reliable value of  $\epsilon_s$  because we have some indications that  $\text{Cd}_3\text{As}_2$  has more than 3 intrinsic TO phonon modes. At least at low temperatures two additional weak modes for  $\nu < 100 \text{ cm}^{-1}$  are present [12].

Cd <sub>3</sub> P <sub>2</sub>				Cd <sub>3</sub> As <sub>2</sub>		
j	$\omega_{tj}$ (cm <sup>-1</sup> )	$\gamma_{tj}$ (cm <sup>-1</sup> )	$B_j^{\dagger}$ (cm <sup>-1</sup> )	j	$\omega_{tj}$ (cm <sup>-1</sup> )	$\gamma_{tj}$ (cm <sup>-1</sup> )
1	227 ± 3	10.4 ± 0.2	-630(±100)-48(±5)i	1	158 ± 1	9.3 ± 0.5
2	254 ± 1	21 ± 2	-235(±15)-60(±100)i	2	189 ± 5	20 ± 5
3	319 ± 2	34 ± 10	-320(±110)-24(±11)i	3	219 ± 2	17 ± 1
$\epsilon_{\infty}=14$			$\epsilon_S=24\pm 2$	$\epsilon_{\infty}=16$		

Table 1. Average values of intrinsic mode parameters of Cd<sub>3</sub>P<sub>2</sub> and Cd<sub>3</sub>As<sub>2</sub>.

#### V. Acknowledgement

We like to thank P.A.M. Nouwens for preparation of the samples, A.H.E. Breuls for assistance with the measurements and Prof. M.J. Steenland for helpful discussions.

#### References

1. M.J. Gelten: Proc. 1st Int. Symp. on Physics and Chemistry of II-V Compounds, Mogilany, (1980) p. 133 (Editors M.J. Gelten and L. Zdanowicz).
2. J.P. Jay-Gerin, M.J. Aubin, L.G. Caron: Phys. Rev. B18 (1978) 3675.
3. J.P. Jay-Gerin, M.J. Aubin, L.G. Caron: Solid State Comm. 21 (1977) 771.
4. J. Cisowski, J. Bodnar: Phys. Stat. Sol. (a) 28 (1975) K49.
5. G.I. Goncharenko, V.Ya. Shevchenko: Sov. Phys. Semicond. 4 (1971) 1375.
6. M.J. Gelten, A. van Oosterom, C.M. van Es: Infrared Physics 16 (1976) 662.
7. A.A. Kukharskii: Sov. Phys. Sol. State 14 (1972) 1501.
8. A.A. Kukharskii: Solid State Comm. 13 (1973) 1761.
9. B.B. Varga: Phys. Rev. 137 (1965) 1896A.
10. M.J. Gelten, L.A. Bosch: to be published in Phys. Stat. Sol. (b) 106 (1981) no. 2.
11. F.A.P. Blom, J.W. Burg: J. Phys. Chem. Solids 38 (1977) 19.
12. M. von Ortenberg, private communication.

4.4

## Intrinsic phonon parameters of $\text{Cd}_3\text{P}_2$

M J Gelten and C M van Es

Department of Physics, Eindhoven University of Technology, Eindhoven, The Netherlands

Received 12 September 1983, in final form 29 December 1983

**Abstract.** Far-infrared reflectivity measurements in the frequency range  $40\text{--}650\text{ cm}^{-1}$  at  $T = 10, 100, 150$  and  $300\text{ K}$  have been performed on degenerate n-type  $\text{Cd}_3\text{P}_2$  samples. The experimental results are fitted with a model dielectric function. We use the Drude/linear oscillators equation for a coupled-plasmon-phonon system. The best fit of the theoretical curve to the experimental data is obtained using six independent transverse phonon modes with temperature-independent eigenfrequencies and oscillator strengths and temperature-dependent damping constants. For the static dielectric constant a temperature-independent value is found of  $23 \pm 1$ .

### 1. Introduction

In the past many measurements have been made in an effort to determine the shape of the conduction band of  $\text{Cd}_3\text{P}_2$ ; for example, measurements of: the thermomagnetic transport properties (Blom and Burg 1977, Radautsan *et al* 1974), optical properties (Haacke and Castellion 1964, Radoff and Bishop 1972, 1973, Gelten *et al* 1978, Gelten 1980), photoconductivity and photoluminescence (Bishop *et al* 1969), spontaneous and stimulated emission (Arushanov 1980) and magnetoabsorption (Wagner *et al* 1971). The papers mentioned above give a good insight into the band structure of the material but do not give many details about the intrinsic phonon modes and the static dielectric constant. All that can be found is some indirect information about the static dielectric constant; this is in a paper published by Jay-Gerin *et al* (1978) and up to now only two papers have been published concerning preliminary measurements of the optical properties of  $\text{Cd}_3\text{P}_2$  in the far-infrared (Gelten 1980, Gelten and van Es 1981). From the data of the last two papers it is clear that  $\text{Cd}_3\text{P}_2$  shows a rather complicated far-infrared reflectivity spectrum, determined by plasmon-phonon coupling effects between free carriers and the multiphonon system of the intrinsic material. The intrinsic phonon system of  $\text{Cd}_3\text{P}_2$  is complicated because of the large number (40) of atoms in the unit cell. There will be 117 possible optical modes, which means that a group theoretical analysis is not useful in the first instance.  $\text{Cd}_3\text{P}_2$  has a tetragonal crystal structure ( $D_{4h}^{2d}$ ), which differs only slightly from a cubic one (Lin-Chung 1971). As we can see from the literature (Heller *et al* 1971, Zdanowicz and Bodnar 1976, Arushanov *et al* 1980a, b, Singh *et al* 1982) most of the physical behaviour of  $\text{Cd}_3\text{P}_2$  is isotropic.

This paper deals with the results of a careful study of the far-infrared reflectivity spectra of degenerate n-type  $\text{Cd}_3\text{P}_2$  at various temperatures. Analysis of all the spectra leads to an accurate determination of the temperature dependence of six intrinsic phonon modes and an accurate value of the static dielectric function.

## 2. Theory

An accurate method of determining the coupled-mode parameters of a plasmon–multiphonon system is described by Gelten and Bosch (1981), starting from the factorised dielectric function given by Kukharskii (1972, 1973). This method, concerning complex poles and zeros of the dielectric function, is unfortunately not useful in our case. The reason is that we cannot apply Kramers–Kronig analysis to our experimental data because we do not have the possibility of measuring the reflectivity of the samples for  $\omega > 600 \text{ cm}^{-1}$  at temperatures below room temperature. Besides, if the phonon frequencies are too close to each other and/or the damping is very strong, the poles-and-zeros method gives just a good description of the structure of the reflectivity curve, but the absolute value from the theory does not agree with that from measurements (Gelten and van Es 1981). Therefore, we have applied the simple and straightforward method of fitting our experimental data with a theoretical curve calculated from the Drude/linear-oscillator equation.

Varga (1965) pointed out that the complex dielectric function  $\hat{\epsilon} = \epsilon_1 - i\epsilon_2$  of a coupled-plasmon–phonon system may be regarded as the sum of two separate contributions: the lattice contribution  $\hat{\epsilon}_L(\omega)$  and the free-carrier contribution  $\hat{\epsilon}_{fc}(\omega)$ . If we also take into account a general and constant background contribution given by the high-frequency dielectric constant  $\epsilon_\infty$ , the complex dielectric function is given by

$$\hat{\epsilon}(\omega) = \epsilon_\infty + \hat{\epsilon}_L(\omega) + \hat{\epsilon}_{fc}(\omega). \quad (1)$$

The free-carrier contribution is given by the Drude equation

$$\hat{\epsilon}_{fc}(\omega) = -\epsilon_\infty \omega_p^2 / (\omega(\omega - i\gamma_p)) \quad (2)$$

where  $\gamma_p$  is the plasmon damping constant, related to the mobility  $\mu$  of the free carriers by  $\gamma_p = e/m^* \mu$ , and  $\omega_p$  is the plasma frequency defined by  $\omega_p^2 = Ne^2/m^* \epsilon_0 \epsilon_\infty$  ( $N$  is the free-carrier concentration and  $m^*$  is the effective mass).

For the lattice part of the dielectric function we make use of the sum equation of classic linear oscillators for our multiphonon system:

$$\hat{\epsilon}_L(\omega) = -\sum_{j=1}^n \frac{f_j \omega_{ij}^2}{\omega^2 - \omega_{ij}^2 - 2i\Gamma_j \omega}. \quad (3)$$

Here  $n$  is the number of intrinsic TO phonon modes, while the intrinsic transverse eigenfrequency, the oscillator strength and the damping constant of  $j$ th phonon are given by  $\omega_{ij}$ ,  $f_j$  and  $\Gamma_j$  respectively. The static dielectric constant  $\epsilon_s$  is now given by

$$\epsilon_s = \epsilon_\infty + \sum_{j=1}^n f_j. \quad (4)$$

The reflectivity  $R$  at normal incidence is given by

$$R = \left| \frac{[\hat{\epsilon}(\omega)]^{1/2} - 1}{[\hat{\epsilon}(\omega)]^{1/2} + 1} \right|^2. \quad (5)$$

Data from the experimental equipment were fed directly into a computer. By means of the equations (1)–(5) we calculate the reflectivity  $R$  with a given set of parameters for phonons and the plasmon. The calculated spectra are compared with these data points by plotting both on a large display. The best fit is determined by visual comparison. By changing the parameters for phonons and the plasmon separately it is possible to determine an accuracy interval for each parameter.

### 3. Experimental arrangement

The preparation of single-crystalline samples of  $\text{Cd}_3\text{P}_2$  was described in a previous paper (Gelten *et al* 1978). Because we do not expect a significant anisotropy effect the measurements were performed with unpolarised radiation and unoriented samples. After polishing, the sample was etched in a 15% bromine-ethanol solution. The electron concentration  $N$  and the mobility  $\mu$  were measured at room temperature by means of the four-point van der Pauw method (van der Pauw 1958). The reflectivity measurements were performed on a Grubb-Parsons Fourier Transform Spectrometer in the wave-number range  $40\text{--}650\text{ cm}^{-1}$  by using mylar beam-splitters of various thicknesses. By varying the number of sample points and the displacement of the moving mirror the resolution of the spectra after Fourier transformation with  $\cos^2$  apodisation is made adjustable. The experimental arrangement is given in figure 1.

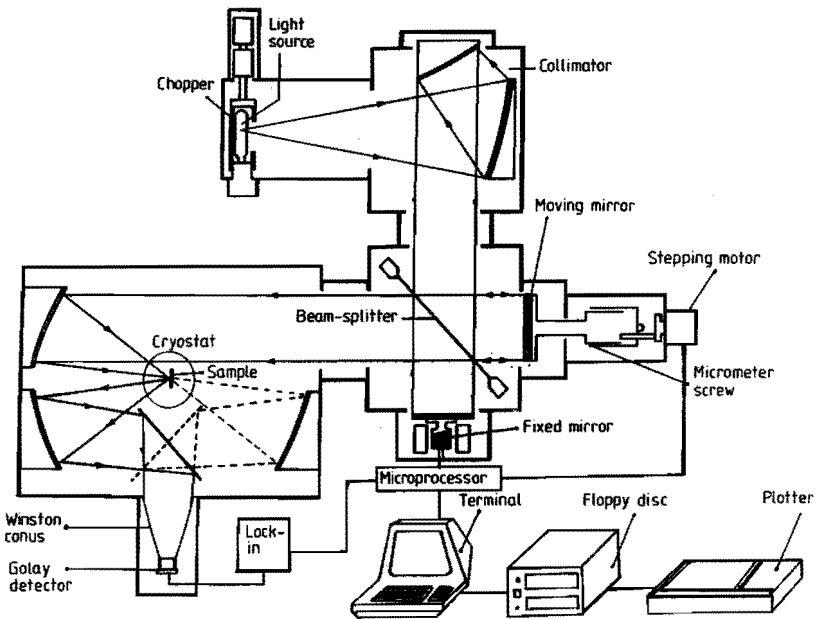


Figure 1. Experimental arrangement. The fixed mirror is vibrating at phase modulation.

The sample chamber was equipped with an adjustable continuous-flow cryostat (Oxford Instruments CF 104) and the measurements were done at temperatures  $T = 10, 100, 150$  and  $300\text{ K}$ . The cryostat was modified as indicated in figure 2. The samples and aluminium calibrating mirror were mounted in a reproducible way. To prevent undesirable reflections the diaphragm and the sample holder were covered with black felt and optical black varnish. The interferometer and the sample chamber were evacuated to a pressure  $p < 10\text{ Pa}$  to prevent intensity loss owing to water-vapour absorption and freezing of water vapour at lower temperatures.



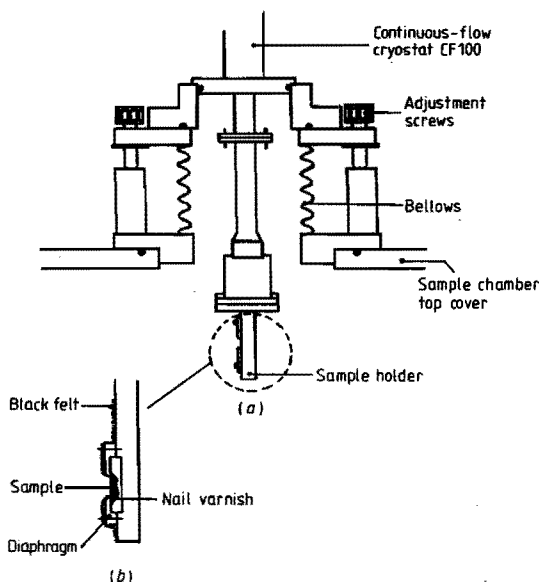


Figure 2. Continuous-flow cryostat for Grubb-Parsons sample chamber. (a) General view. (b) Sample mount.

#### 4. Results and discussion

In figure 3 the reflectivity  $R$  of a typical sample of  $\text{Cd}_3\text{P}_2$  is presented for various temperatures. With a temperature-independent value of  $\epsilon_\infty$  of 14 (Gelten *et al* 1978) we calculate the reflectivity  $R$  using the dielectric function given by equation (1). Because of the plasmon-phonon interaction we have also taken the plasma frequency  $\omega_p$  and the plasmon damping constant  $\gamma_p$  as fitting parameters. Best fits to the data points lead to the sets of phonon-mode parameters given in table 1. From these careful measurements, especially below room temperature, we found conclusive evidence for six intrinsic modes instead of the three modes reported earlier (Gelten and van Es 1981). In general there is a good agreement between the calculated spectra and the data points in the whole wavenumber region. In figure 3 the calculated spectra are shown by full curves.

The large discrepancy between experimental and calculated data in the region  $\omega < 150 \text{ cm}^{-1}$  is mainly caused by deviations of the experimental arrangement as a consequence of the large decrease in radiation intensity.

Because the phonon dips are most pronounced at 10 K, the first parameter set in the fitting procedure is determined at this temperature. The data at higher temperatures could be described very well with the same values of eigenfrequencies and oscillator strengths, while the phonon damping constants increase with increasing temperature. This latter effect agrees with the theory, because the damping constant  $\Gamma_j$ , which is proportional to the lifetime broadening of the phonons, increases at higher temperatures. So the phonon dips look more pronounced at lower temperatures.

From table 1 we can see that there is a reasonable agreement between the transverse eigenfrequencies obtained with the poles-and-zeros method and the method described in this paper. The oscillator strengths and the phonon damping constants are not

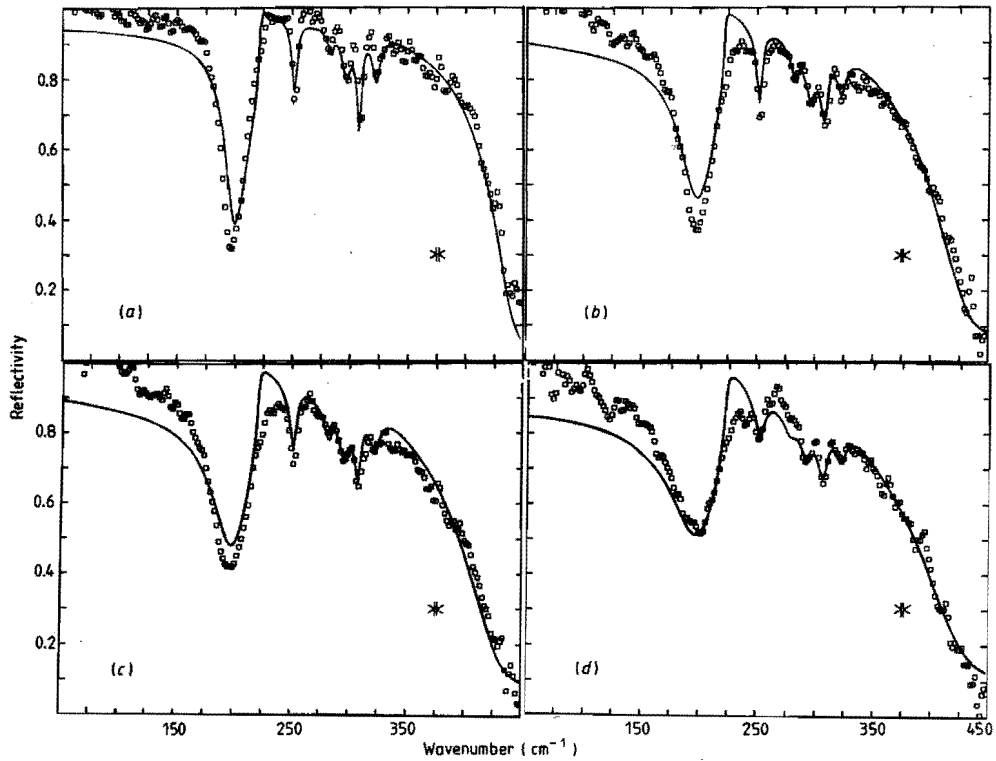


Figure 3. Reflectivity  $R$  at  $T = (a)$  10,  $(b)$  100,  $(c)$  150 and  $(d)$  300 K.

**Table 1.** Sets of phonon parameters of  $\text{Cd}_3\text{P}_2$  (upper part) and sets of plasmon parameters of a particular sample (lower part) at various temperatures. The  $\omega_j$ ,  $\Gamma_j$ ,  $\alpha_j$  and  $\gamma_j$  are in  $\text{cm}^{-1}$ . The  $f_j$  are dimensionless.

$T$	10 K	100 K	150 K	300 K	†	‡
$\omega_{\alpha 1}$	222	222	222	222	$\pm 1$	227
$f_1$	7.5	7.5	7.5	7.5	$\pm 0.5$	5.6
$\Gamma_{11}$	0.3	0.4	0.5	1.0	$\pm 0.1$	10.4
$\omega_{\alpha 2}$	254	254	254	254	$\pm 1$	254
$f_2$	0.7	0.7	0.7	0.7	$\pm 0.1$	1.9
$\Gamma_{12}$	2.5	2.5	3.0	5.0	$\pm 0.5$	21
$\omega_{\alpha 3}$	284	284	284	279	$\pm 1$	—
$f_3$	0.05	0.10	0.10	0.10	$\pm 0.05$	—
$\Gamma_{13}$	2.0	3.0	3.0	5.0	$\pm 0.5$	—
$\omega_{\alpha 4}$	298	298	298	294	$\pm 1$	—
$f_4$	0.15	0.20	0.20	0.20	$\pm 0.05$	—
$\Gamma_{14}$	4.0	5.0	5.0	6.0	$\pm 0.5$	—
$\omega_{\alpha 5}$	310	310	310	309	$\pm 1$	—
$f_5$	0.20	0.20	0.20	0.20	$\pm 0.05$	—
$\Gamma_{15}$	2.0	3.0	3.0	4.0	$\pm 0.5$	—
$\omega_{\alpha 6}$	324	324	324	324	$\pm 1$	319
$f_6$	0.15	0.15	0.15	0.15	$\pm 0.05$	2.0
$\Gamma_{16}$	4.0	5.0	5.0	6.0	$\pm 0.5$	34
$\epsilon_s$	22.75	22.85	22.85	22.85		$24 \pm 2$
$\omega_p$ §	363	366	368	378		
$\omega_p$ ¶	380	367	367	367	$\pm 5$	
$\gamma_p$ §	—	22	27	71		
$\gamma_p$ ¶	45	80	90	120	$\pm 10$	

† Accuracy interval in the fitting procedure.

‡ Preliminary results, after Gelten and van Es (1981).

§ Calculated with the band parameters given by Gelten *et al* (1978).

|| Accuracy in  $\omega_p$  and  $\gamma_p$  at any temperature 5 and 10%, respectively.

¶ Determined from the fitting procedure.

comparable because of the misfit of the absolute value of the reflectivity in the poles-and-zeros method. In spite of this misfit there is a good agreement of the values of the contribution  $\Sigma f_j$  to the static dielectric constant, which is also in excellent agreement with the value found by Jay-Gerin *et al* (1978). It is not surprising that there is a good agreement between the values of  $\epsilon_s$  determined from the poles-and-zeros method and the method of this paper, because the total contribution of the phonon modes for  $\omega > 270 \text{ cm}^{-1}$  is small in comparison with the contribution of the two phonons at 222 and  $254 \text{ cm}^{-1}$ . The error in the static dielectric constant  $\epsilon_s$  of  $\pm 1$  is an average value of the errors in the best fits of various samples.

For this particular sample the room-temperature carrier concentration and mobility were  $N = (1.2 \pm 0.1) \times 10^{24} \text{ m}^{-3}$  and  $\mu = (0.24 \pm 0.02) \text{ m}^2 \text{ V}^{-1} \text{ s}^{-1}$  respectively. Blom and Burg (1977) showed that for samples with carrier concentration  $N > 10^{24} \text{ m}^{-3}$  the concentration does not change with temperature, while the mobility is inversely proportional to the temperature in the temperature range 100–300 K. Taking into account

the band parameters of  $Cd_3P_2$  given by Gelten *et al* (1978) we calculated the plasma frequency and the plasmon damping constant for the various temperatures. There is a good agreement between the calculated values and the values determined by the fitting procedure for the plasma frequency (see table 1). So we can conclude that the values of  $\omega_p$  obtained from our optical data are in good agreement with the carrier concentration of the bulk material. This means that there is no indication of the existence of a surface layer on  $Cd_3P_2$  in contrast to  $Cd_3As_2$  (Schleypen *et al* 1984).

The values of  $\gamma_p$  calculated from the electrical data do not agree with the values fitted to the optical data. Only the temperature dependence of  $\gamma_p$  agrees with the temperature dependence of the mobility found by Blom and Burg (1977). A possible explanation is that mechanical strain and surface damage result in a lower mobility and thus in a higher damping constant at the surface.

## 5. Conclusions

In conclusion we can say that the reflectivity spectra of  $Cd_3P_2$  show a coupling between the plasmon and the multiphonon system. The measurements can be explained theoretically very well with a combination of the Drude equation and a sum of linear oscillators for the dielectric function of the free carriers and phonons, respectively. The fitting procedure results in conclusive evidence for six intrinsic phonon modes with temperature-independent transverse eigenfrequencies and oscillator strengths, whereas the phonon damping constants are dependent on temperature. Using the band-parameter set of  $Cd_3P_2$  given by Gelten *et al* (1978) there is an excellent agreement between the calculated and measured plasma frequencies.

The value of the static dielectric constant is independent of temperature and is given by  $\epsilon_s = 23 \pm 1$ .

## Acknowledgments

The authors are indebted to P A M Nouwens for the preparation of the crystals, to B Eggen and L Konings for assistance with the measurements and to Professor Dr M J Steenland for a careful reading of the manuscript.

## References

- Arushanov E K, Kulyuk L L, Nateprov A N, Radautsan S I and Shtanov A A 1980a *Proc. 1st. Int. Symp. Physics and Chemistry of II-V Compounds (Mogilany) 1980* ed. M J Gelten and L Zdanowicz (Eindhoven: Eindhoven University of Technology) pp 179–82
- Arushanov E K, Lashkhal A V, Mashovets D V, Nataprov A N, Radautsan S I and Sologub V V 1980b *Phys. Status Solidi b* **102** K121–4
- Bishop S G, Moore W J and Swiggard E M 1969 *Proc. 3rd. Int. Conf. Photoconductivity* ed. E M Bell (Oxford: Pergamon)
- Blom F A P and Burg J W 1977 *J. Phys. Chem. Solids* **38** 19–25
- Gelten M J 1980 *Proc. 1st. Int. Symp. Physics and Chemistry of II-V Compounds (Mogilany) 1980* ed. M J Gelten and L Zdanowicz (Eindhoven: Eindhoven University of Technology) pp 133–41
- Gelten M J and Bosch L A 1981 *Phys. Status Solidi b* **106** 635–45
- Gelten M J and van Es C M 1981 *Proc. 4th. Int. Conf. Physics of Narrow Gap Semiconductors (Linz) 1981* ed. E Gornik, H Heinrich, L Palmethofer (Berlin: Springer) pp 167–71

- Gelten M J, van Lieshout A, van Es C M and Blom F A P 1978 *J. Phys. C: Solid State Phys.* **11** 227-37
- Haacke G and Castellion G A 1964 *J. Appl. Phys.* **35** 2484-7
- Heller M W, Babiskin J and Radoff P L 1971 *Phys. Lett.* **36A** 363-4
- Jay-Gerin J-P, Aubin M J and Caron L-G 1978 *Phys. Rev. B* **18** 5675-84
- Kukharskii A A 1972 *Sov. Phys.-Solid State* **14** 1501-6
- 1973 *Solid State Commun.* **13** 1761-5
- Lin-Chung P J 1971 *Phys. Status Solidi b* **47** 33-9
- van der Pauw L J 1958 *Philips Res. Rep.* **13** 1-9
- Radautsan S I, Arushanov E K and Nateprov A N 1974 *Phys. Status Solidi a* **23** K59-61
- Radoff P L and Bishop S G 1972 *Phys. Rev. B* **5** 442-8
- 1973 *Mater. Res. Bull.* **8** 219-28
- Schleypen H M A, von Ortenberg M, Gelten M J and Blom F A P 1984 *Int. J. Infrared and Millimetre Waves* **5** 171-83
- Singh M, Cisowski J, Wallace P R, Portal J C and Broto J M 1982 *Phys. Status Solidi b* **114** 481-6
- Varga B B 1965 *Phys. Rev.* **137** A1896-902
- Wagner R J, Palik E D and Swiggard E M 1971 *The Physics of Semimetals and Narrow Gap Semiconductors* ed. D L Carter and R T Bate (Oxford: Pergamon)
- Zdanowicz W and Bodnar J 1976 *Acta Phys. Polon. A* **49** 3-7

## 4.5 MAGNETOPLASMA REFLECTIVITY STUDIES ON $\text{Cd}_3\text{As}_2$

**H. M. A. Schleijsen,<sup>\*,\*\*</sup> M. von Ortenberg,<sup>+,\*\*</sup>  
M. J. Gelten,<sup>\*\*</sup> and F. A. P. Blom<sup>\*\*</sup>**

*\*Max Planck Institut für Festkörperforschung, Hochfeld  
Magnet Labor F-38042 Grenoble, France*

*\*\*Department of Physics, Eindhoven University of Technology,  
5600 MB Eindhoven, The Netherlands*

Received October 19, 1983

Magnetoplasma reflectivity measurements were performed on  $\text{Cd}_3\text{As}_2$  in order to obtain more experimental details about the structure of the plasma reflectivity edge. The experimental results can be explained by assuming the existence of a surface layer with a carrier concentration-gradient which is responsible for optical interference effects.

Key Words: surface layer, magnetoplasma effect, FIR fourier transform spectroscopy

### Introduction

$\text{Cd}_3\text{As}_2$  is a degenerate n-type semiconductor of the II-V-family. In recent years considerable work has been devoted to this narrow-gap semiconductor, see e.g. [1,2]. Reflectivity studies of the plasma edge of  $\text{Cd}_3\text{As}_2$  often showed additional structures in the region of the plasma minimum, which could not be explained satisfactory [3-5]. In reflectivity measurements by the Eindhoven group these structures were observed as well. In order to get a better understanding of this phenomenon, we studied the behaviour of these structures in magnetic fields. This paper deals

\* on leave from Dept. of Physics, University of Technology, 5600 MB Eindhoven, the Netherlands

\*\* on leave from University of Würzburg, D8700 Würzburg, FRG

with the results of numerous measurements and a model for the interpretation.

### Experimental set-up

We measured the magneto reflectivity spectra in the wavenumber range of 100 to 700  $\text{cm}^{-1}$ , using a rapid-scan Fourier Transform Spectrometer. The FIR-radiation was guided by lightpipes to the sample in a superconducting magnet. The sample was placed as shown in fig. 1 in a special mount fitted with a carbon glass bolometer detector [15]. We measured in Faraday configuration, using unpolarised light. The spectra were taken for temperatures below 2 K. The spectrometer was not calibrated carefully so that the absolute values of the reflectivity may differ from the indicated values by several percent.

Single-crystalline samples of  $\text{Cd}_3\text{As}_2$  were ground and polished with 1.0 and 0.25  $\mu\text{m}$  diamond powder. To etch the sample surface we used either a 15% bromine-methanol solution or a Honeywell etching liquid, consisting of 100 g  $\text{CrO}_3$ , 132 g  $\text{HCl}$  (32%) and 266 g  $\text{H}_2\text{O}$  [6].

The carrier concentration  $N$  and the Hall mobility  $\mu$  of the samples were measured at room temperature by the van der Pauw method [7] and are given in table 1.

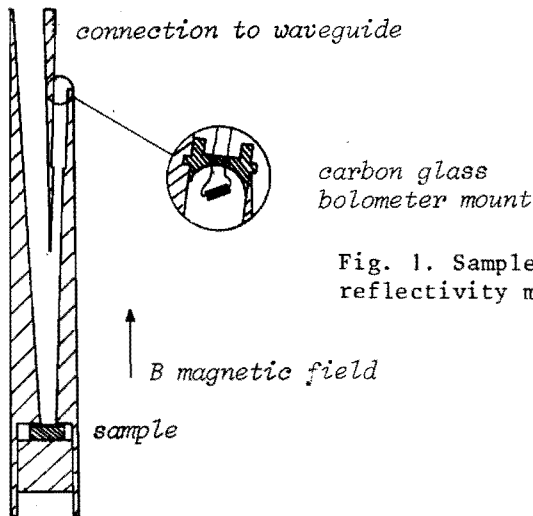


Fig. 1. Sample holder for reflectivity measurements.

TABLE I: Data of the samples

sample no.	N (m <sup>-3</sup> ) at 300 K	$\mu$ (m <sup>2</sup> /Vs)	crystal orientation surface plane
AS 65-7	1.3 . 10 <sup>24</sup>	1.9 (T=300 K)	(1,7,6)
AS 57-2	1.9 . 10 <sup>24</sup>	1.8 (T=300)	(0,0,1)
AS 64-5	0.34 . 10 <sup>24</sup>	27 (T=4.2)	(k,1,0)

### Experimental results

In fig. 2a reflectivity spectra of the high carrier concentration sample AS 57-2 are shown for different magnetic fields. These are some of the rare spectra without additional structures in the plasma minimum. Since we used unpolarised light, which can be decomposed into two modes, the plasma edge splits and shifts to lower wavenumbers for the cyclotron resonance inactive (CRI) mode and to higher wavenumbers for the cyclotron resonance active (CRA) mode. The positions of the plasma minima are indicated by arrows. In the wavenumber range of 100 to 250 cm<sup>-1</sup> we observe phonondips in the reflectivity in accordance with roomtemperature measurements given in [11].

In fig. 2b spectra of the same sample are shown. Now the sample was freshly etched in the Honeywell etching liquid and the structures in the plasma minimum appear. The same is found when etching with bromine-methanol. The arrows mark the positions of the plasma minima of the spectra of fig. 2a. When increasing the magnetic field, we observe that the structures shift over the same distance as the original plasma minima. Therefore we conclude that the structures are pinned to the plasma edge. Besides, we observe that the plasma edge itself tends to shift to lower frequencies when the structures appear.

Fig. 2c shows spectra of sample AS 65-7, with a high carrier concentration, etched in the bromine-methanol solution. Now for high magnetic fields, the structures, pinned to each of the plasma edges, are completely separated. We clearly observe that the structures show an oscillatory behaviour. The period of these oscillations decreases with increasing wavenumber. Besides we see that the amplitude of the oscillations in the CRA mode decreases with increasing magnetic field.

Fig. 2d shows spectra of a low-carrier concentration sample (AS 64-5) with the same behaviour of the oscillations. For high magnetic fields ( $B \geq 8T$ ) the structures even



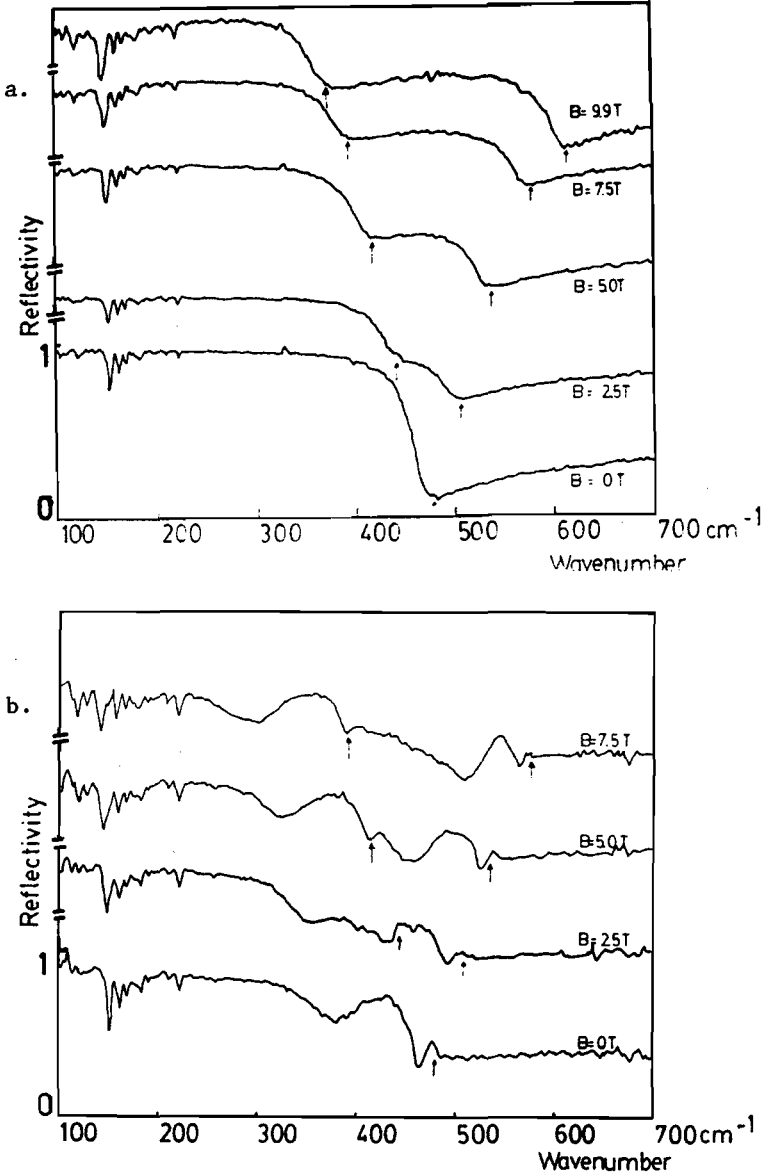


Fig.2. a,b. Reflectivity spectra for different magnetic fields, a) sample AS57-2 unetched, b) sample AS57-2 after Honeywell etching. Note that the spectra are shifted in vertical position.

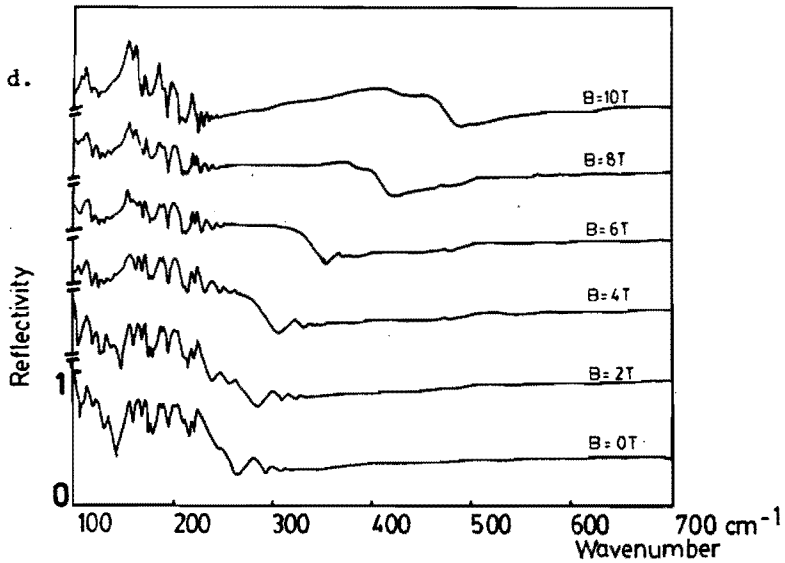
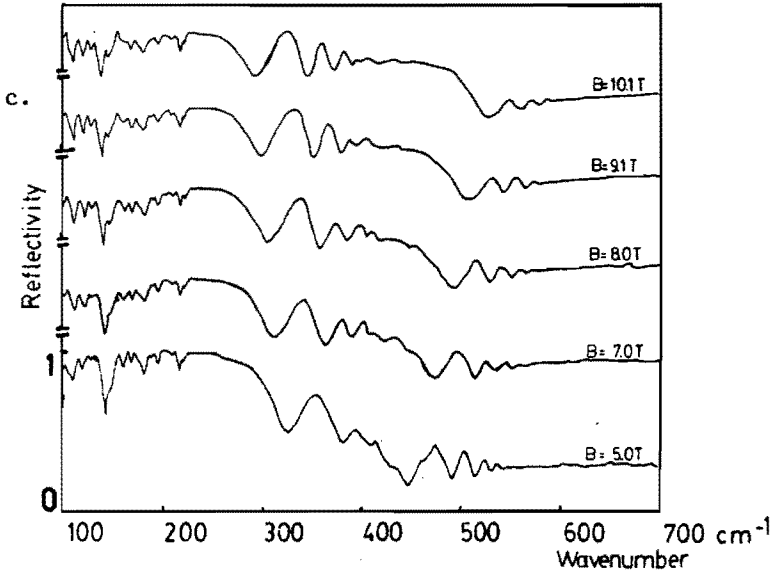


Fig.2. c,d. Reflectivity spectra for different magnetic fields, c) high concentration sample AS65-7, d) low concentration sample 64-5. Note that the spectra are shifted in vertical position.

disappear in the CRA-mode. It should be noted that the results of fig. 2 are typical for  $\text{Cd}_3\text{As}_2$ . Measurements on numerous other  $\text{Cd}_3\text{As}_2$  samples showed similar results.

From previous room temperature reflectivity measurements we determined the plasma frequency  $\omega_p$  of several samples. These optical plasma frequencies were mostly smaller than the plasma frequencies calculated from transport measurement data of these samples. The difference in frequency was greater according as the structures in the plasma edge appeared more clearly. Only in cases without structures the optical and transport plasma frequencies were almost equal to each other. This suggests that the carrier concentration near the surface is smaller than in the bulk material. In such a case a surface depletion layer exists, which will be transparent for I.R. radiation with frequencies in the range between the surface- and bulk-dielectric anomaly (equivalent to the plasma frequency). In this layer optical interference effects can occur. The concept of a surface layer with a low carrier concentration is in agreement with experimental data, which show that the carrier concentration rapidly decreases when the sample thickness becomes smaller than  $20 \mu\text{m}$  [12]. In these measurements the thickness was reduced by lapping and the carrier concentration was determined by the van der Pauw method.

### Theoretical model

Model spectra, calculated with a homogeneous surface layer of about  $10 \mu\text{m}$  thickness, did not show the decreasing oscillation period of the structures as we observed in our measurements.

A better model was developed in which the carrier concentration varies monotonically near the surface. The carrier concentration is assumed to be given by

$$N(z) = N_b + (N_s - N_b)\exp(-z/d) \quad (1)$$

where  $N_b$  and  $N_s$  are the carrier concentration in the bulk and at the surface, respectively,  $z$  is the distance from the surface and  $d$  is an effective surface layer thickness.

The reflectivity  $R$  is completely determined by the  $z$ -dependent dielectric function  $\epsilon(\omega, z)$  as given by:

$$\epsilon(\omega, z) = \epsilon_\infty + \epsilon_{fc}(\omega, z) + \epsilon_{ph}(\omega) \quad (2)$$

where  $\epsilon_\infty$  is the high frequency dielectric constant, equal

to 16 [11],  $\epsilon_{fc}$  and  $\epsilon_{ph}$  are the free carrier and the phonon contribution to  $\epsilon(\omega, z)$  respectively.  $\epsilon_{fc}$  is given by the Drude-model:

$$\epsilon_{fc}(\omega, z) = \frac{-e^2 N(z)}{\epsilon_0 m^*(z)} \cdot \frac{1}{\omega(\omega \pm \omega_c - i\gamma)} \quad (3)$$

where  $\omega_c = eB/m^*(z)$  is the cyclotron frequency and  $\gamma$  is the damping constant of the plasmon, which might be also dependent on  $z$ . Because  $\gamma$  does not shift the plasma edge strongly it is taken as a constant.  $\epsilon_{ph}$  is given by a sum of linear oscillators:

$$\epsilon_{ph}(\omega) = \sum_{i=1}^N \frac{\Delta\epsilon_i \omega_i^2}{\omega_i^2 - \omega^2 + 2i\omega\Gamma_i} \quad (4)$$

where  $\omega_i$  is the wavenumber of the transverse mode for each phonon,  $\Delta\epsilon_i$  is the oscillator strength and  $\Gamma_i$  is the damping parameter. In our calculations we have used the numerical values of the phonon parameters given in table 2. These results were obtained from low temperature measurements [10].

TABLE II: Phonon parameters of Cd<sub>3</sub>As<sub>2</sub> at low temperature

Phonon parameters for Cd<sub>3</sub>As<sub>2</sub> from [10] (T=10K)

i	$\omega_i$	$\Delta\epsilon_i$	$\Gamma_i$
1	152 cm <sup>-1</sup>	2.8	0.9 cm <sup>-1</sup>
2	160 "	1.0	1 "
3	169 "	0.8	2 "
4	182 "	1.0	3 "
5	217 "	0.5	8 "

In Cd<sub>3</sub>As<sub>2</sub> the effective mass is dependent on the carrier concentration. In our calculations we have taken the numerical results for the effective mass of [2] and [13].

In our calculation the actual carrier concentration profile is replaced by a large number (typically 100) of uniform layers. The total reflectivity is obtained by solving the set of equations given by the boundary condi-

tions for the E.M. waves at the interfaces of the layers [14].

To check our method we compared our calculated spectra for various carrier concentration profiles with spectra obtained by Hild et al. [8] who numerically solved the differential equation for the E.M. waves in these profiles.

### Results and discussion

A large number of magnetorefectivity spectra were calculated and two typical sets of spectra are presented in fig. 3a,b. Fig. 3a shows spectra for a high carrier concentration sample (compare with fig. 2a and 2b). These spectra were calculated from the dielectric function without phonon contribution. We clearly see that the oscillatory structures are pinned to the plasma edge which splits and shifts with increasing magnetic field. We observe the decreasing period with increasing wavenumber and the decreasing amplitude in the CRA mode at higher magnetic fields.

Fig. 3b shows spectra for a low carrier concentration sample (compare with fig. 2d). Here the phonon contribution was taken explicitly into account. In these spectra we observe again the decreasing period of the oscillatory structures, indicated by arrows in the zero field spectrum. The structures are again pinned to the plasma edge and disappear in the CRA mode at high magnetic fields.

The disappearance of the structures for the CRA mode with increasing field can be understood from the shift of the plasma edge dielectric anomaly in magnetic fields. The position of this dielectric anomaly for the CRA mode is given by:

$$\omega_+(z) = \omega_c/2 + (\omega_p^2 + \omega_c^2/4)^{1/2} = \frac{eB}{2m^*(z)} + \left[ \frac{e^2 N(z)}{\epsilon_\infty \epsilon_0 m^*(z)} + \left( \frac{eB}{2m^*(z)} \right)^2 \right]^{1/2} \quad (5)$$

For zero field the difference in wavenumber of the dielectric anomaly for bulk and surface is only determined by the carrier concentration difference  $N_b - N_s$ . With increasing magnetic field the dielectric anomaly shifts according to eq. 5. The cyclotron frequency is proportional to the reciprocal of the effective mass. The effective mass is smaller for the low carrier concentration near the surface than for the high carrier concentration in the bulk. Conse-

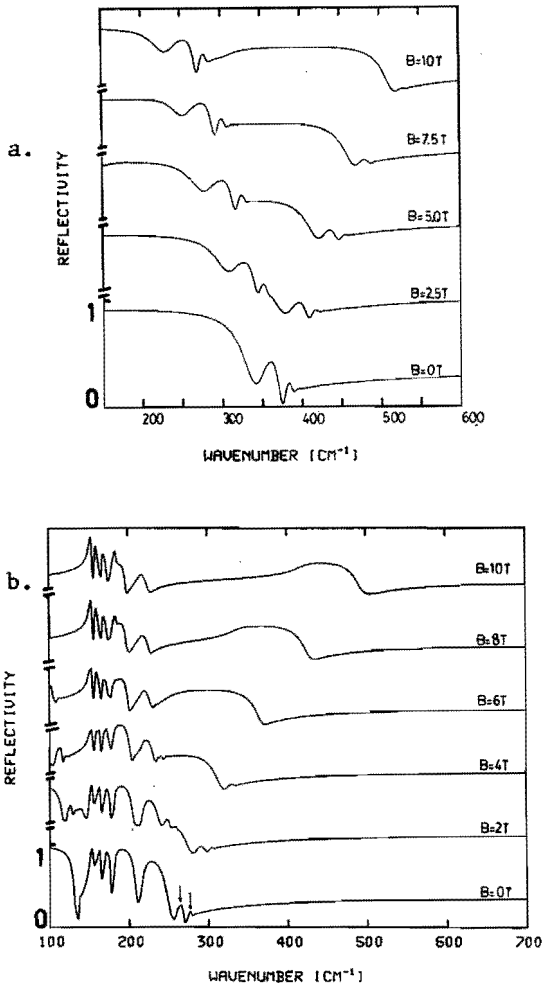


Fig.3. Calculated magnetorefectivity spectra of different samples.

- a) High carrier concentration sample  $N_b = 1.10^{24} \text{ m}^{-3}$ ,  
 $N_s = 5.10^{23} \text{ m}^{-3}$ ,  $d = 10 \text{ } \mu\text{m}$ ,  $\gamma = 10 \text{ cm}^{-1}$   
 No phonon contribution included.
- b) A low carrier concentration sample  $N_b = 3.1.10^{23} \text{ m}^{-3}$ ,  
 $N_s = 1.4.10^{23} \text{ m}^{-3}$ ,  $d = 20 \text{ } \mu\text{m}$ ,  $\gamma = 10 \text{ cm}^{-1}$   
 Phonons included according to table 2.

quently the cyclotron frequency will be larger near the surface and from eq. 5 the shift of the dielectric anomaly will be larger at the surface than in the bulk. So the difference in wavenumber between surface- and bulk-dielectric anomaly will decrease with increasing magnetic field and eventually vanish. In this case the gradient of the dielectric function in the surface layer and consequently the gradient in the refractive index will almost disappear. Thus, the interference effects will vanish.

For low carrier concentrations the effective mass varies more strongly with the carrier concentration and the ratio between bulk- and surface effective mass will be larger than for high carrier concentration samples with the same  $N_b/N_s$  ratio. Thus according to eq. 5 the difference in wavenumber between surface and bulk dielectric anomaly and consequently the oscillations will vanish for smaller magnetic fields, in agreement with the experimental data. In fig. 4 we plotted  $\omega_+$  as a function of the magnetic field  $B$ , for the parameters used in the model calculation (see fig. 3). The arrows in fig. 4 indicate the fields where the oscillations disappear. So we may conclude that our model

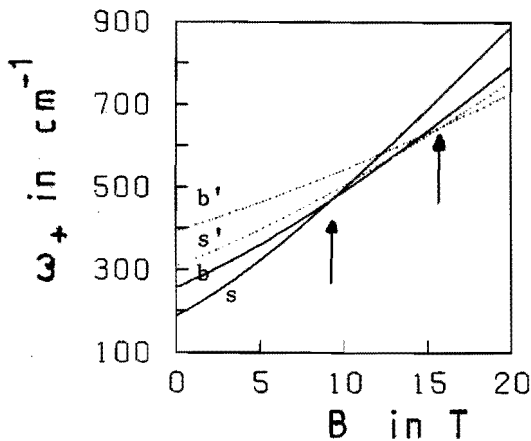


Fig. 4. Shift of the surface and bulk dielectric anomaly in magnetic fields for a low carrier concentration sample (solid lines)  $s$  = surface,  $N_s = 1.4 \cdot 10^{23} \text{ m}^{-3}$ ,  $b$  = bulk,  $N_b = 3.1 \cdot 10^{23} \text{ m}^{-3}$  and for a high carrier concentration sample (dotted lines)  $s'$  = surface  $N_s = 5 \cdot 10^{23} \text{ m}^{-3}$ ,  $b'$  = bulk  $N_b = 1 \cdot 10^{24} \text{ m}^{-3}$ .

describes at least qualitatively all experimental data. However, the origin of the surface layer is not clear up to now, especially if we realize that the effective thickness is about 10 to 20  $\mu\text{m}$ , which is very large.

In Cd<sub>3</sub>As<sub>2</sub> a carrier concentration profile with such a large effective thickness may be caused by a surface layer in another crystallographic phase than the bulk material. A mixed phase between these two phases might cause such a thick layer with gradually changing carrier concentration. There is evidence that under certain circumstances the  $\alpha''$ -phase for Cd<sub>3</sub>As<sub>2</sub> exists at room temperature together with the  $\alpha$ -phase [9].

This phenomenon is only known for Cd<sub>3</sub>As<sub>2</sub> and does not exist in other II-V compounds. This may be the reason why the effect of oscillations near the plasma edge has only been observed in the material Cd<sub>3</sub>As<sub>2</sub>.

#### Conclusions

We have obtained more experimental data to get a better insight in the oscillatory behaviour of the plasma edge of Cd<sub>3</sub>As<sub>2</sub>. We have proposed a simple model with a carrier concentration profile near the surface which explains at least qualitatively all experimental magneto reflectivity data. The origin of the rather thick surface layer of some  $\mu\text{m}$  is still a problem.

#### Acknowledgement

We greatly acknowledge the assistance of P.A.M. Nouwens for growing the crystals. We would like to thank C.M. van Es for many helpful discussions and assistance with the numerical calculations.



### References

1. Proc. of 1st. Symposium on Physics and Chemistry of II-V compounds, Mogilany, Poland, ed. by M.J. Gelten and L. Zdanowicz Eindhoven University of Technology, 1980.
2. F.A.P. Blom, Lecture notes in Physics 133 ed. by W. Zawadzki (Springer Verlag New York 1980) p. 191.
3. E.D. Haidemenakis, M. Balkanski, E.D. Palik, J. Tavernier in Proc. Int. Conf. on Semicond. Kyoto 1966, Journal of Phys. Soc. of Japan 21 Suppl. 189 (1966).
4. G.I. Goncharenko, M.I. Elinson, V.I. Kovalev, V.Y. Shevchenko Sov. Phys. Semicond. 5, 1431 (1972).
5. J. Thielemann, M. v. Ortenberg, F.A.P. Blom, K. Strobel, Proc. Conf. Physics of Narrow Gap Semicond., Linz Austria 1981 ed. by E. Gornik p. 207.
6. A.F. Bogenschütz Aetzpraxis für Halbleiter, Carl Hauser München (1967).
7. L.J. v.d. Pauw, Philips Res. Rep. 13, 1 (1958).
8. F. Hild, A. Grofcsik, Infrared Physics 18, 23 (1978).
9. L. Zdanowicz, A. Kierski, J. Sturc in [1] p. 79.
10. L. Konings, M.J. Gelten and C.M. v. Es, internal report Eindhoven University of Technology (1982) in Dutch.
11. M.J. Gelten, C.M. v. Es, Proc. Int. Conf. on the Physics of Narrow Gap Semicond. Linz Austria, 1981 ed. by E. Gornik p. 167.
12. M.G. Menting, internal report Eindhoven University of Technology (1978) in Dutch.
13. M.J. Gelten, C.M. v. Es, F.A.P. Blom and J.W.F. Jongeneelen, Sol. St. Comm. 33. 833 (1980).

14. H. Mayer, Physik dünner Schichten, Wissenschaftliche Verlagsgesellschaft Stuttgart 1950.
15. J.P. Kotthaus, C. Gaus, P. Stallhofer in Physics in High Magnetic Fields, proceedings of the Oji International Seminar on the Application of High Magnetic Fields in the Physics of Semiconductors and magnetic materials, Hakone 1980, ed. by S. Chikazumi and N. Miura, Springer Verlag Berlin 1981, p. 118.

## CHAPTER 5. RECENT DEVELOPMENTS: THE BODNAR MODEL

In spite of the tetragonal crystal structure and the early observation of the conduction band anisotropy by Rosenman {36} and Doi et al. {37}, most of the experimental data have been interpreted in terms of the isotropic Kane type band model. At the start of our research program this band model was the best one available for application to experimental data. Especially sections 3.3 and 3.4 show the success of this model by combining optical with electrical transport data. It has been shown in chapter 3 that some modifications of the Kane model sufficed to make it suitable for the description of our interband optical data.

After completion of this part of our work Bodnar published the results of a calculation of the band structure for tetragonal narrow gap semiconductors {38}. This model was based on the k.p approximation, similar to the Kane model, and took into account the tetragonal crystal field splitting. The anisotropic Bodnar model was experimentally verified for  $Cd_3As_2$  by Shubnikov-de Haas measurements, see e.g. Blom and Gelten {39}, Blom et al. {40} and the thesis of Neve {10}. Following the generally accepted convention for the notation of the Bodnar equation {10}, the bands  $c$ ,  $v_1$ ,  $v_2$  and  $v_3$  defined in chapter 3 are now given by the following expression, valid near the center of the Brillouin zone.

$$\gamma(E') = f_1(E')(k_x^2 + k_y^2) + f_2(E')k_z^2 \quad (5.1)$$

with

$$\gamma(E') = E'(E' - E_g) \left[ E'(E' + \Delta) + \delta \left( E' + \frac{2\Delta}{3} \right) \right]$$

$$f_1(E') = P_{\perp}^2 \left[ E'(E' + \frac{2\Delta}{3}) + \delta \left( E' + \frac{\Delta}{3} \right) \right]$$

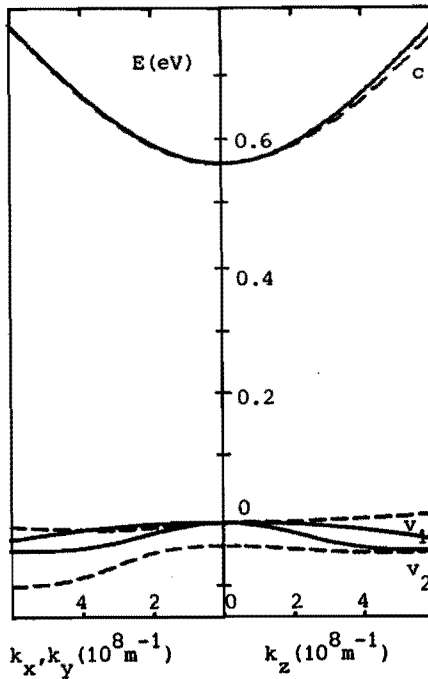
$$f_2(E') = P_{\parallel}^2 \left[ E'(E' + \frac{2\Delta}{3}) \right]$$

$$\text{and } E' = E - \frac{\hbar^2}{2m_0} (k_x^2 + k_y^2 + k_z^2)$$

In the above equations the band parameters have the following meaning:  $E_g$  is the energy gap,  $\Delta$  is the spin orbit splitting energy,  $\delta$  is the tetragonal crystal field splitting and  $P_{\perp}$  and  $P_{\parallel}$  are interband momen-

tum matrix elements, similar to the Kane matrix element  $P$  introduced in chapter 3. Eq. (5.1) is valid for both the normal and the inverted band ordering and for both positive and negative values of  $\delta$ . For  $\delta = 0$  and  $P_{\perp} = P_{\parallel} = P$  eq. (5.1) reduces to eqs. (3.1) and (3.2) given in section 3.2.

There is only very little known about the anisotropy effects in  $\text{Cd}_3\text{P}_2$ . The literature reports only one quantitative estimate of the tetragonal crystal field splitting  $\delta$  [41]. In order to evaluate the influence of anisotropy we have plotted in fig. 5.1 the band structure curves for  $\text{Cd}_3\text{P}_2$  in two different cases:



- isotropic ( $E_g = 0.56$  eV;  $\Lambda = 0.1$  eV;  $P = 6.7 \cdot 10^{-10}$  eVm;  $m_{v1} = 0.5 m_0$ )  
 --- anisotropic ( $E_g = 0.56$  eV;  $\Lambda = 0.1$  eV;  $P_{\perp} = P_{\parallel} = 6.7 \cdot 10^{-10}$  eVm;  
 $\delta = 0.08$  eV)

Fig. 5.1. Plot of the band structure of  $\text{Cd}_3\text{P}_2$  for the isotropic and anisotropic models. Valence band  $v_3$  has been omitted.

a) According to eqs. (3.1) and (3.3) for the isotropic (Kane) model using the experimentally determined band parameters from our interband measurements (see section 3.3).

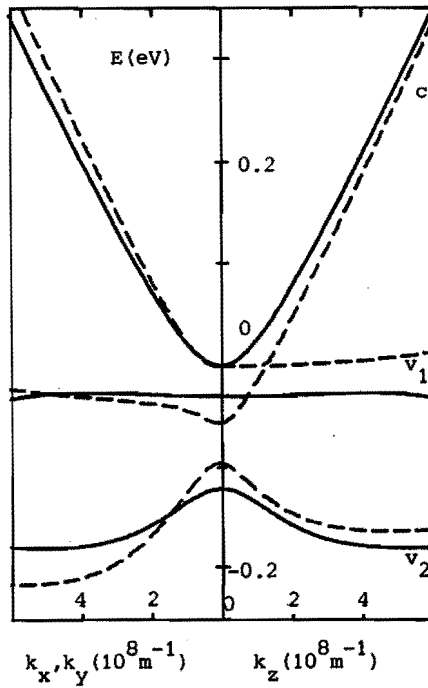
b) According to eq. (5.1) for the anisotropic (Bodnar) model using for  $E_g$ ,  $\Delta$  and  $P_{\perp} = P_{\parallel} = P$  the values of case a) and for  $\delta$  a value of 0.08 eV as given by Singh et al. [41].

A comparison between the isotropic and anisotropic cases leads to the following comments. The differences between both conduction bands are negligibly small for all directions in k-space so that the fermi energy and consequently the Burstein-Moss shift will not be affected significantly. The differences in bands  $v_1$  are larger but it should be noted that in contrast with the isotropic valence band  $v_1$ , the anisotropic one has not been corrected for higher bands because this correction is not known quantitatively. However, qualitatively we may expect that such a correction will bend the anisotropic band  $v_1$  downwards as pointed out in section 3.2. This will lead to a smaller difference between the isotropic and anisotropic heavy hole valence bands  $v_1$ . After all, it can be concluded that the tetragonal correction of the band structure will influence the joint density of states  $\rho_{v_1c}$  between bands  $v_1$  and c only slightly (see section 3.3). Assuming that the interband matrix element  $M_{v_1c}$  will not change very much by the tetragonal perturbation and realising that small anisotropy effects will be averaged out in the calculation of the absorption coefficient, it may be concluded that the theoretical values of the absorption coefficient of transition A (see section 3.3) will be modified only slightly by introduction of the tetragonal band structure correction. It can be seen from fig. 5.1. that the crystal field splitting  $\delta$  mainly shifts the light hole valence band  $v_2$  to lower energies. This means that the onset of transition B in the absorption spectra will occur at higher photon energies compared with the isotropic case. This might be the reason why this transition could not be detected in our experiments. It has, however, no influence on the quantitative interpretation of our measurements because the fit of the experimental and theoretical curves was completely based on transition A.

In contrast with  $Cd_3P_2$ , the anisotropy effects in  $Cd_3As_2$  have been studied extensively in the last few years. In fact the validity of the Bodnar model has been experimentally verified on  $Cd_3As_2$  and at present

an accurate set of band parameters is known. For a good comparison we have plotted in fig. 5.2 the band structure curves for  $\text{Cd}_3\text{As}_2$  in two different cases similar to  $\text{Cd}_3\text{P}_2$ :

- a) According to eqs. (3.1) and (3.4) for the isotropic (modified Kane) case using the experimentally determined band parameters of our interband measurements (see section 3.4).
- b) According to eq. (5.1) for the anisotropic (Bodnar) case using the experimentally determined values of the band parameters given by Neve [10].



- isotropic ( $E_g = -0.12$  eV;  $\Delta = 0.3$  eV;  $P = 7.10 \cdot 10^{-10}$  eVm;  
 $E_T = -0.026$  eV;  $E_R = -0.030$  eV;  $k_1 = 4.10^8$  m $^{-1}$ )
- anisotropic ( $E_g = -0.095$  eV;  $\Delta = 0.27$  eV;  $P_{//} = 7.35 \cdot 10^{-10}$  eVm;  
 $P_{\perp} = 7.40 \cdot 10^{-10}$  eVm;  $\delta = 0.095$  eV)

Fig. 5.2. Plot of the band structure of  $\text{Cd}_3\text{As}_2$  for the isotropic and anisotropic models. The valence band  $v_3$  has been omitted.

We want to emphasize first that, surprisingly, the anisotropic band  $v_1$  in the Bodnar model shows the essential features of the isotropic one given by the phenomenological eq. (3.4): the degeneracy with band c is lifted and its maximum is shifted from  $k = 0$ . Like in the  $Cd_3P_2$  case the anisotropic band  $v_1$  should be corrected for higher band interactions leading to a still better agreement with the isotropic band  $v_1$ . After these corrections the differences between all corresponding bands show the same behaviour: in the region of  $k$ -space around the fermi energy the differences are small and their sign is opposite for the  $k_z$ - and  $(k_x, k_y)$ -directions. This means that the joint density of states for both transitions A and B is hardly influenced by the anisotropy effects. If we assume that the interband matrix elements mentioned in section 3.4 are not influenced by the tetragonal crystal field perturbation, the anisotropy effects will be averaged out in the calculation of the absorption coefficient. In contrast with  $Cd_3P_2$  the position of the light hole valence band  $v_2$  with respect to the conduction band is not strongly influenced by the value of  $\delta$ . Together with the fact that the fermi energies in the isotropic and anisotropic cases will be nearly the same, this means that in the absorption spectrum the onsets of both transitions A and B are hardly influenced by the tetragonal crystal field correction.

In conclusion we may say that, though the anisotropic Bodnar model will give a more accurate description of the band structure of  $Cd_3P_2$  and  $Cd_3As_2$ , the use of the isotropic and much simpler Kane like model appears to be justified after all. Especially, the general conclusion that band structure inversion exists in the system with end components  $Cd_3P_2$  and  $Cd_3As_2$ , remains valid.

GENERAL REFERENCES

- {1} R. Dornhaus, G. Nimtz; *Narrow Gap Semiconductors*,  
Ed. G. Höhler, Springer Tracts in Modern Physics, 98 (1983) 119,  
(Springer Verlag, Berlin)
- {2} D.R. Lovett; *Semimetals and Narrow-Bandgap Semiconductors*, (Pion Ltd.,  
London, 1977)
- {3} R.K. Willardson, A.C. Beer; *Semiconductors and semimetals*, 18 (1981)  
(Academic Press, New York)
- {4} W. Zdanowicz, L. Zdanowicz; *Ann. Rev. Mater. Science*, 5 (1975) 301
- {5} E.K. Arushanov; *Prog. Crystal Growth Charact*, 3 (1981) 211
- {6} W. Zdanowicz; *Landolt-Börnstein Numerical Data*, III/17e, p. 178;  
Ed. K.H. Hellwege (Springer Verlag, Berlin, 1983)
- {7} Proceedings of the first int. symp. on the physics and chemistry of  
II-V compounds, Mogilany, Poland 1980, Eds. M.J. Gelten and L.  
Zdanowicz (Eindhoven University of Technology, Eindhoven, 1980).
- {8} F.A.P. Blom; *Thermomagnetic effects in Cadmium Arsenide*, Ph. D. Thesis  
Eindhoven University of Technology, 1970
- {9} F.A.P. Blom; *Proceedings Int. Summer School on Narrow Gap Semicond.*  
*Physics and Applications*, Ed. W. Zawadzki, *Lecture Notes in Physics*  
133, 191 (Springer Verlag, Berlin, 1980)
- {10} J.J. Neve; *The Shubnikov-de Haas effect in  $Cd_3As_2$ ,  $CdSnAs_2$  and*  
 *$(Cd_{1-x}Mn_x)_3As_2$* , Ph. D. Thesis, Eindhoven University of Technology,  
1984
- {11} F.A.P. Blom, J.W. Burg; *J. Phys. Chem. Solids* 38 (1977) 19
- {12} V.B. Anzin, Yu.V. Kosichkin, Yu.N. Kotlov, A.I. Nadezhdinsky;  
*Cryogenics* 16 (1976) 375
- {13} W. Seith; *Diffusion in Metallen* (Springer Verlag, Berlin, 1955)
- {14} B. Koltirine, M. Chaumereuil; *Phys. Stat. Sol.* 13 (1966) K1
- {15} R.J. Wagner, E.D. Palik, E.M. Swiggard; *The Physics of Semimetals and*  
*Narrow-gap Semiconductors*, Ed. D.L. Carter, R.T. Bate; *J. Phys. Chem.*  
*Solids Suppl.* 1 (1971) 471
- {16} P.L. Radoff, S.G. Bishop; *Phys. Rev.* B5 (1972) 442
- {17} E.O. Kane; *J. Phys. Chem. Solids* 1 (1957) 249
- {18} W. Zawadzki; *Adv. Physics* 23 (1974) 435
- {19} W. Szymanska, P. Boguslawski, W. Zawadzki; *Phys. Stat. Sol.* (b)  
65 (1974) 641
- {20} P.J. Lin-Chung; *Phys. Rev.* 188 (1969) 1272



- {21} P.J. Lin-Chung; Phys. Stat. Sol. (b) 47 (1971) 33
- {22} P. Plenkiewicz, B. Dowgiallo-Plenkiewicz; Phys. Stat. Sol. (b) 52  
(1979) 379
- {23} P. Plenkiewicz, B. Dowgiallo-Plenkiewicz; Phys. Stat. Sol. (b) 95  
(1979) 29
- {24} B. Dowgiallo-Plenkiewicz, P. Plenkiewicz; Phys. Stat. Sol. (b) 94  
(1979) K57
- {25} B. Dowgiallo-Plenkiewicz, P. Plenkiewicz; Phys. Stat. Sol. (b) 96  
(1979) 517
- {26} M.J. Aubin, L.G. Caron, J.P. Jay-Gerin; Phys. Rev. B15 (1977) 3872
- {27} L.G. Caron, J.P. Jay-Gerin, M.J. Aubin; Phys. Rev. B15 (1977) 3879
- {28} T.C. Harman, J.M. Honig, P. Trent; J. Phys. Chem. Solids 28 (1967)  
1995
- {29} T.S. Moss, G.J. Burrell, B. Ellis; Semiconductor Opto-electronics,  
(Butterworths, London, 1973)
- {30} P. Grosse; Freie Elektronen in Festkörpern (Springer Verlag, Berlin,  
1979)
- {31} E.K. Arushanov, A.F. Knyazev, K.G. Lisunov, A.N. Nateprov, S.I.  
Radautsan; Sov. Phys. Semicond. 17 (1983) 555
- {32} W. Zawadzki; Handbook of Semiconductors, 1 p. 713, Ed. W. Paul  
(North Holland Publishing Comp., Amsterdam, 1982)
- {33} J. Thielemann, M. von Ortenberg, F.A.P. Blom, K. Strobel; Proc. 4th.  
Int. Conf. Phys. Narrow Gap Semicond. Linz, 1981, Lecture Notes  
in Physics 152 p. 207 (Springer Verlag, Berlin, 1982)
- {34} E.D. Haidemenakis, M. Balkanski, E.D. Palik, J. Tavernier; Proc. Int.  
Conf. Semicond. Physics, Kyoto 1966, J. Phys. Soc. Japan 21  
suppl. (1966) 189
- {35} G.I. Goncharenko, M.I. Elinson, V.I. Kovalev, V.Ya. Shevchenko  
Sov. Phys. Semicond. 5 (1972) 1431
- {36} I. Rosenman; J. Phys. Chem. Solids 30 (1969) 1385
- {37} H. Doi, T. Fukuroi, T. Fukase, Y. Muto, K. Tanaka; Sci. Rep. Inst.  
Tohoku Univ. A20 (1969) 190
- {38} J. Bodnar; Proc. Int. Conf. Phys. Narrow Gap Semiconductors, Warsaw,  
1977, p. 311 (Polish Scientific Publ., Warsaw, 1978)
- {39} F.A.P. Blom, M.J. Gelten; Proc. 14th Int. Conf. Phys. Semicond.,  
Edinburgh, 1978, p. 545 (The Institute of Physics, London, 1979)

- {40} F.A.P. Blom, J.W. Cremers, J.J. Neve, M.J. Gelten; Solid State Comm.  
33 (1980) 69
- {41} M. Singh, J. Cisowski, P.R. Wallace, J.C. Portal, J.M. Broto;  
Phys. Stat. Sol. (b) 114 (1982) 481

## Temperature dependence of electron concentration in cadmium arsenide

F. A. P. Blom and M. J. Gelten

Department of Physics, Eindhoven University of Technology, Eindhoven, Netherlands

(Received 30 December 1977)

From measurements of the temperature dependence of the electron concentration in  $\text{Cd}_3\text{As}_2$ , we found values for the conduction-band parameters that are in good agreement with those recently reported by Aubin, Caron, and Jay-Gerin. However, in contrast with these authors we found no small overlap, but a relatively large gap of 26 meV between the heavy-hole band maximum and the conduction-band minimum.

In two recent papers<sup>1,2</sup> Aubin, Caron, and Jay-Gerin proposed an electronic-energy-band structure of  $\text{Cd}_3\text{As}_2$ . By gathering the literature values of electron effective masses from electrical transport studies and interpreting these data in Kane's model for the  $\alpha$ -Sn type inverted structure, these authors deduced the dispersion relation for the conduction band. The available data on the optical gap were used to determine the position and shape of the heavy-hole band, resulting in band schemes at 300 and 77 K as shown in Fig. 4 of Ref. 1 and Fig. 4 of Ref. 2, respectively. The ever present high degeneracy of this material (a characteristic electron concentration of about  $2 \times 10^{18} \text{ cm}^{-3}$  corresponding to a Fermi energy of about 0.15 eV) excluded up to now the determination of both conduction- and valence-band parameters from transport measurements only.

We prepared  $\text{Cd}_3\text{As}_2$  samples with net donor concentrations almost an order of magnitude lower than those reported in the literature.<sup>3</sup> Samples with initial concentrations of about  $2 \times 10^{18} \text{ cm}^{-3}$  were subjected to various heat treatments in either cadmium or arsenic atmospheres. Reduction of net donor concentrations was found to be most effective by applying a two-stage annealing procedure in arsenic vapor. The samples were first annealed during 1 week at 250 °C, followed by a much longer annealing time (2–4 months) at 100 °C. Substantial decrease in net donor concentration with time only started during the second stage of the treatment. A time of over 2 months is needed before a minimum value is achieved. Once the samples are stabilized in this way, their electron concentrations remain constant with time when maintained in air at room temperature.

In these samples the degeneracy is partly lifted, and measurements of the electron concentration  $n$  as function of temperature can be used to obtain numerical values for some important band parameters of the above mentioned model. The  $n$ - $T$  dependences of four samples in the temperature range from 4.2 to 360 K are given in Fig. 1. The net donor concentrations ( $N_D - N_A$ ) of the samples

are  $2.30 \times 10^{17}$ ,  $3.95 \times 10^{17}$ ,  $4.75 \times 10^{17}$ , and  $7.70 \times 10^{17} \text{ cm}^{-3}$ , respectively. For each net donor concentration  $n(T)$  can be calculated by solving simultaneously the equations

$$n - p = N_D - N_A, \quad (1)$$

$$n = \frac{1}{3\pi^2} \left( \frac{k_B T}{P} \right)^3 {}^0K_{3/2}(\eta, \beta, \Delta/k_B T), \quad (2)$$

$$p = \frac{1}{2\pi^2} \left( \frac{2m_h^* k_B T}{\hbar^2} \right)^{3/2} F_{1/2}(E_v/k_B T - \eta). \quad (3)$$

In Eqs. (1)–(3)  $n$ ,  $p$ ,  $N_D$ , and  $N_A$  are the concentrations of electrons, heavy holes, donors, and

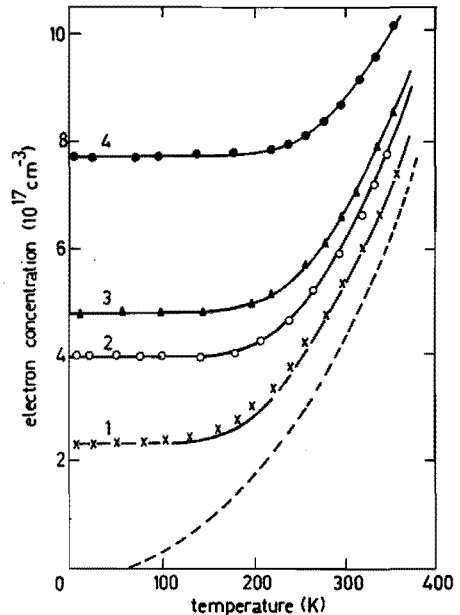


FIG. 10 Electron concentration as function of temperature for various net donor concentrations ( $2.30$ ,  $3.95$ ,  $4.75$ , and  $7.70$ )  $\times 10^{17} \text{ cm}^{-3}$  for samples 1, 2, 3, 4 respectively. The dashed curve represents the corresponding intrinsic concentration.

acceptors, respectively. The symbol  ${}^0L_k^{m_0}(\eta, \beta, \Delta/k_0T)$  represents a generalized  ${}^0L_k^m(\eta, \beta)$  integral,<sup>5</sup> by fully taking into account the free-electron term  $\hbar^2k^2/2m_0$  as well as finite spin-orbit splitting  $\Delta$ .  $F_{1/2}(E_f/k_0T - \eta)$  is a Fermi-Dirac integral of order  $\frac{1}{2}$ . It should be noticed that the band model we use here is essentially that of Aubin, Caron, and Jay-Gerin (Fig. 4 of Ref. 1), apart from the fact that we make no assumptions about the position of the maximum of the heavy-hole band in  $k$  space. The conduction band is described by the largest root of the secular equation for the three-band Kane model for the  $\alpha$ -Sn type structure.<sup>4</sup> Due to the lack of information about higher-lying bands in  $\text{Cd}_3\text{As}_2$ , corrections due to these bands can not be included. The  $K$  integral in Eq. (2) is similar to the integral introduced by Ermolovich and Kravchuk<sup>6</sup> for the InSb type structure. These authors define a four-parameter integral, in which the effective mass at the bottom of the conduction band acts as the fourth parameter. However, expressing this quantity in terms of the Kane matrix element  $P$  reduces this four-parameter integral to our three-parameter  $K$  integral, multiplied by a constant factor containing  $P$ .

For the heavy-hole band we assume an isotropic parabolic band with a thermal energy gap  $E_t$  between its top and the conduction-band minimum. The zero of energy is taken at the bottom of the conduction band, thus a positive  $E_t$  would signify an overlap between the heavy-hole and conduction bands. If the heavy-hole band maximum is displaced from  $\Gamma$  as has been suggested by some authors,<sup>1,2,7</sup> Eq. (3) still holds. Due to the introduction of the density-of-states effective mass in Eq. (3), this equation remains valid regardless of the number of equivalent extrema associated with the heavy-hole band.

Adopting temperature-independent values for  $\Delta$  of 0.30 eV,<sup>8</sup> and for the Kane matrix element  $P$  of  $7.0 \times 10^{-3}$  eV cm,<sup>9</sup> a computer fitting of the experimental  $n(T)$  data yielded the following numerical results (in the temperature range from 100 to 400 K):

$$E_0 = 0.12 + 3.3 \times 10^{-4} T \text{ eV}; \quad E_t = -26 \text{ meV};$$

$$m_t^*/m_0 = 0.50m_0.$$

The positive sign of  $E_0$  is caused by the fact that in the secular equation we used for the  $\alpha$ -Sn structure,<sup>4</sup>  $E_0$  represents the absolute energy separation between  $\Gamma_6$  and  $\Gamma_8$ . Comparing the above numerical results with those given in Refs. 1 and 2, we have to distinguish between the bands originating from the third-order secular equation (light-electron, light-hole, and split-off valence band) and the heavy-hole band. The magnitude of the

direct gap  $E_0$  at  $\Gamma$  as well as the sign and magnitude of its temperature coefficient are in good agreement with the values reported by Aubin *et al.* Since the values of  $P$  and  $\Delta$  are also nearly the same, we may conclude that positions and shapes of the light-electron band, light-hole, and split-off valence bands are well established now and that they exhibit the  $\alpha$ -Sn type ordering. Recent analysis by Bodnar<sup>10</sup> of Shubnikov-de Haas and de Haas-van Alphen effects in terms of a band model which takes into account the tetragonal field splitting, also give strong evidence for an  $\alpha$ -Sn like structure.

Considering the numerical data for the heavy-hole band, we conclude that remarkable differences with the work by Aubin *et al.* are found. Whereas these authors deduce from the few available optical data that there should exist a zero indirect gap or even a small overlap, our analysis of  $n(T)$  gives a negative value of  $E_t$ . Secondly, our value of the effective mass is much higher than 0.12 $m_0$ , the value obtained by Aubin *et al.* as well as by Haidemenakis *et al.*<sup>11</sup> from low-temperature magneto-optical experiments. Concerning our results it has to be remarked that in the fitting procedure  $E_t$  and  $m_t^*$  are highly correlated. This is illustrated in Fig. 2, which shows that the combination  $m_t^*/m_0 = 0.50$ ,  $E_t = -26$  meV is not the unique one leading to a good fit to the experimental results of Fig. 1. Smaller values of  $m_t^*$  result in smaller—but strongly temperature dependent—values of  $E_t$ , and conversely. For instance, a value of  $m_t^* = 0.12m_0$  requires  $E_t$  to vary from about -10 meV at 100 K to an overlap of 30 meV at 300 K. On the other hand, regarding  $E_t$  as fixed at zero gives

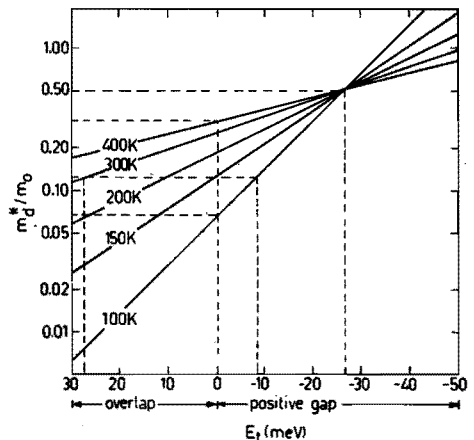


FIG. 2. Correlation between  $m_t^*$  and  $E_t$  for the same set of values for  $E_0$ ,  $P$ , and  $\Delta$  as in Fig. 1.

rise to an  $m_d^*$  increasing from  $0.07m_0$  at 100 K to  $0.22m_0$  at 300 K. For the given values of  $E_0$ ,  $P$ , and  $\Delta$ , the only set of temperature-independent values of  $E_r$  and  $m_d^*$ , which gives a good fit to the experimental results over the whole temperature and concentration ranges, is the combination  $E_r = -26$  meV and  $m_d^* = 0.50m_0$ . The fact that  $E_r$  and  $m_d^*$  may be expected to have only very small temperature coefficients, because they are influenced only by bands far away, makes this set of values the more reliable.

Aubin *et al.* proposed a complex heavy-hole band with off-axis maxima and a smoothing out towards  $\Gamma$  with a residual gap  $E_r$  (see Fig. 4 of Ref. 1). From the above given analysis of the experimental data it is not possible to decide whether  $E_r$  is a direct or an indirect gap. Therefore we also tried to fit our data by assuming a quartic model for the heavy-hole band,<sup>12</sup> involving two sets of electrons and one set of holes. However, we could not obtain a definite answer, also because of the fact that interpretation in this model requires the introduction of some extra fitting parameters, such as the effective mass of the heavy electrons. Conclusive evidence for the Aubin model of the heavy-hole band should come from optical data on low-concentration samples. We started optical absorption measurements on very thin samples with electron concentrations of about  $5 \times 10^{17}$  cm<sup>-3</sup>. The absorption coefficient was calculated assuming direct transitions from a heavy-hole band described by a quartic model to the conduction band. This quartic model gives a much better agreement with the experimental optical data than a simple parabolic heavy-hole band at  $\Gamma$ . With  $E_r = -26$  meV a value of  $4 \times 10^6$  cm<sup>-1</sup> was found for the wave number

corresponding to the heavy-hole band maximum. More extensive absorption measurements and calculations for geometrically more complex heavy-hole band forms are necessary.

Regarding the large difference between our value of  $m_d^* = 0.50m_0$  and that of  $0.12m_0$  from the literature<sup>1,11</sup> one has to realize that in our case we are dealing with the density-of-states effective mass. For a heavy-hole band exhibiting a number of equivalent extrema ( $N_v$ ), the relation  $m_d^{*3/2} = N_v m^{*3/2}$  should be applied. This leads to a value of  $N_v$  of about 8, a result which is not unreasonable in view of the band-structure calculations by Lin-Chung.<sup>7</sup> Concerning our value of  $m_d^*$  it has to be clearly stated that this type of curve fitting of transport coefficients versus temperature can result in a nonphysical value. Both Fermi surface and optical data are necessary before final conclusions about the phenomenological band structure may be drawn.

Finally we comment on the conclusion by Aubin *et al.* that, if the shape of the heavy-hole band does not depend on temperature, the overlap with the conduction band increases as the temperature is lowered. This is in disagreement with our results, as can be seen in Fig. 2. For a constant  $m_d^*$  smaller than  $0.50m_0$ ,  $E_r$  always decreases ("overlap" decreases) with decreasing temperature. This also means that the absolute value of the residual  $E_r$  should increase with lowering temperature, in contradiction to the suggestion in Ref. 2.

#### ACKNOWLEDGMENTS

We thank P. Nouwens and R. van Bree for technical assistance, and C. van Es and P. H. Monen for the computer programming.

<sup>1</sup>M. J. Aubin, L. G. Caron, and J.-P. Jay-Gerin, Phys. Rev. B **15**, 3872 (1977).

<sup>2</sup>L. G. Caron, J.-P. Jay-Gerin, and M. J. Aubin, Phys. Rev. B **15**, 3879 (1977).

<sup>3</sup>F. A. P. Blom and M. J. Gelten, Proceedings of the International Conference on the Physics of Narrow-Gap Semiconductors, Warszawa (1977) (to be published).

<sup>4</sup>W. Zawadzki, Adv. Phys. **23**, 435 (1974).

<sup>5</sup>W. Zawadzki, R. Kowalczyk, and J. Kolodziejczak, Phys. Status Solidi **10**, 513 (1965).

<sup>6</sup>Yu. B. Ermolovich and A. F. Kravchuk, Fiz. Tekh. Poluprovodn. **10**, 1966 (1976) [Sov. Phys. Semicond. **10**, 1173 (1976)].

<sup>7</sup>P. J. Lin-Chung, Phys. Rev. **188**, 1274 (1969).

<sup>8</sup>V. V. Sobolev, N. N. Syrbu, T. A. Zyubina, and Y. A. Ugal, Fiz. Tekh. Poluprovodn. **5**, 327 (1971) [Sov. Phys. Semicond. **5**, 279 (1971)]; M. J. Aubin and J. P. Cloutier, Can. J. Phys. **53**, 1642 (1975). A possible small

temperature dependence of  $\Delta$  is ignored in our case, because the value of this quantity has not been measured directly but determined by applying the empirical  $\frac{2}{3}$  rule to the spin splitting in the  $\Lambda$  direction.

<sup>9</sup>This value is obtained by reinterpreting previous results [F. A. P. Blom and J. Th. Schrama, Phys. Lett. A **30**, 245 (1969)] without simplifying the secular equation. The introduction of a weak temperature dependence of  $P$ , which was reported in Ref. 1, has no significant effect on the confidence limits of the band parameters. The same conclusion has been drawn for HgSe by S. L. Lehoczky, J. G. Broerman, D. A. Nelson, and C. R. Whitsett, Phys. Rev. B **9**, 1598 (1974).

<sup>10</sup>J. Bodnar, in Ref. 3.

<sup>11</sup>E. D. Haidemenakis, M. Balkanski, E. D. Paltk, and J. Tavernier, J. Phys. Soc. Jpn. Suppl. **21**, 189 (1966).

<sup>12</sup>T. C. Harman, J. M. Honig, and P. Trent, J. Phys. Chem. Solids **28**, 1995 (1967).

## SUMMARY

Cadmium phosphide ( $\text{Cd}_3\text{P}_2$ ) and cadmium arsenide ( $\text{Cd}_3\text{As}_2$ ) are n-type semiconductors from the II-V family and have a tetragonal crystal structure. They have a small bandgap and show in many aspects great similarity with the well known semiconductors CdTe and HgTe which crystallize in a cubic structure. On the contrary they show interesting differences because of anisotropy effects.

There were indications that the system  $\text{Cd}_3(\text{As}_x\text{P}_{1-x})_2$  ( $0 \leq x \leq 1$ ) showed the phenomenon of band structure inversion analogous to the system  $\text{Hg}_x\text{Cd}_{1-x}\text{Te}$ . This phenomenon means in fact that the symmetry properties of the conduction band and the light hole valence band interchange. This leads to a normal band ordering and an open energy gap in one end compound ( $\text{Cd}_3\text{P}_2$ ), whereas the other end compound ( $\text{Cd}_3\text{As}_2$ ) shows an inverted band ordering with a thermal bandgap equal to zero.

To get a better knowledge of the electron properties in their respective energy bands a comprehensive study has been started in which both optical measurements and electrical transport measurements were carried out.

This thesis describes primarily the results of the optical measurements. It contains previously published papers in a chronological order linked by some elucidating text and gives the results of absorption and reflectivity measurements carried out on n-type samples of  $\text{Cd}_3\text{P}_2$  and  $\text{Cd}_3\text{As}_2$  with a large electron concentration (degenerate material). All measurements are performed between the temperature of liquid helium (4.2 K) and room temperature (300 K) in the spectral region from the near infrared (wavelength several  $\mu\text{m}$ ) to the far infrared (wavelength several hundreds of  $\mu\text{m}$ ).

After a general introduction in chapter 1, some experimental details are described in chapter 2.

Chapter 3 deals with the interband absorption measurements in the near infrared. After a general treatment of band structure inversion we present a description of the band structure models used for the interpretation of the measurements. The experimental results of  $\text{Cd}_3\text{P}_2$  can be interpreted in an isotropic band model according to Kane.

After a phenomenological correction this model also suits to describe the measurements on  $\text{Cd}_3\text{As}_2$ . On the one hand this gives the experimental proof of the existence of the band structure inversion, on the other hand a number of important band structure parameters can be determined by fitting the theoretical and the experimental results.

Chapter 4 presents the experimental results of far infrared reflectivity measurements. These are carried out for a better understanding of the structure of the plasma edge which is mainly determined by the free carrier properties and is strongly influenced by the existence of optical phonons in both  $\text{Cd}_3\text{P}_2$  and  $\text{Cd}_3\text{As}_2$  (plasmon-phonon coupling). The large number of optical phonons leads to a complicated structure in the reflectivity spectrum. A new theoretical model has been developed for the interpretation of reflectivity spectra due to plasmon-multiphonon coupling. The most relevant intrinsic phonon parameters of  $\text{Cd}_3\text{P}_2$  and  $\text{Cd}_3\text{As}_2$  have been determined experimentally. From plasma-reflectivity measurements in high magnetic fields an explanation has been found for the unique phenomenon of oscillations in the reflectivity spectrum of  $\text{Cd}_3\text{As}_2$  near the plasma frequency.

Finally, in chapter 5 the influence of anisotropy effects on the band structure of  $\text{Cd}_3\text{P}_2$  and  $\text{Cd}_3\text{As}_2$  is discussed. Application of a recently developed model, the so called Bodnar model, does not require reconsideration of the previous conclusions.

## SAMENVATTING

Cadmiumfosfide ( $\text{Cd}_3\text{P}_2$ ) en cadmiumarsenide ( $\text{Cd}_3\text{As}_2$ ) zijn n-type halfgeleiders uit de II-V familie en bezitten een tetragonale kristalstructuur. Ze hebben een kleine bandafstand en vertonen in een aantal opzichten gelijkenis met de meer bekende halfgeleiders CdTe en HgTe die een kubische structuur bezitten. Ze vertonen echter ook interessante verschillen door anisotropie-effecten.

Het vermoeden bestond dat het systeem  $\text{Cd}_3(\text{As}_x\text{P}_{1-x})_2$  ( $0 \leq x \leq 1$ ) het verschijnsel van bandenstructuur-inversie vertoonde analoog aan het systeem  $\text{Hg}_x\text{Cd}_{1-x}\text{Te}$ . Bij dit verschijnsel wisselen de symmetrie-eigenschappen van de geleidingsband en de lichte gatenband. Hierdoor vertoont de ene eindverbinding ( $\text{Cd}_3\text{P}_2$ ) een normale bandordening met een open energiegap terwijl de andere eindverbinding ( $\text{Cd}_3\text{As}_2$ ) een geïnverteerde bandordening heeft die leidt tot een thermische bandafstand gelijk aan nul.

Om een beter inzicht te krijgen in het gedrag van elektronen in hun energiebanden is een uitvoerig onderzoek opgezet waarbij zowel optische metingen als elektrische transportmetingen uitgevoerd worden.

Dit proefschrift beschrijft in hoofdzaak de resultaten van de optische metingen. Het bestaat uit reeds gepubliceerde artikelen in chronologische volgorde met enige tussentekst als toelichting en geeft de resultaten van absorptie- en reflectiemetingen die verricht zijn aan n-type preparaten van  $\text{Cd}_3\text{P}_2$  en  $\text{Cd}_3\text{As}_2$  met een hoge elektronenconcentratie (gedegeneerd materiaal). Alle metingen zijn verricht tussen de temperatuur van vloeibaar helium (4.2 K) en kamertemperatuur (300 K) in het spectrale gebied dat zich uitstrekt van het nabije infrarood (golflengte enkele  $\mu\text{m}$ ) tot het verre infrarood (golflengte enkele honderden  $\mu\text{m}$ ).

Na een algemene inleiding in hoofdstuk 1 worden enkele experimentele bijzonderheden beschreven in hoofdstuk 2.

In hoofdstuk 3 worden de interband-absorptiemetingen in het nabije infrarood behandeld. Na een algemene beschouwing over bandenstructuur-inversie volgt een beschrijving van de bandenstructuurmodellen die voor interpretatie van de metingen gebruikt zijn. De meetresultaten aan  $\text{Cd}_3\text{P}_2$  kunnen worden geïnterpreteerd in een isotroop bandenmodel van Kane. Na een fenomenologische aanpassing blijkt dit model ook te voldoen om de metingen aan  $\text{Cd}_3\text{As}_2$  te beschrijven. Enerzijds wordt hiermee het experimentele bewijs geleverd dat de bandenstructuur-inversie inder-



daad optreedt, anderzijds kan door aanpassing van de theorie en de experimenten een aantal essentiële bandenstructuurparameters goed bepaald worden.

Hoofdstuk 4 behandelt de resultaten van reflectiemetingen in het verre infrarood. Deze zijn verricht om een beter inzicht te verkrijgen in de structuur van de plasmakant, die bepaald wordt door eigenschappen van de vrije ladingsdragers en zowel in  $\text{Cd}_3\text{P}_2$  als  $\text{Cd}_3\text{As}_2$  sterk beïnvloed wordt door de aanwezigheid van optische fononen (plasmon-fonon-koppeling). Door het grote aantal optische fononen ontstaat een gecompliceerde structuur in het reflectiespectrum. Een nieuw theoretisch model is ontwikkeld voor de interpretatie van reflectiespectra ten gevolge van plasmon-multi-fonon-koppeling. De belangrijkste intrinsieke fononparameters van  $\text{Cd}_3\text{P}_2$  en  $\text{Cd}_3\text{As}_2$  zijn experimenteel bepaald. Uit de resultaten van plasmareflectiemetingen in hoge magneetvelden is een verklaring gevonden voor het unieke, al jaren bekende, verschijnsel van opslingeren in het reflectiespectrum van  $\text{Cd}_3\text{As}_2$  in de buurt van de plasmafrequentie.

Tenslotte wordt in hoofdstuk 5 nog een beschouwing gegeven over de invloed van anisotropie-effecten op de bandenstructuur van  $\text{Cd}_3\text{P}_2$  en  $\text{Cd}_3\text{As}_2$ . Een recent ontwikkeld model, het zogenaamde Bodnar-model, geeft geen aanleiding om de eerder getrokken conclusies te herzien.

## DANKWOORD

Het onderzoek, dat in dit proefschrift is beschreven, kon slechts worden uitgevoerd doordat vele personen van de afdeling der Technische Natuurkunde, in het bijzonder van de Vakgroep Vaste Stof, in de Loop der jaren hun medewerking hebben verleend. Allen die in meer of mindere mate bij dit onderzoek betrokken zijn geweest dank ik van harte voor hun bijdrage en de plezierige wijze waarop ik met hen mocht samenwerken.

Enkele personen wil ik voor hun grote inzet in het bijzonder vermelden:

- Prof.dr. M.J. Steenland ben ik naast zijn stimulerende belangstelling erkentelijk voor de grote mate van vrijheid die hij mij gaf om onze overeenstemmingsrelatie volgens de WUB in te vullen. Voor zijn warme persoonlijke contacten, ook na zijn pensionering, dank ik hem zeer.
- Prof.dr.ir. W.J.M. de Jonge ben ik erkentelijk voor zijn kritische steun tijdens het schrijven van dit proefschrift.
- Frans Blom dank ik voor de wijze waarop hij mij in het vakgebied van de kleine-bandafstand halfgeleiders introduceerde en de collegiale wijze waarop hij onze samenwerking gestalte gaf.
- Peter Nouwens verdient dank voor zijn plichtsgetrouwe en nauwgezette manier van werken bij het vervaardigen van de samples.
- Vele stagiairs en afstudeerders droegen hun steentje bij. Met name wil ik de bijdragen noemen van Ton van Oosterom, Noud van Lieshout, Giel Menting, Jan Jongeneelen, Leon Bosch, Sten Groh, Ton Breuls, Ric Schleijpen en Huub Deckers. Allemaal bedankt!
- Mijn dank gaat verder uit naar de secretaressen die het typewerk verzorgden voor alle publicaties, in het bijzonder Rianne van Vinken en Frida Verbeek die bij de laatste fase van het typewerk hun beste beentje hebben voorgezet.
- Mijn gezin ben ik dank verschuldigd voor het scheppen van de goede sfeer buiten de werkuren. Ik heb gemeend deze dankbaarheid gestalte te geven door dit proefschrift aan hen op te dragen.
- In deze opsomming is de laatste en zeker niet de minste plaats bestemd voor Kees van Es vanwege zijn grote inzet bij het voltooiën van dit onderzoek. Telkens als mijn functioneren een aanpassing behoefde was hij bereid de hiaten op te vullen. Kees, mijn dank is groot: voor mij promoveer jij ook een beetje.

## CURRICULUM VITAE

- 14-03-1944      *Geboren te Halsteren*
- 1956-1961      *Opleiding HBS-B aan het Dr. Mollerlyceum  
te Bergen op Zoom*
- 1961-1966      *Studie aan de Technische Hogeschool te Eindhoven,  
afdeling der Technische Natuurkunde. Afgestudeerd  
in de groep Atoomfysica onder leiding van Prof. Dr.  
A.A. Kruithof*
- 1966-heden     *Wetenschappelijk Medewerker aan de THE, afdeling der  
Technische Natuurkunde, in de groep Lage Temperaturen,  
later de groep Halfgeleiderfysica van de Vakgroep  
Vaste Stof, onder leiding van Prof. Dr. M.J. Steenland.*

STELLINGEN

behorende bij het proefschrift van

M.J. Gelten

Eindhoven, 14 juni 1985

1. Bij het meten van Langmuir sondekaracteristieken in een cesiumgas-ontlading dient de sonde tijdens de meting op een constante temperatuur te worden gehouden.

*J.G.A. Hölscher, M.J. Gelten; Appl. Sci. Res. 18 (1967) 167*

2. De door Brebner en Déverin gebruikte benadering voor de uitdrukking voor de dubbele breking in GaS en GaSe leidt tot onaanvaardbaar grote fouten in de door hen bepaalde waarden van de ordinare en extraordinaire brekingsindices.

*J.L. Brebner, J.-A. Déverin; Helv. Phys. Acta 38 (1965) 650*

3. De door Aubin et al. gegeven interpretatie van interband magneto-optische oscillaties in  $Cd_3As_2$  berust op een onjuist gebruik van de Shubnikov- de Haas periode van elektronen in de geleidingsband.

*M.J. Aubin, A. Rambo, E. Arushanov; Phys. Rev. B23 (1981) 3602*

4. Bij de vergelijking van het magneetveld afhankelijke deel van de soortelijke warmte van TMMC met klassieke modelsystemen corrigeren Borsa et al. hun meetresultaten ten onrechte voor de bijdrage van lineaire spingolf excitaties.

*F. Borsa, M.G. Pini, A. Rettori, V. Tognetti; Phys. Rev. B28 (1983) 5173*

5. Nicoli en Tinkham geven op onvoldoende wijze aan hoe zij bij de bepaling van de absorptie intensiteiten van spin cluster resonanties in  $CoCl_2 \cdot 2H_2O$  hun transmissiemetingen gecorrigeerd hebben voor de reflectie-coëfficiënt van de samples temeer daar deze zal variëren met de golflengte.

*D.F. Nicoli, M. Tinkham; Phys. Rev. B9 (1974) 3126*

6. De door Mouwen geïntroduceerde overgangswaarschijnlijkheid voor interne sociale interacties kan nader worden gepreciseerd door de introductie van een normeringsfactor die zowel afhankelijk is van de opiniesprong als van de opinieafstand tussen elkaar beïnvloedende groepen.

*C.A.M. Mouwen; Intermediair jaargang 17, juni 1981, p. 31*

7. Het is opvallend dat in deze tijd het stijldansen een grote populariteit geniet, hoewel bij deze sport de heer een leidinggevende functie heeft ten opzichte van zijn dame.

8. One Apple a day  
keeps the physics away.